11-12-2007

Effects of Nutrients From the Water Column on the Growth of Benthic Microalgae in Permeable Sediments

Brian P. Darrow
University of South Florida

Effects of Nutrients From the Water Column on the Growth of Benthic Microalgae in Permeable Sediments

by

Brian P. Darrow

A dissertation submitted in partial fulfillment
of the requirements for the degree of
Doctor of Philosophy
College of Marine Science
University of South Florida

Major Professor: John J. Walsh, Ph.D.
Gabriel A. Vargo, Ph.D.
Kent A. Fanning, Ph.D.
Robert H. Weisberg, Ph.D.
Richard A. Jahnke, Ph.D.

Date of Approval:
November 12, 2007

Keywords: Marine Ecology, Diatoms, Numerical Modeling, Nutrient Cycles, Phytoplankton

This work is dedicated to my wife Raffi and my two daughters, Alice and Wendy. I cannot think of three better women with whom to share my life. I just finished my dissertation. I'm going to Disney World.

Acknowledgments

This work was funded by various grants to John Walsh, Kent Fanning, Bob Weisberg and Gabe Vargo from the National Aeronautics and Space Administration, the National Science Foundation, and the Office of Naval Research. Additional funding was also provided by research fellowships from the Tampa Bay Parrotheads in Paradise, the Sanibel Captiva Shell Club, St. Petersburg Progress and the United States Geological Survey.

I'd like to thank my major advisor, John Walsh for his challenging tutelage, stimulating conversations and fatherly advice over the last 9 years. I am indebted to my committee members, Bob Weisberg, Kent Fanning, Gabe Vargo, and Rick Jahnke for suggestions that have greatly improved this manuscript as well as my graduate school career.

This work would not have been possible without the technical assistance of Dwight Dieterle. His patient guidance has been invaluable in discovering silly coding errors and getting things to work throughout my graduate school career. Finally, I'd like to thank Jason Lenes for his friendship and inspiration. Many creative solutions to complex problems were hatched while shooting the breeze on the third floor landing of the Knight Oceanographic Research Center.

Table of Contents

List of Tables

List of Figures

Effects of Nutrients from the Water Column on the Growth of Benthic Microalgae in Permeable Sediments

Brian P. Darrow

ABSTRACT

In some continental shelf sediments integrated benthic microalgal biomass is greater than the integrated phytoplankton biomass in the overlying water column. In addition, benthic microalgae may account for up to 10% of the primary production responsible for the coastal fishery yield of the eastern United States.

A three-dimensional model of the eastern Gulf of Mexico examines the effects of water-column nutrient sources on the growth of benthic microalgae. To parameterize the exchange of nutrients across the sediment/water interface in these permeable sediments, a non-local exchange submodel was constructed and tested within the framework of the model's grid.

Based on the results of the three dimensional simulations, the growth of benthic microalgae from water-column nutrients is highly dependent on the light limitation of overlying phytoplankton. When light is available to phytoplankton in high enough quantities, water-column nutrients are used up before reaching the

sediments. When the overlying phytoplankton are light limited, nutrients are able to reach the sediments where the shade adapted benthic microalgae can grow.

Introduction

The principle of competitive exclusion states that no two species competing for exactly the same resources can stably coexist. The apparent violation of this principle by the many species of freshwater and marine phytoplankton has been the impetus for countless experiments, discussion and research papers in the field of ecology since George Evelyn Hutchinson (1961) first articulated the “paradox of the plankton”.

Hutchinson realized that a body of water is not as homogeneous as it seems on the surface. Physical, chemical and biological conditions change on every possible time scale. This continual change means that no one species can be adapted to the conditions at a single point in space at all times. Likewise, conditions at any spatial point in a body of water are likely to be different from those at other spatial points at any given time. If the water is in constant motion, as bodies of water tend to be, conditions at one space may move to another space, or mix with conditions at other spaces creating completely new conditions. It is in this very heterogeneous and continually changing environment that many species of phytoplankton coexist.

Every species of phytoplankton uses the sun's energy through photosynthesis to convert inorganic carbon, to organic carbon. Phytoplankton are a significant sink of CO_2 because of the vast size of the Earth's oceans relative to its landmass. It may, therefore, seem that all phytoplankton are one functional group with the purpose of keeping Earth's carbon budget in balance.

In reality, each phytoplankton species plays a role in defining the environmental conditions in which it thrives. Some species support productive fisheries while others kill fish. Some species rapidly sink to the depths, transporting their carbon away from the surface layer, while others become buoyant when they die. Clearly, the success of one species of phytoplankton over another in a given environment can have serious social, environmental, economic and political impacts.

Such wide ranging impacts have recently led to extensive studies of the factors that lead to the success of the harmful dinoflagellate, *Karenia brevis* in the Gulf of Mexico. Blooms of *Karenia brevis* occur regularly off the west coast of Florida on the shallow West Florida shelf. The first documentation of such a bloom was recorded in 1884 (Walker, 1884), and the causative organism, then known as *Gymnodinium brevis*, was first identified in 1948 (Davis, 1948). Throughout time, several causes have been suggested, ranging from volcanic heating to agricultural pollution. Recent studies have shown that the causes of the toxic blooms are complex, such that a very specific succession of conditions is required for a large bloom to develop and persist (Walsh *et al.*, 2006).

An important condition for the initiation of *Karenia brevis* blooms is a phosphorus-rich nutrient source (Walsh *et al*, 2006). Such a nutrient source favors the initiation of nitrogen fixing organisms, which then undergo cell lysis, releasing their nitrogen to the water-column for use by other species, like *Karenia brevis*. For this reason, the West Florida shelf is an ideal location for *Karenia brevis* blooms because of a rich source of fossil phosphorus near the surface of the landmass and underlying the continental shelf.

The eastern Gulf of Mexico comprises a complex nutrient habitat for algae. The region is dominated by the West Florida shelf, which extends approximately 700 km along the west coast of Florida and ranges 100-150 km in width. In the northeastern portion of the Gulf of Mexico, the Louisiana, Mississippi and Alabama shelves are narrower, ranging from 56 km in width near DeSoto canyon to about 10 km off the Mississippi River delta. The Mississippi River, itself, encompasses the world's second largest drainage basin, draining approximately 40% of the continental United States, with an average discharge of over 18,500 $m^3 s^{-1}$ to the Gulf of Mexico (Morgan & Dale, 2007). In total, approximately 25 other rivers discharge to the Gulf of Mexico between the Mississippi river delta and the Florida Keys. Most of these are in Florida and drain relatively small, coastal regions surrounding the Gulf (Nordlie, 1990).

Despite such riverine discharge, nutrient concentrations in the eastern Gulf of Mexico are generally low, often below detection levels (Masserini and Fanning, 2000), except in the most nearshore areas. There are, however,

several seasonal and regional features, which help to bring about the ecological complexity of the region. The most obvious of these is the Mississippi River.

In September 1991, near-surface nitrate concentrations greater than 30 μM were measured in the low salinity plume of the Mississippi River above the Louisiana shelf. Silicate concentrations greater than 40 μM with phosphate concentrations larger than 1 μM (Smith and Hitchcock, 1994) were also observed. Relatively high nutrient concentrations were again measured during May 1999 (Figs. 1,2) within a similar low salinity plume. Like other years (Gilbes *et al.*, 1996; Muller-Karger *et al.*, 1991) the May 1999 low salinity plume was carried southeastward by oceanic currents to the West Florida Shelf, thus impacting a large area of the Gulf. The Mobile, Apalachicola and Suwannee rivers (Del Castillo *et al.*, 2000) have been observed to similarly interact with oceanic currents (Gilbes *et al.*, 1996), episodically producing low salinity, nutrient rich plumes that may deliver nutrients to the continental shelf directly or through the degradation of algal biomass and grazer byproducts within the plume.

In addition to the intermittent peaks in discharge of the various rivers, further complexity is added because of regional differences in characteristics of riverine waters. Each low salinity plume associated with a river flowing into the eastern Gulf of Mexico exhibits a different relationship between dissolved organic matter (DOM) and salinity (Conmy and Coble, 2002). Furthermore, enhanced surface phosphate concentrations (Fig. 3) in the southern portion of the shelf are likely the result of the seasonal outflow of southern rivers (Nordlie, 1990) draining the regions of the shallow Bone Valley and Hawthorn phosphate deposits.

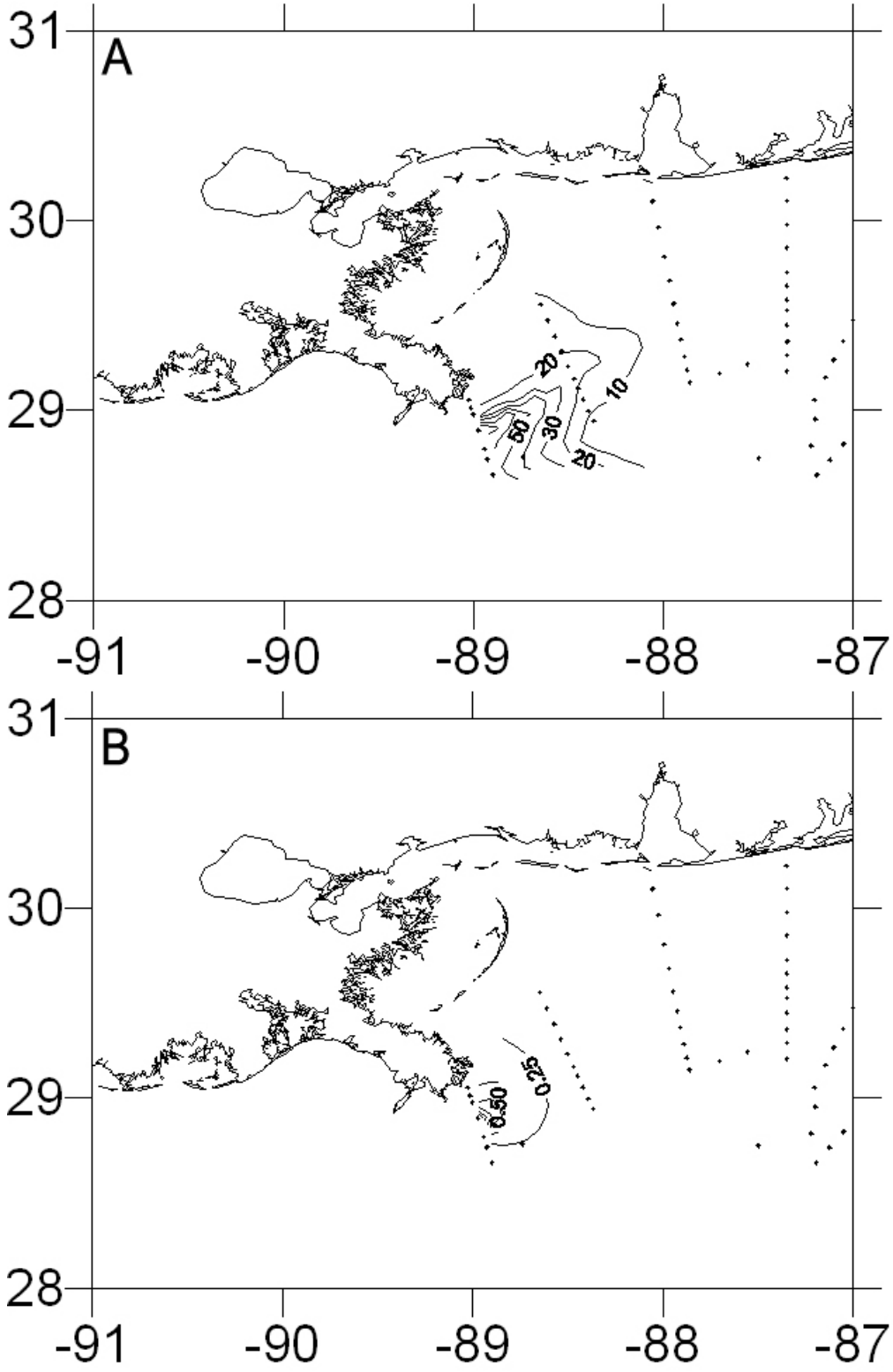

Figure 1. The surface distribution of (A) NO_3+NO_2 and (B) PO_4 off the coast of Louisiana during the May 1999 NEGOM cruise.

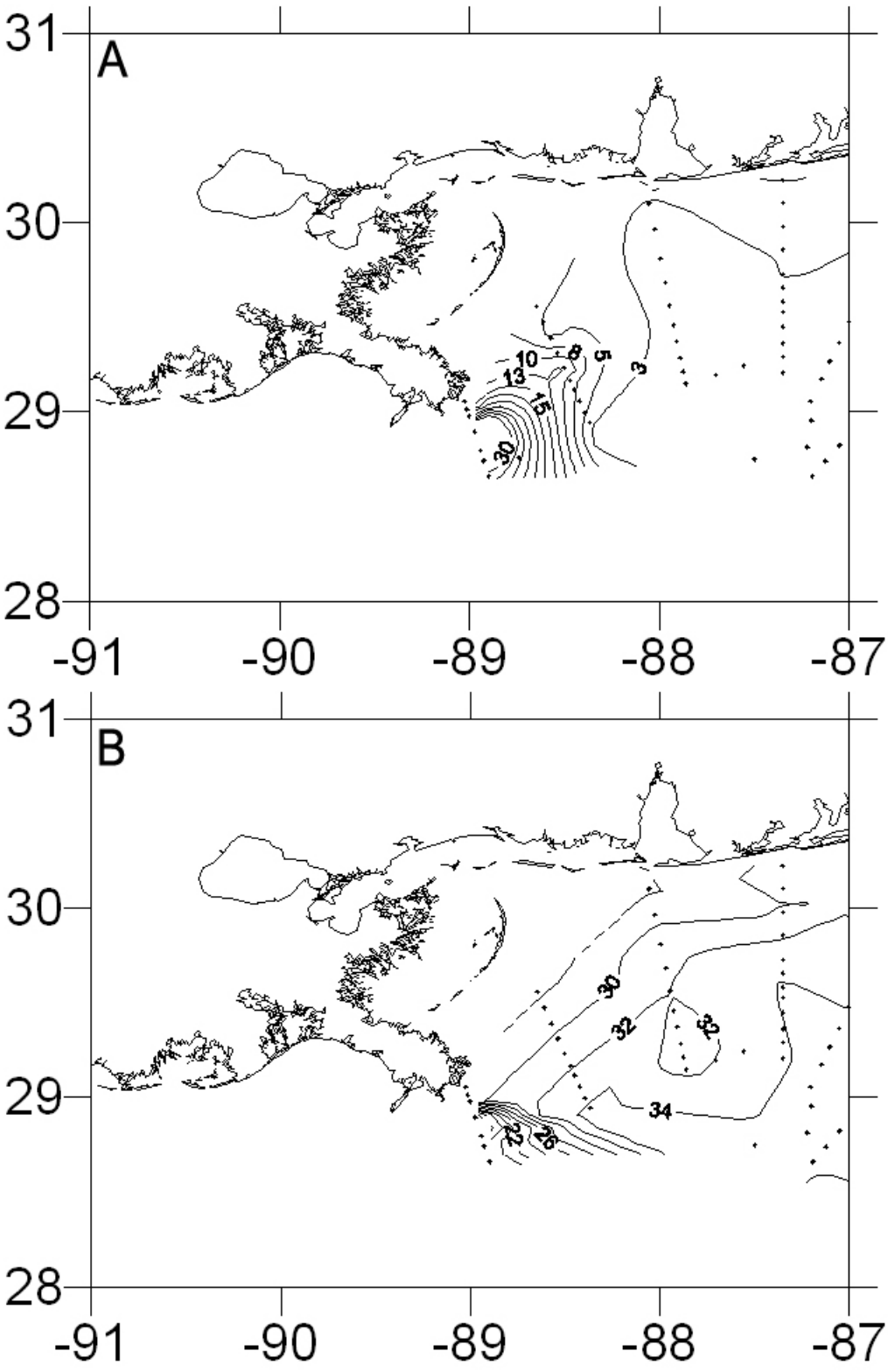

Figure 2. The surface distribution of (A) SiO_4 and (B) salinity off the coast of Louisiana during the May 1999 NEGOM cruise.

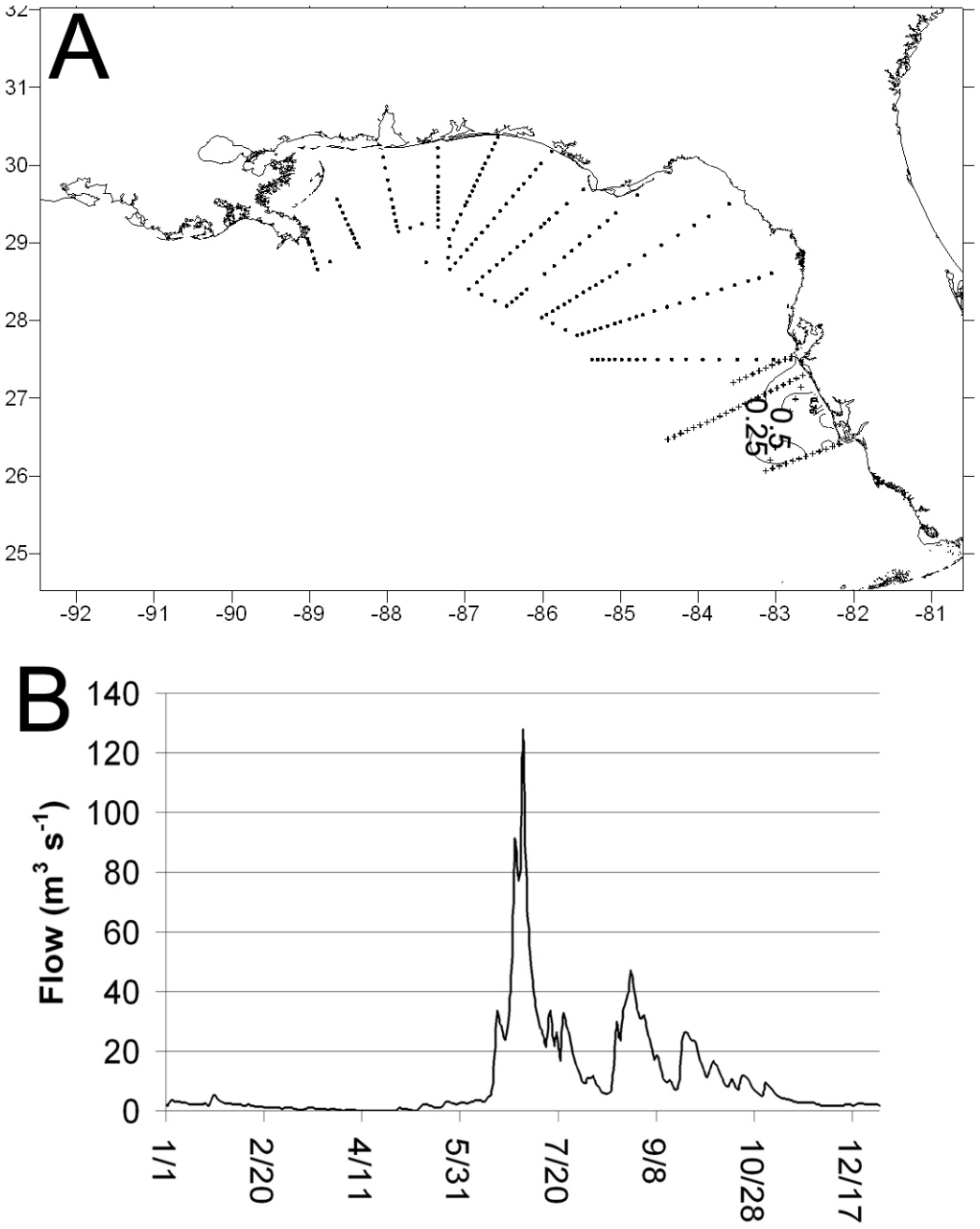

Figure 3. A) August 1999 surface phosphate concentrations (□mol/kg) in the eastern Gulf of Mexico during the NEGOM (□) and ECOHAB(+) cruises and B) the flow of the Peace river near Charlotte Harbour.

Another source of nutrients to the euphotic zone of the eastern Gulf of Mexico is the introduction of slope water due to upwelling events induced either by the intrusion of the Loop Current onto the continental shelf, and/or by local wind forcing. This phenomenon was observed in April 1982 (Paluskiewicz, *et al*., 1983) during a Loop Current frontal eddy intrusion onto the West Florida shelf where the 1.0 μmol kg^{-1} isopleth of nitrate+nitrite intersected the 60 m isobath. Similar observations were made in 1998 (Walsh *et al.*, 2003) after Loop Current water intruded (He and Weisberg, 2003) onto the outer shelf, coincident with upwelling favorable winds. The 1.0 μmol kg^{-1} isopleth of nitrate+nitrite and the 3.0 μmol kg^{-1} isopleth of silicate reached the 20 m isobath over much of the shelf (Figs. 4,5), in contrast to 1999 (Figs. 6 and 7), when the prevailing winds were not favorable for upwelling, and these isopleths were located in much deeper waters.

The Miocene facies of the Hawthorne phosphate deposit (Fig. 8) extend out onto the continental shelf approximately between Tarpon Springs, FL and Port Charlotte, FL (Ryder, 1985; Sinclair *et al.*, 1985), where they lie within a few meters of the sediment surface (Birdsall, 1977). Sediments off St. Petersburg Beach, FL have 3.4% phosphorite, while those off Venice, FL contain as much as 4.6% phosphorite (Bates, 1963). Such phosphorite percentages have been found in the sediments on the West Florida shelf past the 18 m isobath, with no significant amounts being found beyond approximately the 30 m isobath, thus providing a potential additional source of phosphate, to the shelf in that region.

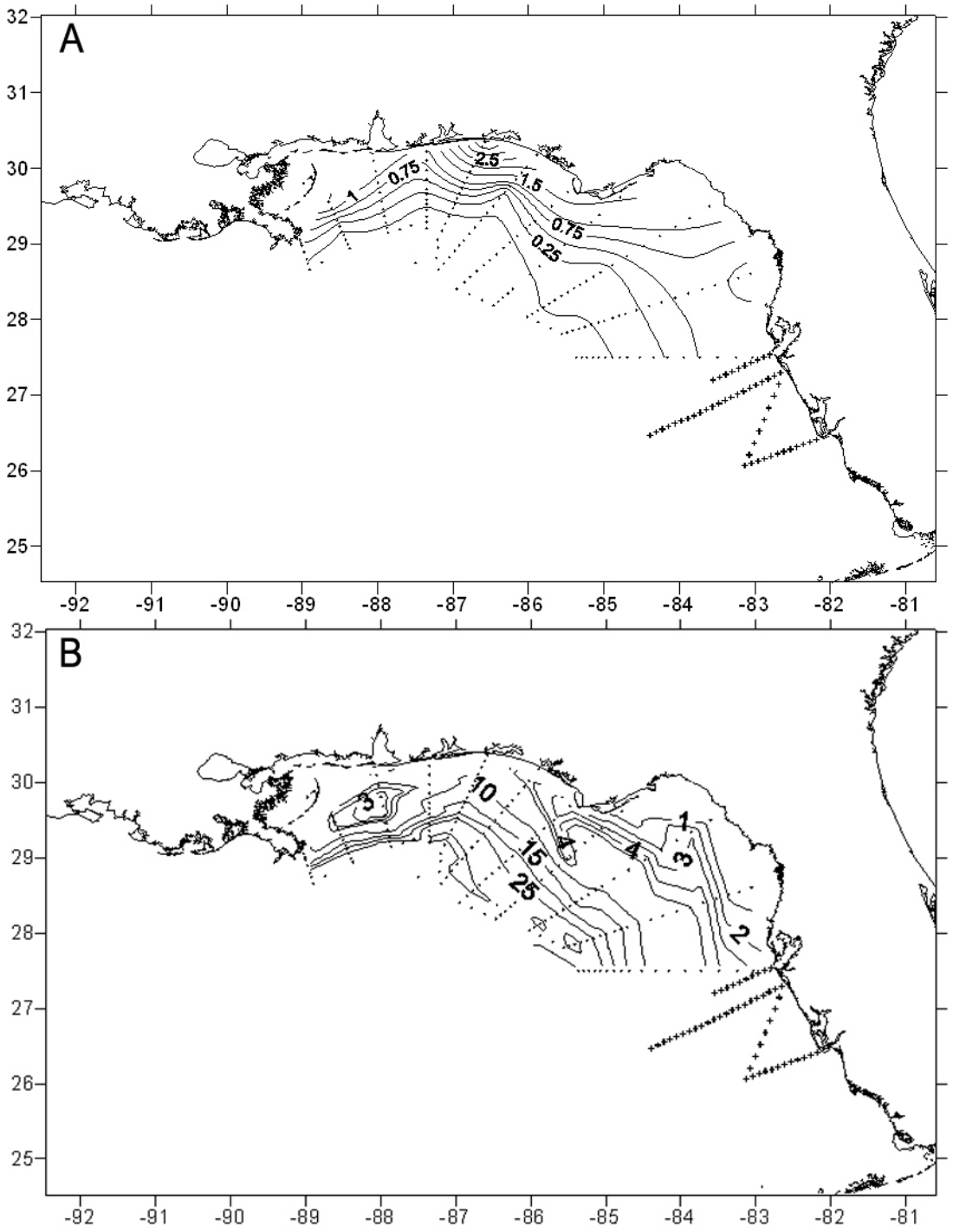

Figure 4. Near-bottom A) chlorophyll ($\mu g\ l^{-1}$) and B) $NO_2 + NO_3$ ($\mu mol\ kg^{-1}$) observations during the NEGOM (♦) cruise May 4-15 1998. ECOHAB cruise stations (+) are included for reference, but there were no ECOHAB observations during May 1998.

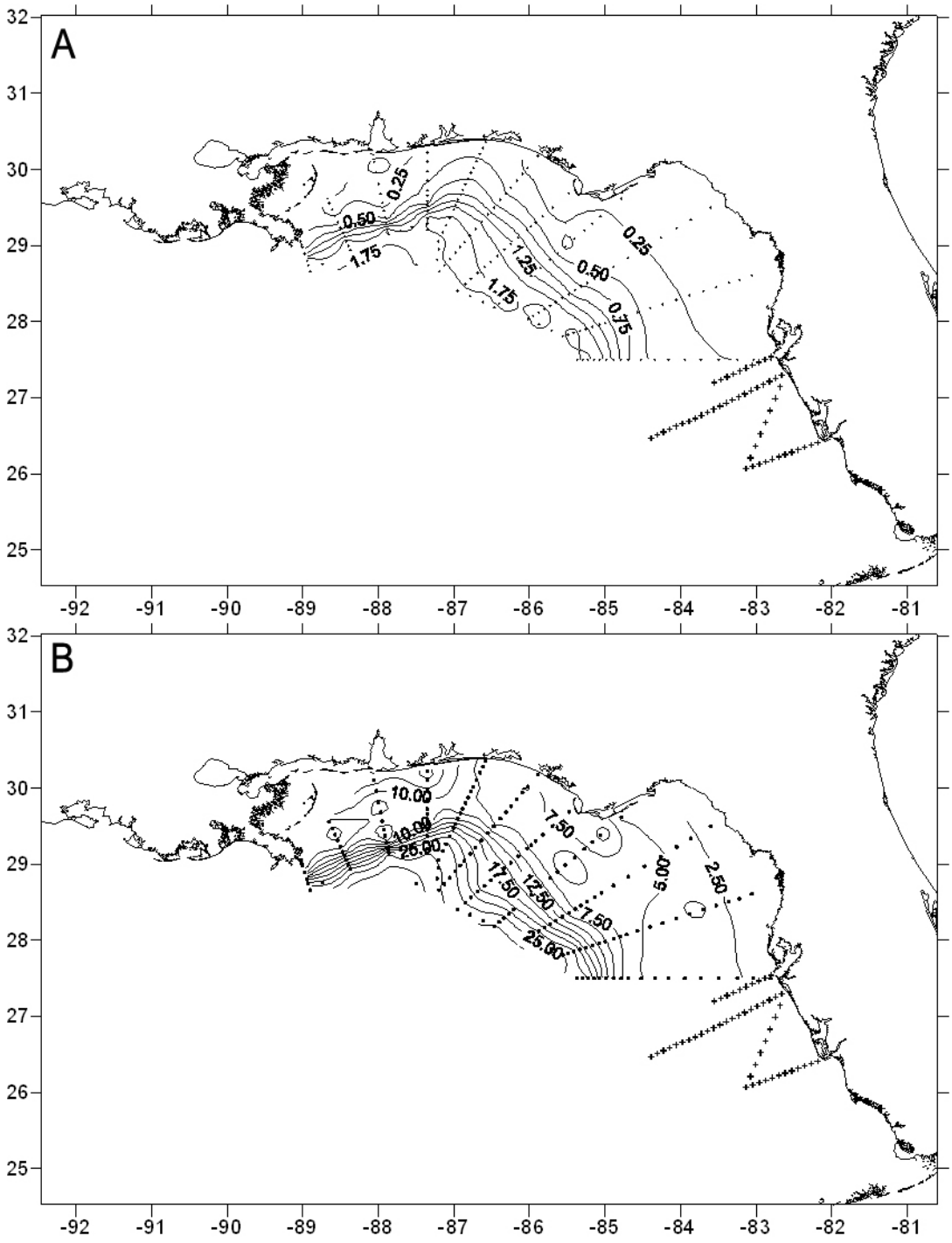

Figure 5. Near-bottom A) PO_4 (μmol kg^{-1}) and B) SiO_4 (μmol kg^{-1}) observations during the NEGOM (♦) cruise May 4-15 1998. ECOHAB cruise stations (+) are included for reference, but there were no ECOHAB observations during May 1998.

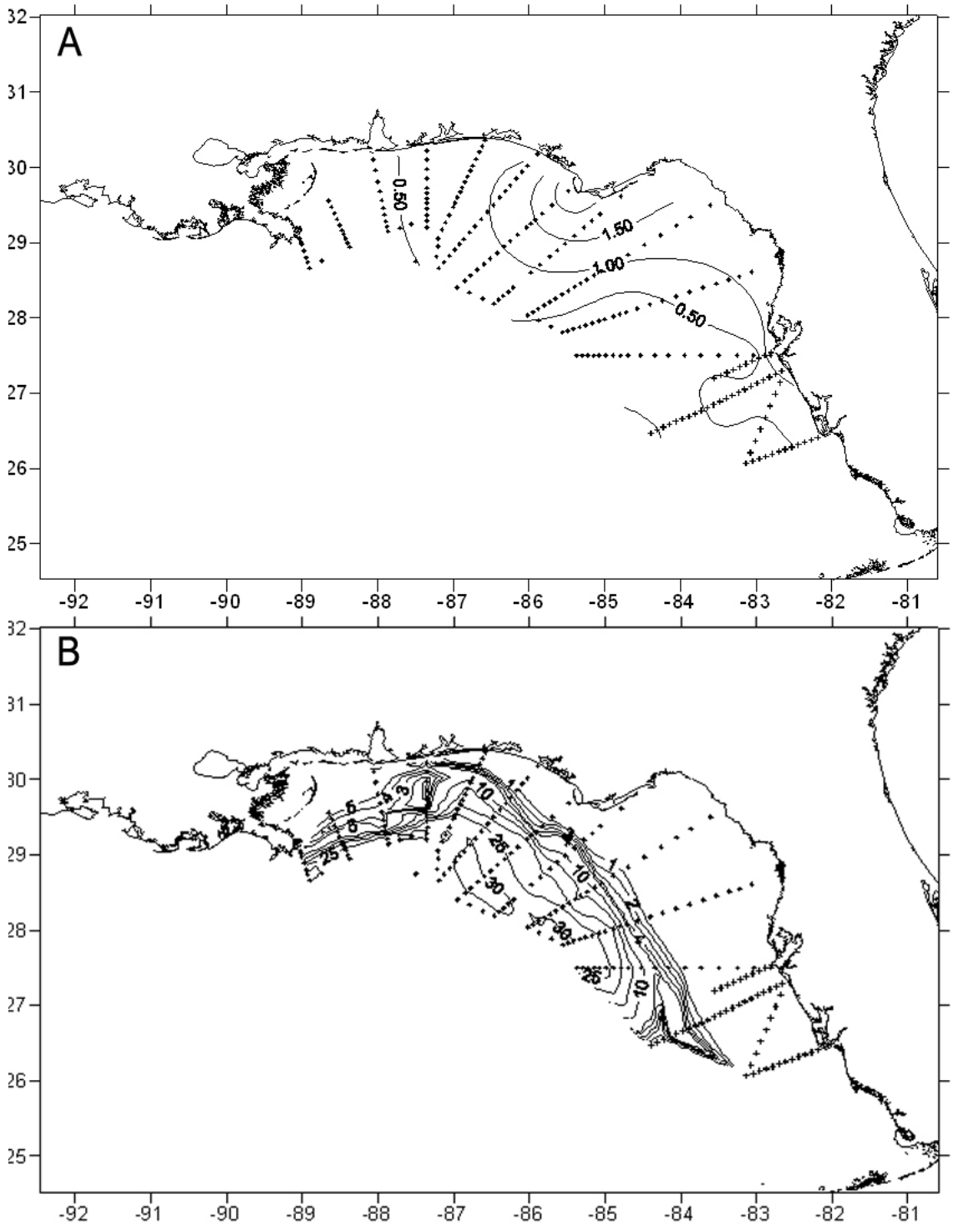

Figure 6. Near-bottom observations of A) chlorophyll ($\mu g\ l^{-1}$) and B) $N0_2+NO_3$ ($\mu mol\ kg^{-1}$) during the May 1999 NEGOM (♦) and ECOHAB (+) cruises.

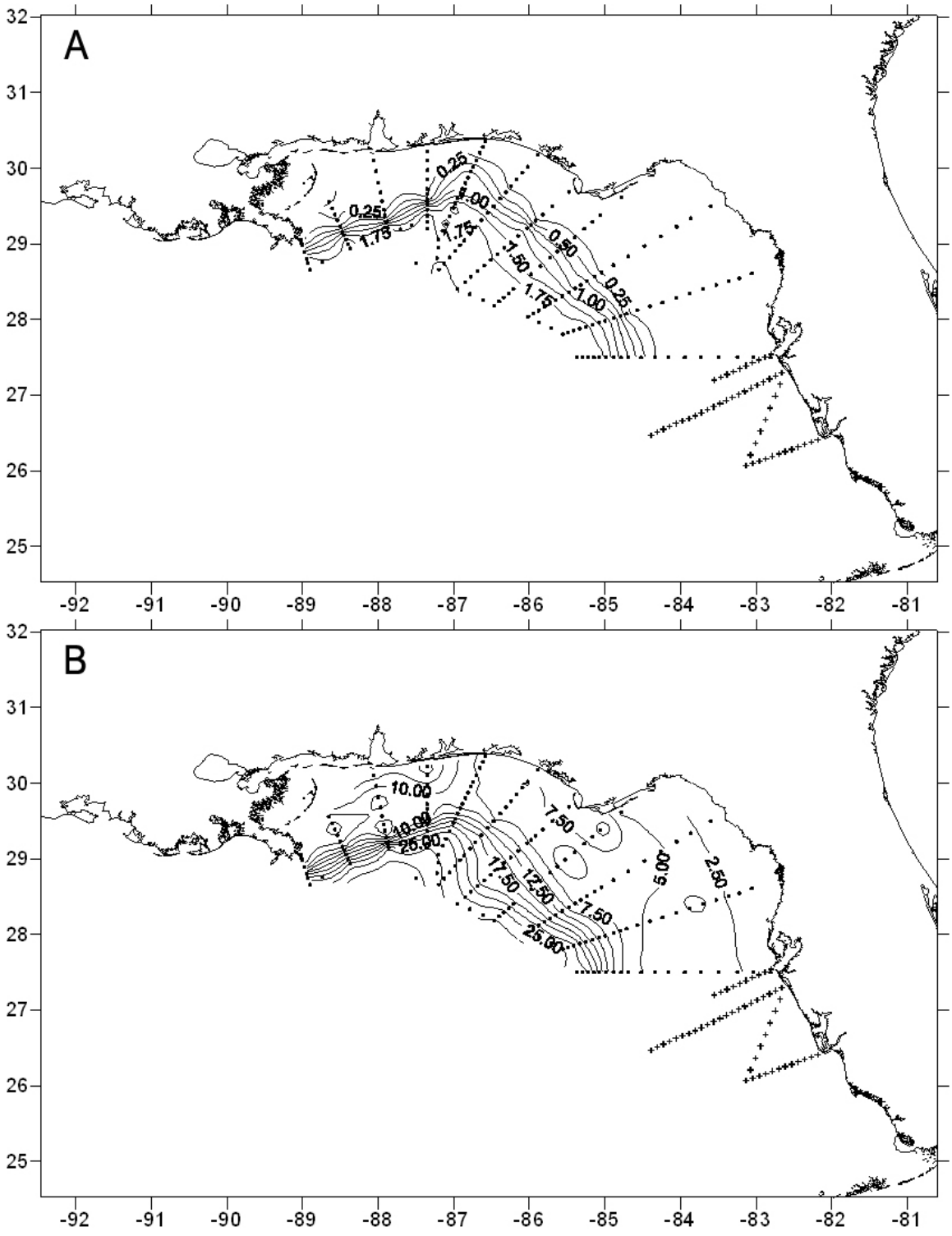

Figure 7. Near-bottom observations of A)PO_4 (μmol kg^{-1}) and B)SiO_4(μmol kg^{-1}) during the May 1999 NEGOM (♦) and ECOHAB (+) cruises.

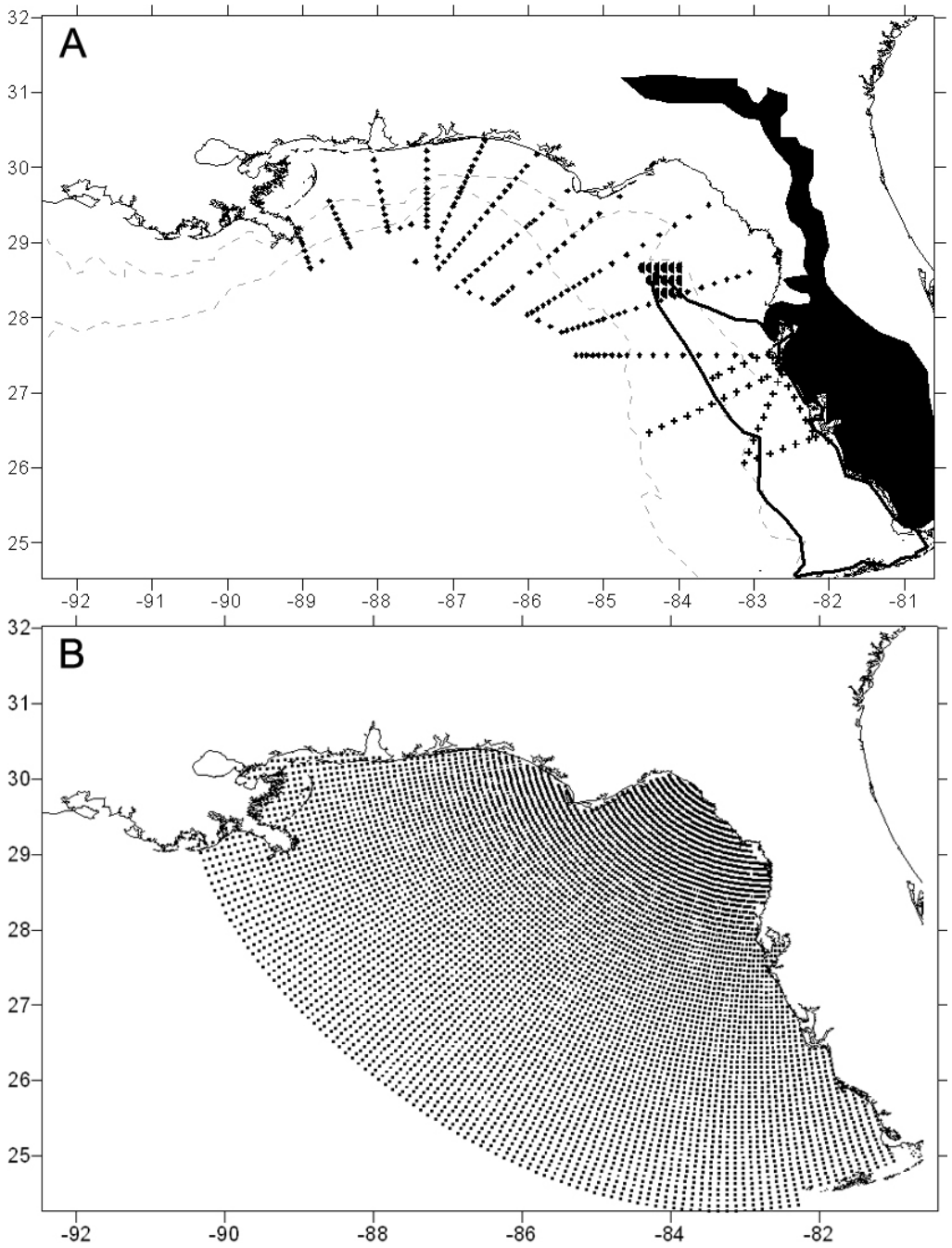

Figure 8. A) The land (shaded) and marine (—) extent of near-surface phosphate rich Miocene strata based on well cores (Bates, 1963) and sediment phosphorite percentages (Birdsall, 1977) relative to the 20 m and 200 m isobaths, the NEGOM (◆), ECOHAB(+), and ECOHAB Middle Grounds (◖) stations in the eastern Gulf of Mexico. B) The model grid.

Increased phosphorus, in relation to nitrogen, may thus be delivered to the euphotic zone in the eastern Gulf of Mexico in a number of ways. Phosphorus rich waters may be upwelled from outside the euphotic zone in the deep water of the Gulf of Mexico. Rivers, eroding the fossil phosphorus deposits of peninsular Florida may deliver phosphate in greater quantities, relative to nitrogen and silica, to the continental shelf than rivers along the northern Gulf coast. Likewise, porewaters overlying the underwater phosphate deposits may be a source of phosphate to the overlying water column. Finally, the faster turnover rate of phosporus relative to nitrogen (Darrow *et al*, 2003) may lead to decreased near-bottom N/P ratios following the decline of surface phytoplankton blooms. An understanding of these sediment related phosphorus delivery methods requires a more detailed consideration of the sediments than has been attempted in previous simulation analyses.

The ocean sediments have traditionally been regarded as an area where diffusion rules the transport of matter over minute spatial scales. While this idea still holds true in many parts of the ocean, studies primarily in continental shelf regions (Riedl *et al.*, 1972; Riedl and Machan, 1972) have shown that large areas of sediment, especially on the continental shelves, are highly permeable. Simply put, sediment permeability is the capacity of sediments to transmit fluid. Exchange of materials in the surface of high permeability sediments is typically dominated by advective processes in the pore-waters (Huettel and Gust, 1992) that often results in the upwelling of nutrient rich pore-water to the sediment surface (Huettel *et al.*, 1996). The coarse-grained carbonate and quartz sands

that dominate the eastern Gulf of Mexico sediments (Brooks, 1973) are characterized by such high permeabilities.

In addition to physical complexities, nutrient dynamics near the poorly understood sediment/water interface are further affected by benthic microalgae. Though previous simulation analyses (Darrow *et al.*, 2003) have included the microphytobenthos, a large scale study of their role in production and nutrient cycling in the eastern Gulf of Mexico has not yet been attempted. Although sediments in the South Atlantic Bight (SAB) are primarily quartz sediments, compared to mostly carbonate sediments on the WFS, the sediments of the two regions are characterized by similar permeabilities. Studies in the SAB have clearly shown that microphytobenthos are widespread across the continental shelf (Cahoon and Cooke, 1992; Cahoon *et al.*, 1990; Nelson *et al.*, 1999).

The microphytobenthos have been estimated to provide at least 10% of the primary production leading to the coastal fishery yield of the Atlantic coast of the United States from New York to Georgia (Mallin *et al.*, 1992). Benthic microalgae are a known food source for many different types of benthic macrofauna in shallow waters, including shrimp and other crustaceans (Miller *et al.*, 1996), some of which are of economic importance in the eastern Gulf of Mexico. Interactions of benthic microflora with the water column trophic structure have been demonstrated through multiple pathways (Thomas and Cahoon, 1993). The isotopic signature of benthic microalgae has been traced to fishes such as the tomtate (a type of grunt) and red porgy through demersal zooplankton (Bolden, 1990; Cahoon and Tronzo, 1992), and benthic

invertebrates (Manooch, 1977), respectively. Tomtate, specifically, have been found in the gut of the economically important Red Grouper in the Gulf of Mexico (Schirripa *et al.*, 1999) along with several species of crabs and other crustaceans (Moe, 1969).

In addition to their potentially important ecological role as primary producers in economically significant components of shelf ecosystems, benthic microalgae may play an important role as a particulate storage pool of nutrients on the continental shelf. Alteration of nutrient and oxygen fluxes across the sediment water interface due to benthic microalgae has been shown in the laboratory (Sundback and Graneli, 1988), in microecosystems (Admiraal, 1977), and in the field (Jahnke *et al.*, 2000).

Previous simulation analyses (Darrow *et al.*, 2003) suggested that a mechanism for the reduction of nutrient flux across the sediment/water interface might be the uptake of pore-water nutrients by the microphytobenthos. Consequently, lower concentrations of nutrients in the pore-waters, and thus, a smaller gradient across the interface, lead to less diffusion, assuming that bioturbation and other mixing processes remain the same. Benthic microalgae are also known to create biofilms (Miller *et al.*, 1996), which may trap nutrients in the sediments. On the other hand, increased benthic macrofaunal activity (Marinelli, 1992), due to the presence of the microalgal food source, may lead to increased bioturbation of the sediments, and therefore increased flux.

There may also be a profound impact on the water column upon the death of benthic flora, through grazing or through the mechanism of resuspension.

Experiments on estuarine sediments (De Jonge and Bergs, 1987; De Jonge and Beusekom, 1995) have shown significant wind and tidal resuspension of benthic diatoms. Furthermore, such sand movement can effectively pulverize the algal cells (Delgado *et al.*, 1991), causing them to lyse, and release their organic contents to the water column. Simple sediment resuspension models (Darrow, 2002) have shown that sediment suspension is possible on the West Florida shelf at the 30 m isobath, when significant wave height exceeds 3.5 m. The critical shear stress of the sediment layer may be exceeded even as deep as 70 m, under even rougher conditions.

The euphotic zone, designated by irradiance greater than 1% of the surface irradiance, extends to the bottom over much of the continental shelf in the eastern Gulf of Mexico (Fig. 9). It is greatest on the oligotrophic West Florida shelf where the percentage of surface irradiance reaching the bottom is greater than 25% in some locations (Fig. 9) and the 1% light level can extend past the 100 m isobath (Joyce and Williams, 1969).

Though no extensive studies have occurred, benthic microflora have been observed on the West Florida shelf in 1992 and 1993 (Figs. 10,11). They were studied more recently during ECOHAB middle grounds cruises in July and August, 2000, and by Jim Nelson and Charles Robertson off central Florida in November 2001 (Table 1).

Table 1. Average chlorophyll (mg m^{-2}) stocks integrated over the top 0.5 cm of sediment on the West Florida shelf during 2000-2001 (Nov-01 benthic data courtesy of Jim Nelson and Charles Robertson)

Date	Water-column	Sediments	# Stations
Jul-00	14.6	5.4	15
Aug-00	15.3	21.0	15
Nov-01	16.3	15.8	3

.

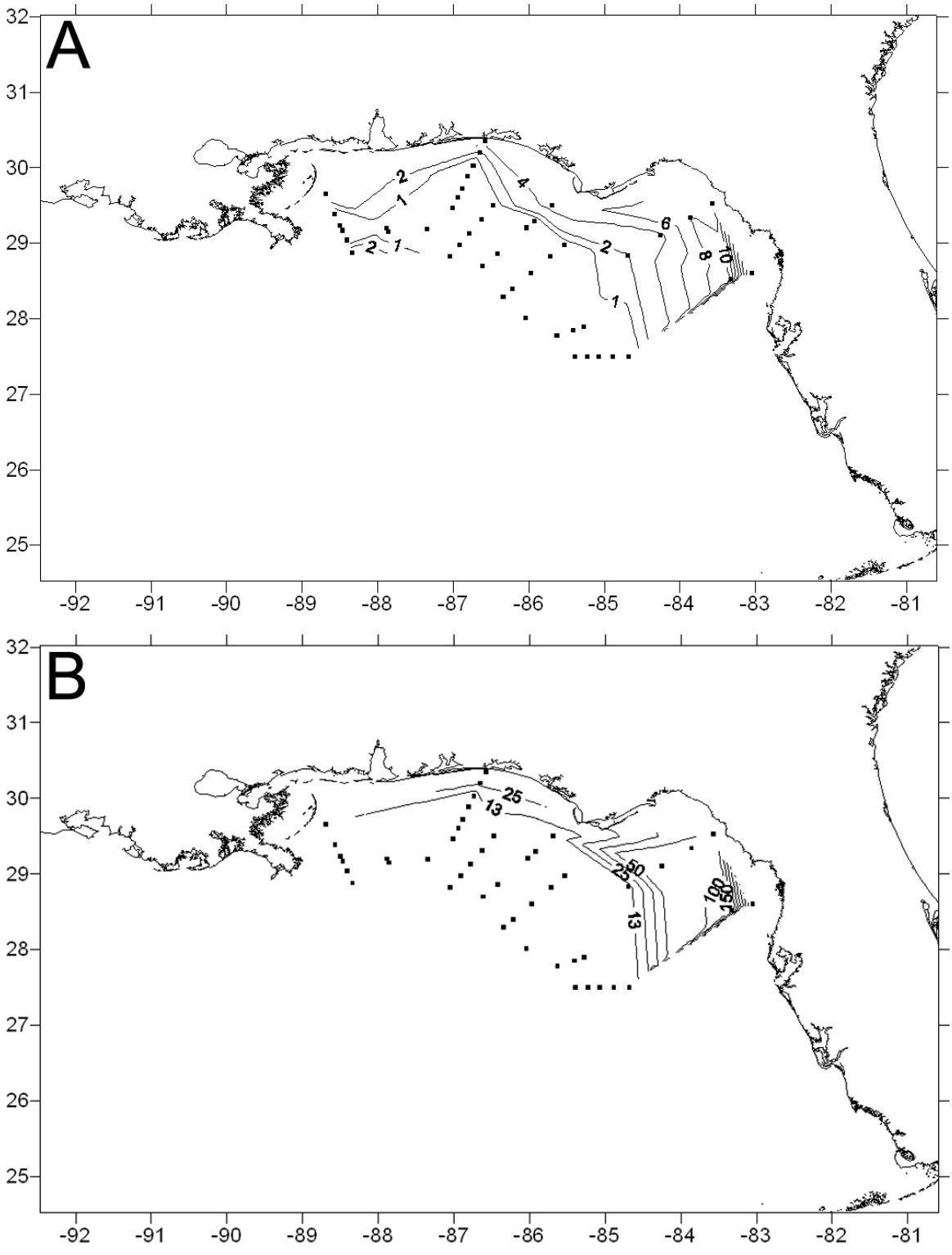

Figure 9. The observed A) percentage of surface PAR and B) total PAR ($\mu E\ m^{-2}\ s^{-1}$) reaching the ocean floor during the NEGOM cruise July 25 – August 9, 1998.

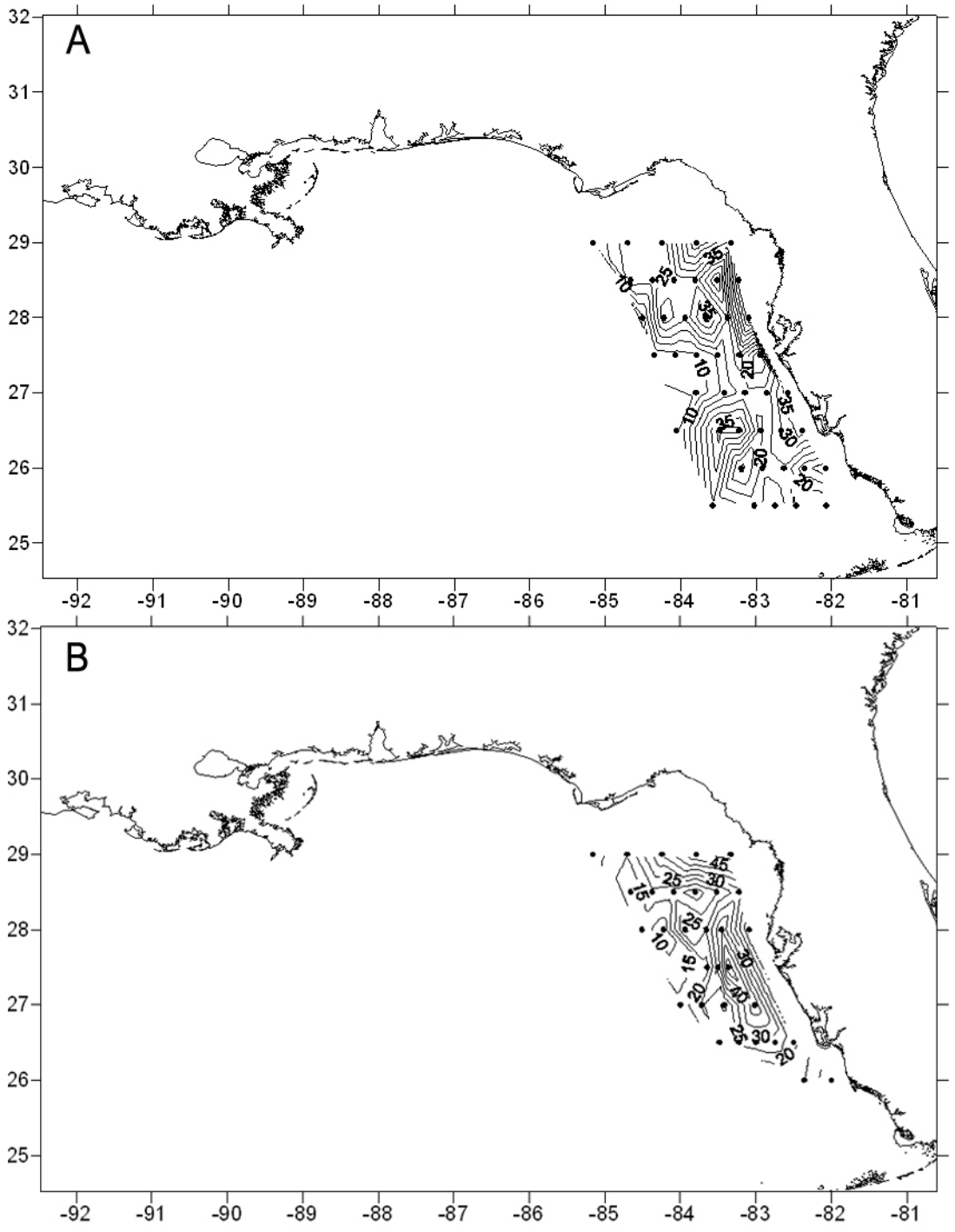

Figure 10. Observed benthic chlorophyll stocks (mg m^{-2}) integrated over the top 0.5 cm of sediment in A) July 1992, B) October 1992 during the Coastal Production (●) cruises.

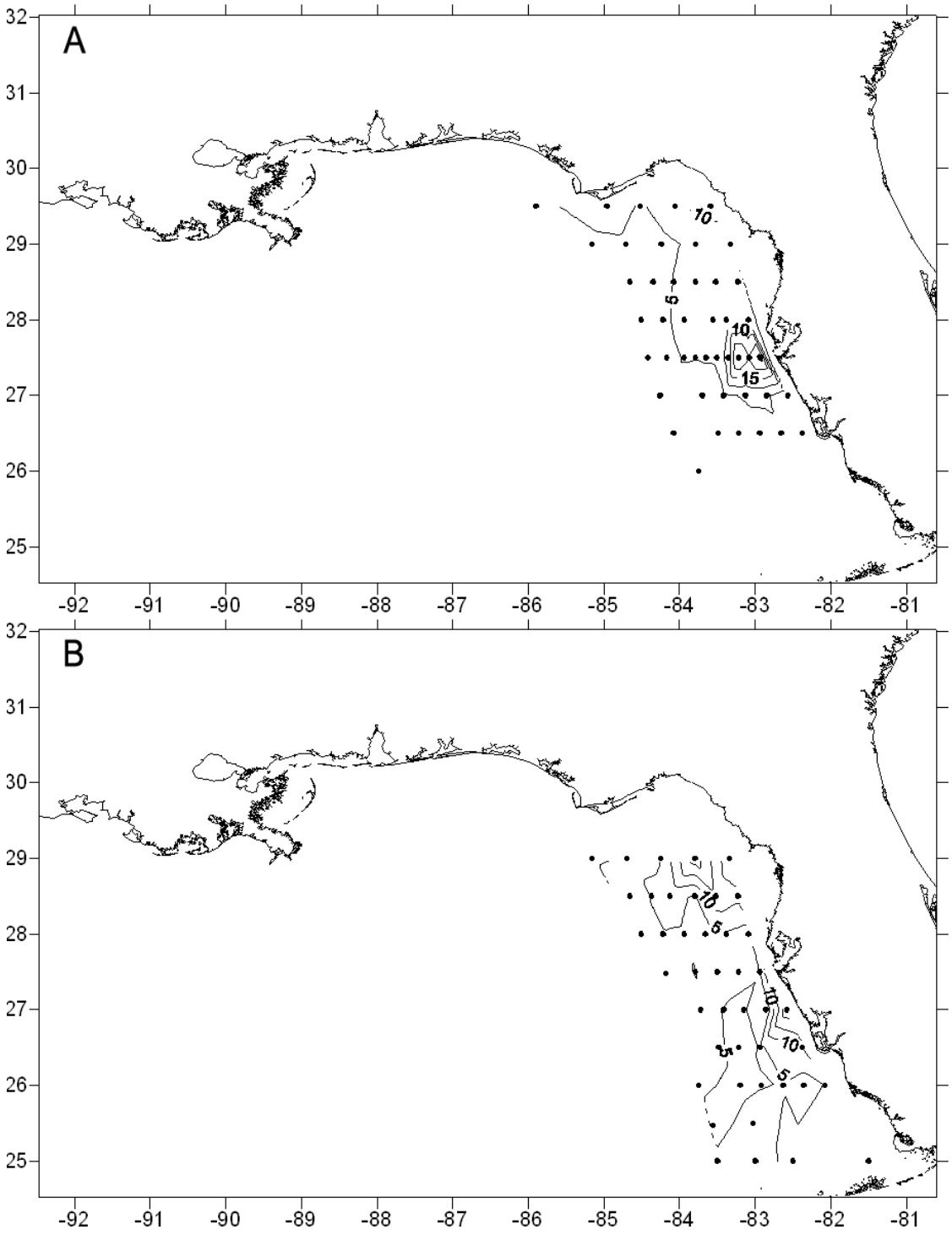

Figure 11. Observed benthic chlorophyll stocks (mg m^{-2}) integrated over the top 0.5 cm of sediment in A) April 1993, B) August 1993 during the Coastal Production (●) cruises.

Given that average observed benthic chlorophyll stocks vary from 5.4 mg m^{-2} to 30 mg m^{-2} during the seven months of available measurements, one might wonder what factors lead to high chlorophyll concentrations vs. low ones. Light is certainly a factor. Previous analyses (Darrow *et al.*, 2003) showed that benthic photosynthesis is reduced on cloudy days. Field observations (Jahnke *et al.*, 2000) in benthic chambers indicate a significant correlation between light flux to the bottom and benthic primary production when average benthic PAR flux is less than 83.3 $\mu E\ m^{-2}\ s^{-1}$. In some areas of the eastern Gulf of Mexico, however, the benthic PAR flux exceeds 83.3 $\mu E\ m^{-2}\ s^{-1}$ (Fig. 9). Given the generally oligotrophic conditions (Masserini & Fanning, 2000) and episodic nutrient enhancements (Gilbes et al, 1996; Fig. 3, Fig. 4), one might expect nutrient limitation to also play a role in benthic primary production.

Benthic macroalgae and seagrasses can also be important producers on the continental shelf. Although growing specimens of macroalgae have been found at depths as great as 400 m (Humm, 1957), these producers are most dominant nearshore in waters of less than 10 m depth (El-Sayed *et al.*, 1972; Iverson and Bittaker, 1986).

Although the growth and production of benthic microflora is important in terms of total community production and fishery yield on continental shelves, the mechanisms of their death and decline deserve equal attention in terms of nutrient recycling to the water column. Previous studies in the northeastern Gulf of Mexico (Fanning *et al.*, 1982) indicate that the resuspension of as little as 1

mm of organic rich sediment could enhance productivity in the water-column by as much as 200% in areas influenced by the Mississippi and Mobile rivers. A simple simulation analysis (Darrow, 2002) calculated that integrated water column primary production could be briefly enhanced by ~225 mg C m^{-2} day^{-1} upon suspension and lysis of a population of benthic diatoms living in carbonate sands of otherwise poor organic content on the West Florida shelf.

During fall overturn, such resuspension and lysis of benthic microflora could be a nutrient source for phytoplankton in the water column like *K. brevis*. If the biotic remineralization of organic matter from the suspended benthos outpaces the dissolution of silica, the slow growing dinoflagellates could outcompete the faster diatoms. Suspended organic and lithogenic particles would also attenuate light for the shade adapted *K. brevis* (Millie *et al.*, 1995), giving it a further competitive advantage.

This three-dimensional simulation analysis assesses the role of two water-column nutrient sources (upwelled deepwater nutrients and recycled nutrients from a dying phytoplankton bloom) in the growth of benthic microalgae living in the high permeability sediments of the eastern Gulf of Mexico. Using two cases of the simulation, the hypothesis that water column nutrients play a significant role in the growth of benthic microalgae is tested. The role of upwelled nutrients with and without the addition of fallout from a surface phytoplankton bloom is tested within the framework of the spring and summer 1998 physical conditions in the eastern Gulf of Mexico.

Methods

1. Transport Model

1.1 Pelagic Transport

Advective transport (Tr_a) in the water column is described by:

$$Tr_a(dQ) = -\frac{\left[\frac{\partial}{\partial\xi}(h_2 udQ) + \frac{\partial}{\partial\varsigma}(h_1 vdQ) + h_1 h_2 \frac{\partial}{\partial\sigma}(\omega Q)\right]}{h_1 h_2} \quad (1a)$$

where Q represents any particular state variable to which the transport applies, ξ is the horizontal curvilinear coordinate in the cross shore direction, ζ is the horizontal curvilinear coordinate in the alongshore direction, σ is the depth dependent vertical coordinate, h_1 and h_2 are the length of the grid box in the x and y directions respectively, and u, v and ω represent the velocities in the x,y and z directions taken from a circulation model of the West Florida Shelf (Weisberg & He, 2003) adapted from the (POM) Princeton Ocean Model (Blumberg & Mellor, 1987).

Strong horizontal diffusion is implicit in the numerical algorithm for advective transport (Blumberg & Mellor, 1987), such that explicit horizontal turbulent mixing is ignored and only the vertical component of diffusive transport (Tr_d) is modeled:

$$\mathrm{Tr_d(dQ)} = \frac{\partial}{\partial \sigma}\left(\frac{\mathrm{K_h}}{\mathrm{d}}\frac{\partial \mathrm{Q}}{\partial \sigma}\right) \tag{1b}$$

where K_h is the coefficient of vertical eddy diffusivity derived from a second moment turbulence closure submodel (Mellor and Yamada, 1982) embedded within the circulation model. Total transport (Tr_b) is then the sum of Tr_a and Tr_d in the water column.

1.2 Benthic Transport

Processes in the sediment occur over millimeter scales. The present application of these processes to a kilometer scale model thus requires some approximations. Nonlocal exchange models (Boudreau, 1997) have been employed to approximate enhanced exchange of dissolved species due to pore-water irrigation by benthic macrofauna:

$$NLE = \alpha\phi(C_0 - C) \tag{2}$$

where NLE represents non-local exchange (μmol m^{-3}), α is the non-local exchange parameter (Boudreau, 1997), ϕ is the sediment porosity, C_0 is the concentration of the chemical species being exchanged in the overlying water, and C is pore water the concentration of that species in the sediment layer in question.

The non-local exchange formulation is used in the present simulation to approximate advective porewater exchange within the sediments. Advective porewater exchange is the result of pressure perturbations caused by the irregular flow of water over obstructions (modeled as sediment ripples) on the sediment surface. The maximum pressure perturbation (P_{max}) can be determined as:

$$P_{\max} = 0.14\rho u^2 (\frac{\delta}{0.34H})^{3/8} \quad (3)$$

where ρ is the density of the water, u is the mean current velocity over the ripple, δ is the ripple height and H is the depth of the water (Huettel & Gust, 1992). The mean current velocity is calculated from the near-bottom flow fields of a circulation model of the eastern Gulf of Mexico (He & Weisberg, 2003). The density of the water is calculated from the near-bottom temperature and salinity calculations of the same circulation model. The depth of the water column is dynamically calculated based on the bathymetry and the sea surface height of the circulation model at each time step. The ripple height is calculated from a sediment transport model (Li & Amos, 1995). Wave data for the sediment

transport model was obtained from 1998 NOAA buoy data in the eastern Gulf of Mexico.

From the maximum pressure perturbation, the porewater flow (W_0) can be calculated by:

$$W_0 = \left(\frac{2k}{\rho \nu L_D}\right) P_{max} \quad (4)$$

where ν is the kinematic viscosity of the fluid (obtained from the circulation model), L_D is the ripple wavelength (calculated by the sediment transport model), and k is the sediment permeability. The sediment permeability is calculated by:

$$k = \frac{\left(5.6x10^{-3}\phi^3 d_s^2\right)}{\left(1-\phi\right)^2} \quad (5)$$

where ϕ is again the sediment porosity and d_s is the mean sediment grain diameter (Boudreau, 1997). Both parameters were obtained from Gulf of Mexico observations in the usSEABED (Reid, *et al.*, 2001) database. Permeabilities were calculated for the sediments underlying each point on the horizontal grid (Fig. 8B). Equation 5 is known to be inaccurate in areas where porosity is greater than 0.8 (Boudreau, 1997). Therefore, at points where sediment porosity was greater than 0.8 according to the usSEABED database, sediment permeability was assumed to be 1.0 x 10^{-14} cm^2.

The non-local exchange parameter (α) at the surface sediment layer can then be determined from:

$$\alpha_0 = \frac{2W_0}{h_0} \quad (6)$$

Where W_0 is again the porewater flow, and h_0 is the thickness of the surface sediment layer, assumed to be 2 mm in this model. The non-local exchange parameter decays exponentially in the sediment on the length scale of the wavelength of the sediment ripple (Boudreau, 1997).

In order to test the non-local exchange approximation for porewater advection in the sediments without interference from biochemical processes, a simulation case considered only the physical factors affecting a single tracer in the sediments and the overlying water-column. Concentrations of the tracer in the bottom layer of sediments in this "tracer case" were set to 1000 mmol kg^{-1} at randomly chosen points within three pre-determined regions of the model grid – the northern Gulf coast, the West Florida shelf and the continental slope off the west coast of Florida (Fig. 12). These concentrations were held constant over a 90 day model run from February 27 to May 28 1998. The model was run twice. One run considered diffusion only and a second run used diffusion and the non-local exchange (NLE) approximation.

Under these conditions, molecular diffusion would tend to produce a linear profile of the tracer in the sediments (Fig 13A) since the concentration of the deepest layer is held constant at 1000 mmol m^{-2}. The concentration of tracer in

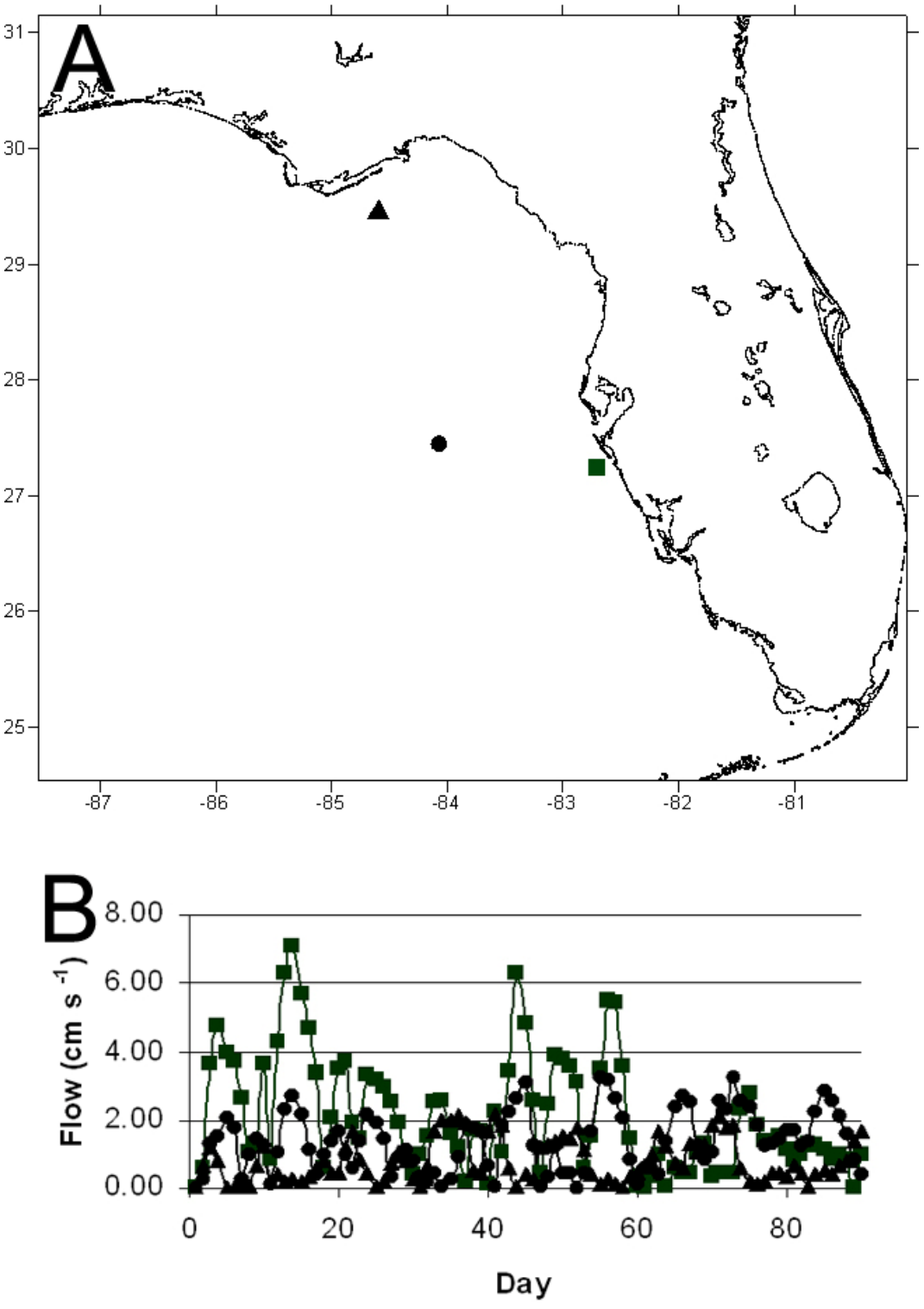

Figure 12. Geographical locations of (A) site 1(■), site 2(●) and site 3(▲)of the "tracer case" of the model, along with the flow (B) at those locations over time.

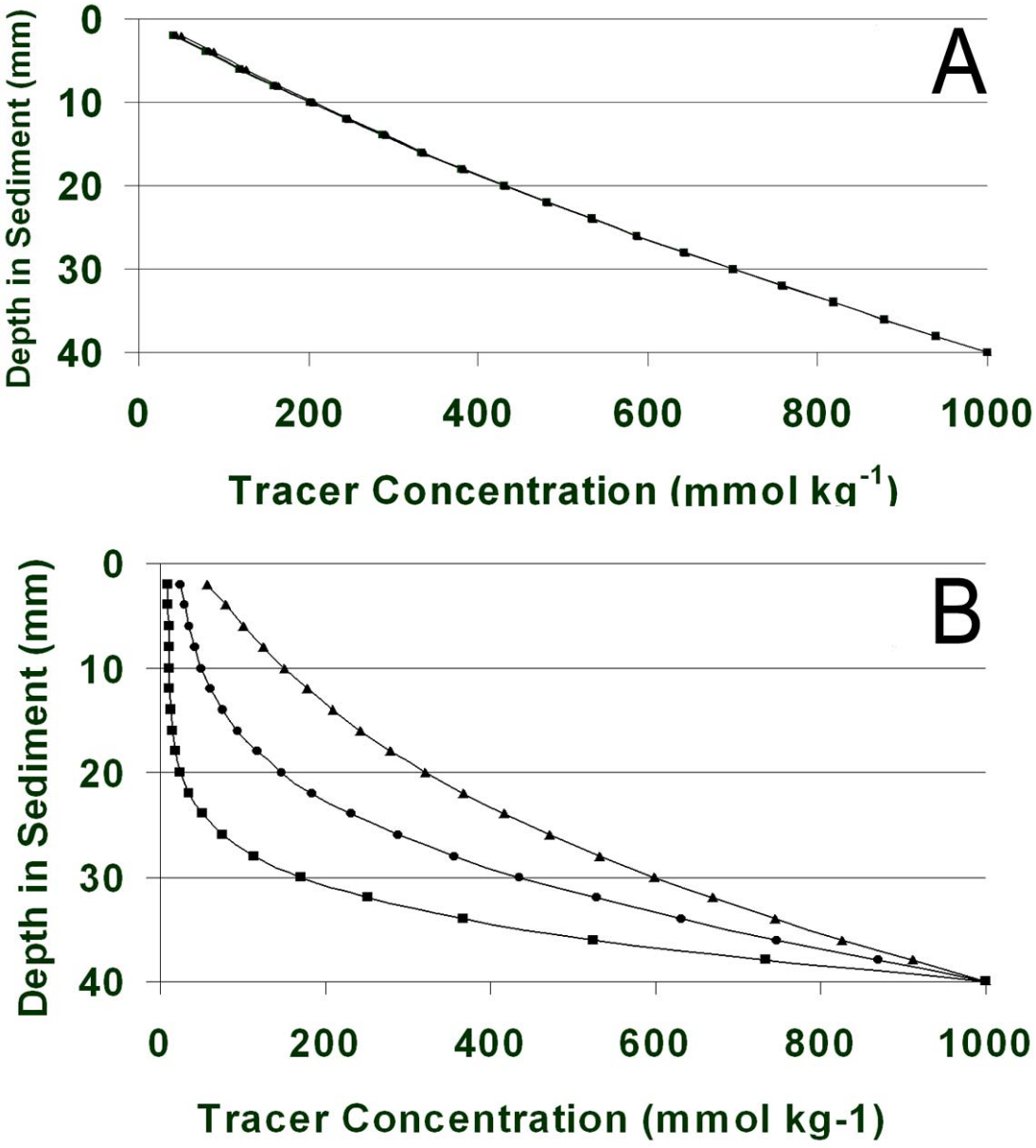

Figure 13. Sediment profiles of tracer at stations 1 (■), 2(●), and 3(▲) during 17 March 1998 (day 18) of A) the diffusion only tracer case and B) the NLE tracer case of the model.

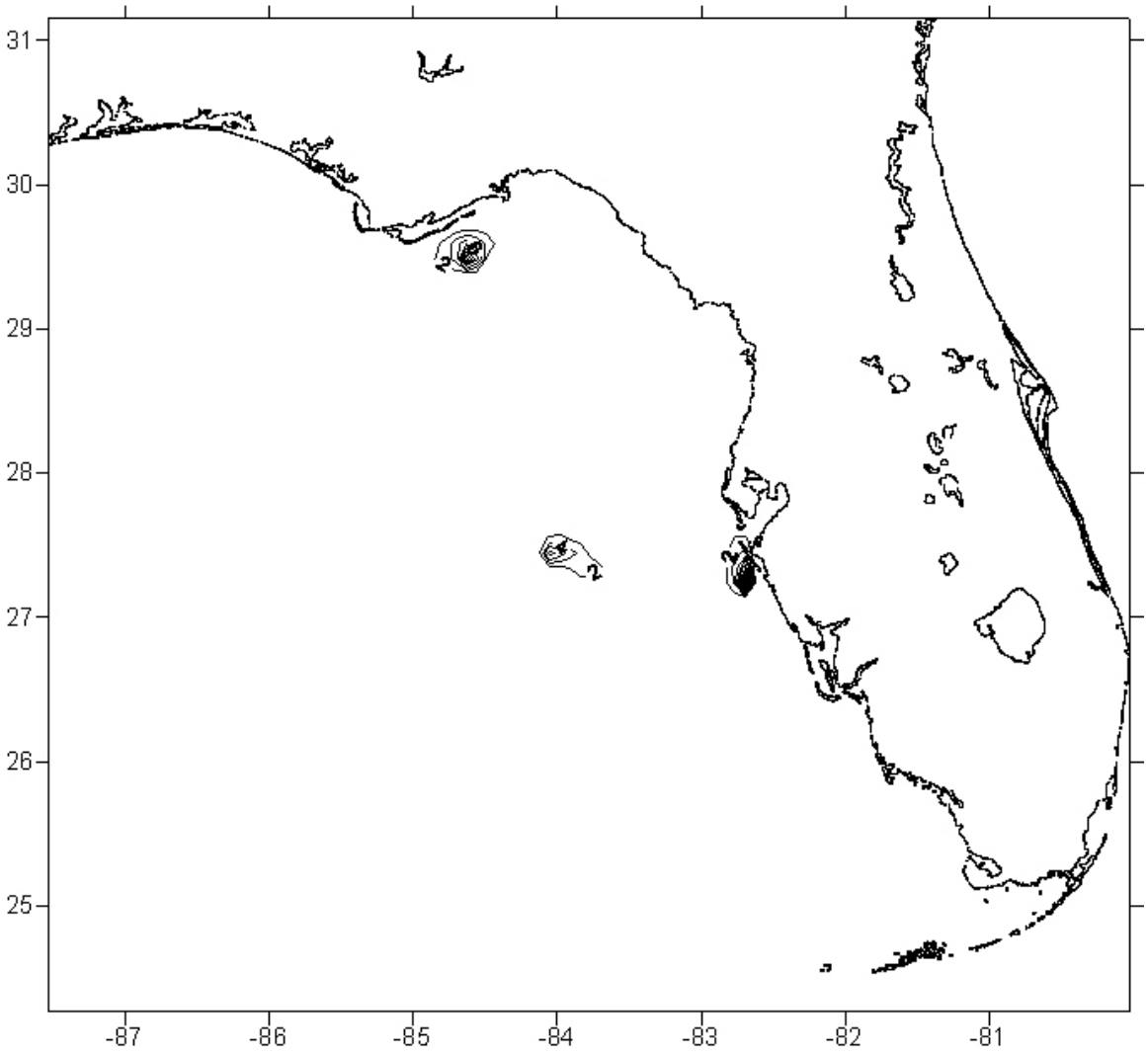

Figure 14. Tracer concentration (mmol kg^{-1}) in the near-bottom water during 17 March 1998 (day 18) of the NLE tracer case of the model.

tracer at sites 1 and 2 (Fig. 14B)

the water column is almost constant at near zero because the tracer diffusing out of the sediment is flushed away by the currents. At site 3, where the simulated near-bottom flow was relatively slow compared to sites 1 and 2 (Fig. 12b), the profile of tracer in the sediment was nearly linear by day 18 of the simulation (Fig 13b). In contrast, comparatively swift near-bottom flow at site 1 resulted in greater flushing of the surface sediments at sites 1 and 2. The vertical profile of tracer at sites 1 and 2 (Fig. 14B) is similar to those observed by Jahnke et al. (2000) under similar flow conditions on the South Atlantic Bight.

In the days leading up to day 54 of the simulation in April 1998, flow over site 1 was somewhat reduced (Fig. 12B), relative to early in the simulation. As a result, the surface sediments were not flushed to the extent they were on day 18 (Fig. 15B). Flow at site 2 had increased somewhat, however leading to increased flushing of the surface sediments there (Fig. 15B). The near-bottom tracer at the offshore site 2 moved shoreward, while the near-bottom tracer at sites 1 and 3 moved cyclonically around the eastern Gulf of Mexico against the coastline (Fig. 15A).

By day 90, flow over all three sites had slowed to less than 2 cm s^{-1} (Fig 12B). As a result, sediment profiles at all three sites were similar (Fig 16). Flushing of the surface sediment was minimal compared to that at station 1 on day 18 (Fig. 14B).

Calculated “non-local” exchange rates at the sediment/water interface in the model ranged from 0 day^{-1} to 3 day^{-1}, and were consistent with previous estimates (Jahnke *et al* 2005) of non-local exchange rates required to produce

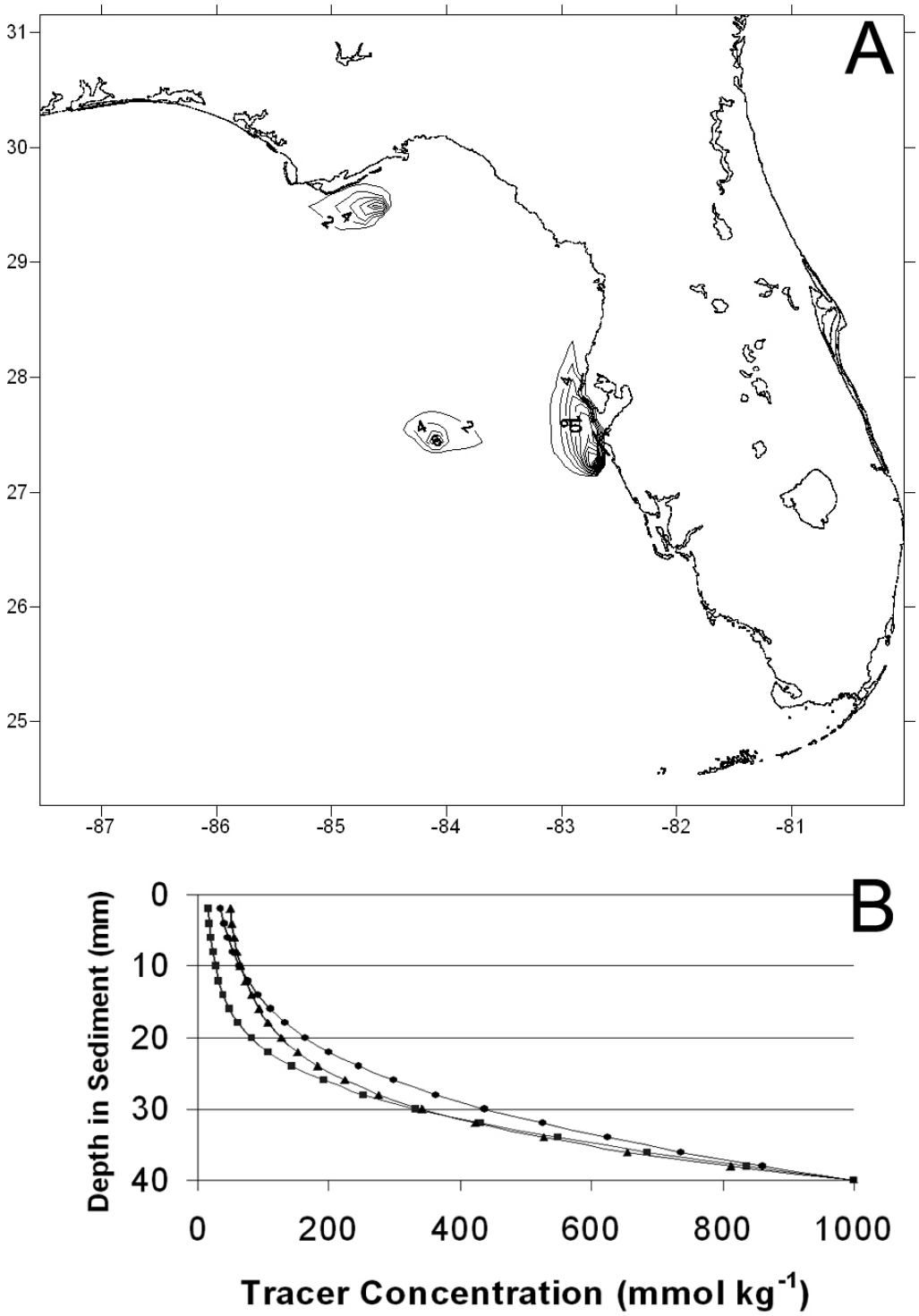

Figure 15. A) Concentration of tracer in the near-bottom water (mmol kg^{-1}) and B) sediment profiles of tracer at stations 1 (■), 2(●), and 3(▲) during 22 April 1998 (day 54) of NLE tracer case of the model.

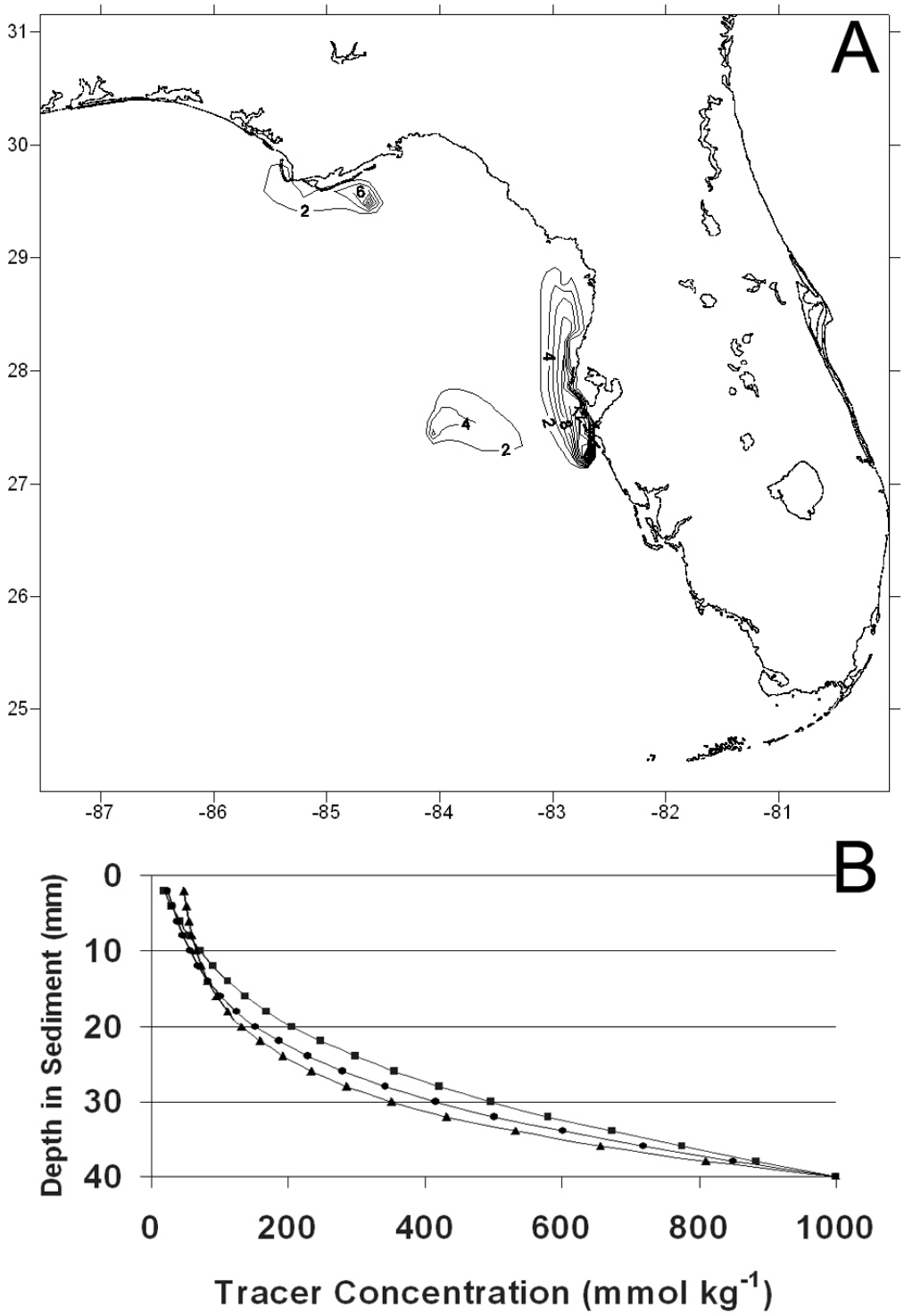

Figure 16. A) Concentration of tracer in the near-bottom water (mmol kg^{-1}) and B) sediment profiles of tracer at stations 1 (■), 2(●), and 3(▲) during 28 May 1998 (day 90) of the NLE tracer case of the model.

the sediment profiles of observed nutrients on the SAB. As such, the sediment transport model is assumed to be a suitable approximation of pore-water advection processes in permeable continental shelf sediment environments such as those on the South Atlantic Bight and the West Florida shelf.

1.3 Optics

In almost every ecological system, light plays a key role in primary production. Particularly in light limited benthic habitats, small changes in PAR flux through the water column can alter benthic light flux significantly and can therefore determine the growth of algae living there. Thus, a detailed light model is employed to simulate the dynamics of the benthic and pelagic microalgae in the ecological simulation. In this case, a spectral solar irradiance model (Gregg and Carder, 1990) is corrected for cloud cover, and used to derive solar irradiance at 8 visible spectral wavelength integrals just below the ocean surface ($I_{0(\lambda)}$), thus representing photosynthetically active radiation (PAR) in distinct 25 nm bands. Although smaller bands might result in a more detailed determination of the light field, the 25 nm bands represent a compromise between a detailed determination of PAR at depth vs. the computation time of the model.

Within the water column, light energy is absorbed and scattered by the water itself, algae, and colored dissolved organic matter (Kirk, 1995) as well as non-living particulate matter (detritus) and bacteria (Nelson and Robertson, 1993). In addition, to the above factors, light is scattered and absorbed by

sediment particles as it travels through the benthos. These processes account for the attenuation of spectral irradiance as it travels through the ecosystem. Spectral irradiance at a given depth, z ($I_{z(\lambda)}$), was calculated according to Beer's law of exponential decay:

$$I_{z(\lambda)} = I_{0(\lambda)} e^{-k_\lambda z} \tag{7}$$

where λ denotes the wavelength of interest, and k_λ is an attenuation coefficient described by,

$$k_\lambda = \frac{k_{w(\lambda)} + \sum\{k_{Q(\lambda)} \int_0^z Q(z)dz\}}{z} + \frac{k_{s(\lambda)} + \sum\{k_{Q(\lambda)} \int_z^h Q(h)dh\}}{h} \tag{7a}$$

The second term of equation 7a applies only to the benthos and Q now represents pelagic diatoms (P_1), and pelagic microflagellates (P_2) in the first term, benthic diatoms (P_3) in the second term, and detritus (D), bacteria (B), and CDOM in both terms. Their specific attenuation coefficients ($k_{Q(③)}$) are then represented by $k_{P1(\lambda)}$, $k_{P2(\lambda)}$, $k_{P3(\lambda)}$, $k_{D(\lambda)}$, $k_{B(\lambda)}$, and $k_{C(\lambda)}$, respectively. The specific attenuation coefficients of water and wet sandy sediment are respectively $k_{w(\lambda)}$ and $k_{s(\lambda)}$.

The specific attenuation coefficients at each wavelength for each parameter are determined from published values. In the case of the wet, sandy sediments (Kuhl and Jorgensen, 1994) and water (Pope and Fry, 1997; Smith

and Baker, 1981), total attenuation coefficients at each spectral wavelength are known. Due to the dissolved nature of CDOM, backscattering is ignored in the present model (Gordon *et al.*, 1988) and attenuation coefficients for CDOM are equal to published CDOM absorption coefficients in the eastern Gulf of Mexico(Carder *et al.*, 1989). Attenuation coefficients for phytoplankton, benthic microalgae (Bidigare *et al.*, 1990), bacteria (Morel and Ahn, 1990) and detritus (Roesler *et al.*, 1989) are, instead, equal to the sum of the wavelength specific absorption coefficients and the corresponding scattering coefficients.

2. Biological Model

2.1 Primary Producers

Fueled by light energy, and nutrient fertilization the dynamics of the three functional groups of microalgae are modeled. The processes affecting the rate of change with time (t) for the pelagic diatoms (P_1) and microflagellates (P_2) are described by:

$$\frac{\partial dP_1}{\partial t} = Tr_t(dP_1) - \frac{\partial}{\partial \sigma}(w_1 P_1) + dg_1 P_1 - d\gamma_1 P_1 - d\varepsilon_1 P_1 - d\psi_1 P_1 - dl_1 P_1 \quad (8)$$

$$\frac{\partial dP_2}{\partial t} = Tr_t(dP_2) + dg_2 P_2 - d\gamma_2 P_2 - d\varepsilon_2 P_2 - d\psi_2 P_2 - dl_2 P_2 \quad (9)$$

where w_1 represents the sinking rate of the pelagic diatoms. The terms, g_n, ε_n, ψ_n, γ_n and l_n represent the respective growth, respiration, excretion, grazing and lysis rates of the pelagic microalgae.

The benthic diatoms (P_3) are described by:

$$\frac{\partial hP_3}{\partial t} = Tr_t(hP_3) + hP_3(g_3 + \varepsilon_3 - \psi_3 - \gamma_3 - l_3) \tag{10}$$

where g_3, ε_3, ψ_3, $\gamma_{3,\text{ and }} l_3$ are, again, the growth, respiration, excretion, grazing and lysis rates of the benthic diatoms.

The specific biological rates, g_n expand to non-linear, time dependent expressions,

$$g_{1,3} = [\mu_{1,3}]\begin{bmatrix} \min\left(I_z / I_{sat}\, e^{(1-Iz/Isat(1,3))}\right), \left(NO_3 / \{k_{NO3(1,3)} + NO_3\}\right), \\ \text{or}\left(NH_4 / \{k_{NH4(1,3)} + NH_4\}\right), \left(PO_4 / \{k_{PO4(1,3)} + PO_4\}\right), \\ \left(SiO_4 / \{k_{sio4(1,3)} + SiO_4\}\right) \end{bmatrix} \tag{8a,10a}$$

for benthic and pelagic diatoms, and

$$g_2 = [\mu_2]\begin{bmatrix} \min\left(I_z / I_{sat}\, e^{(1-Iz/Isat(2))}\right), \left(NO_3 / \{k_{NO3(2)} + NO_3\}\right), \\ \text{or}\left(NH_4 / \{k_{NH4(2)} + NH_4\}\right), \left(PO_4 / \{k_{PO4(2)} + PO_4\}\right) \end{bmatrix} \tag{9a}$$

for pelagic microflagellates, which are not dependent on silicate as a nutrient source. In the above equations, $k_{NO3(n)}$, $k_{NH4(n)}$, $k_{PO4(n)}$, and $k_{SiO4(n)}$ represent the Michaelis-Menten half-saturation constants, with respect to each microalgal functional group, for uptake of nitrate, ammonia, phosphate and silicate respectively. $I_{sat(n)}$ is the saturation light intensity for each functional group effecting photo-inhibition. The maximal microalgal gross growth rate, μ_n is a function of temperature (Eppley, 1972):

$$\mu_n = \mu_{t(n)} e^{0.0633(T-27)} \qquad (8b,9b,10b)$$

where T is the temperature (˚C) obtained from the POM and $\mu_{t(n)}$ is a functional group specific maximum growth rate normalized to a 24 h period at 27˚C (Eppley, 1972).

2.2 Secondary Producers

The secondary producers (micro/mesozooplankton and multiple benthic grazers) are not explicitly simulated but their activities do, instead, provide closure for this ecological simulation. The proposed simulation's grazing rates are determined as Michaelis-Menten functions of the microalgal biomass (Mullin *et al.*, 1975):

$$\gamma_i = \gamma_{mi}\left(P_i - P_i^{'}\right)/\left[k_{zi} + \left(P_i - P_i^{'}\right)\right] \qquad (11)$$

where i is the functional group of microalgae (1,2 or 3), γ_{mi} is the maximum grazing rate for the herbivore grazing the corresponding microalgal functional group, and k_{zi} is the corresponding half-saturation constant for grazing. Each microalgal functional group is subject to a "refuge" population, P', below which grazing does not occur.

2.3 Microbial Loop

The role of heterotrophic bacteria in the recycling of nutrients is significant (Azam *et al.*, 1983), and measurements of bacterial production in the Gulf of Mexico have been as high as 156 μg C l^{-1} day^{-1} (Pakulski *et al.*, 2000). Though these microbes are quite diverse, their dynamics in the marine environment are still difficult to discern and they are often treated as a homogenous assemblage (Ducklow, 2000). With respect to bacteria, the primary concern of this model is to simulate the remineralization of organic matter to inorganic matter that can be used by the simulated microalgae as well as the nitrification of ammonia to nitrate to be used by benthic diatoms in the sediments. Such nitrification occurs whether or not light is present (Eriksson, P.G. & S.E.B. Weisner,1999). Thus, the model's bacterioplankton are divided into two distinct functional groups – the ammonifying (B_a) and nitrifying (B_n) bacteria. In the water-column, these are described by:

$$\frac{\partial dB_{a1}}{\partial t} = Tr_t(dB_{a1}) + dg_4 B_{a1} - d\beta_{a1} B_{a1} - dmB_{a1} \quad (12a)$$

$$\frac{\partial dB_{n1}}{\partial t} = Tr_t(dB_{n1}) + dg_5 B_{n1} - d\beta_{n1} B_{n1} - dmB_{n1} \quad (13a)$$

and in the sediments, they are described by:

$$\frac{\partial hB_{a2}}{\partial t} = Tr_t(hB_{a2}) + hg_6 B_{a2} - h\beta_{a2} B_{a2} - hmB_{a2} \quad (12b)$$

$$\frac{\partial hB_{n2}}{\partial t} = Tr_t(hB_{n2}) + hg_7 B_{n2} - h\beta_{n2} B_{n2} - hmB_{n2} \quad (13b)$$

where β represents published bacterial respiration rates (del Giorgio and Cole, 2000) and m represents the bacterial mortality rates. Like the microalgae, bacterial growth rates ($g_{4\text{-}7}$) are a function of temperature (Walsh and Dieterle, 1994) such that:

$$g_{4-7} = 0.008\ e^{0.092T} \quad (12c,13c)$$

where T is again the temperature obtained from the circulation model and the temperature in the sediments is assumed to be the same as the near-bottom sigma level of the circulation model (Weisberg & He, 2003).

3. Nutrient model

3.1 Non-living particles

The fecal pellets of the model's grazers are explicitly described state variables, Z_1, Z_2, Z_3, representing the egested products of organisms feeding on pelagic diatoms, pelagic microflagellates, and benthic diatoms respectively. They are described in the model by:

$$\frac{\partial dZ_1}{\partial_t} = Tr(dZ_1) - \frac{\partial}{\partial\sigma}(w_{z1} Z_1) + d\ [(1-\delta_1)\alpha_1\gamma_1 P_1 - k_{fp} Z_1] \quad (14a)$$

$$\frac{\partial dZ_2}{\partial_t} = Tr(dZ_2) - \frac{\partial}{\partial\sigma}(w_{z2} Z_2) + d\ [(1-\delta_2)\gamma_2 P_2 - k_{fp} Z_2] \quad (14b)$$

$$\frac{\partial hZ_3}{\partial_t} = Tr(hZ_3) + h\ [(1-\delta_3)\alpha_3\gamma_3 P_3 - k_{fp} Z_3] \quad (14c)$$

where $w_{z1,2}$ are the fecal pellet sinking rates. Note that the fecal pellets of the benthic grazers (and those of the pelagic grazers) are not allowed to sink through the sediments and are therefore assumed to remain in the sediment layer in which the matter was originally ingested. The parameters, $\alpha_{1,2,3}$ represent the fraction of grazed microalgae which are actually ingested, ie. not lost due to sloppy feeding (Banse, 1992; Jumars *et al.*, 1989). Grazer respiration is represented by $\delta_{1,2,3}$ such that the term $[(1-\delta_{1,2,3})\alpha_{1,2,3}\gamma_{1,2,3}P_{1,2},M]$ is the grazer assimilated carbon, all of which is converted to fecal pellets to provide closure in

the model since the grazer biomass is not explicitly represented. Finally, k_{fp} is the fecal pellet degradation rate.

The other form of non-living particulate organic carbon in the model is detritus. It primarily consists of particulate cell material from dead or dying microalgae. Its dynamics are described in the water column by:

$$\frac{\partial dD_1}{\partial_t} = Tr\ (dD_1) - \frac{\partial}{\partial \sigma}(w_{D1} D_1) + d\ [(l_1 P_1) - k_D D_1] \quad (15a)$$

$$\frac{\partial dD_2}{\partial_t} = Tr\ (dD_2) - \frac{\partial}{\partial \sigma}(w_{D2} D_2) + d\ [(l_2 P_2) - k_D D_2] \quad (15b)$$

and in the sediments by:

$$\frac{\partial hD_3}{\partial_t} = Tr\ (hD_3) + h\ [(l_3 P_3) - k_D D_3] \quad (15c)$$

where $w_{D1,2}$ are the sinking rates of the detrital products of the pelagic diatoms and microflagellates respectively. Like the sediment fecal pellets, sediment detritus is assumed to remain in the sediment layer where it was generated.

The parameters k_{fp} and k_D represent the degradation rates of the fecal pellets and detritus respectively. Because the fecal pellets and detritus are algal products, they are assumed to have the same carbon to nitrogen and carbon to phosphorus ratios as the proposed model's microalgae. As the non-living particulate organic material is degraded, DOC, DON, and DOP are thus

proportionally produced. The inorganic particulate silica contained within some of the detritus and fecal pellets, however, is not subject to the same degradational processes as the organic materials. Due to the differential sinking rates of fecal pellets (100 m day^{-1}) and detritus (5 m day^{-1}), the particulate silica in the water-column is separated into two distinct groups: detrital silica (Si_D) and fecal pellet silica (Si_{fp}). These are described in the model by:

$$\frac{\partial dSi_D}{\partial t} = Tr\ (dSi_D) - \frac{\partial}{\partial \sigma}(w_D Si_D) + d\left[\left(\frac{Si}{C}\right)_r \left((1-\alpha_1+\delta_1\alpha_1)\gamma_1 P_1 + l_1 P_1\right)\right] - d\eta Si_D \quad (16a)$$

$$\frac{\partial dSi_{fp}}{\partial t} = Tr\ (dSi_{fp}) - \frac{\partial}{\partial \sigma}(w_{fp} Si_{fp}) + d\left[\left(\frac{Si}{C}\right)_r (1-\delta_1)\alpha_1\gamma_1 P_1\right] - d\eta Si_{fp} \quad (16b)$$

where η is the dissolution rate of particulate silica. Note that particulate silica is added to the model's detrital pool through the sloppy feeding and respiration of grazers in the third term of equation 16a in order to maintain a mass balance with the organic matter. The fecal pellets and detritus in the sediments are not subject to a sinking flux, such that the particulate silica dynamics there can be described by one equation:

$$\frac{\partial hSi_s}{\partial t} = Tr\ (hSi_s) + h\left[\left(\frac{Si}{C}\right)_r (\gamma_3 P_3 + l_3 P_3)\right] - h\eta Si_s \quad (16c)$$

3.2 Dissolved Organic Matter

Dissolved organic matter is important in marine ecosystem studies of phytoplankton dynamics for two reasons. Organic matter colors the water, thus affecting the attenuation of light in the water column and the sediments, and it also acts as a reservoir of carbon, nitrogen and phosphorus which have varying levels of reactivity. Despite extensive study of the properties of dissolved organic matter, however, only 4-11% of DOC and 7-14% of DON have been characterized in the surface ocean (Benner, 2002).

Given the range of properties of marine DOM (Benner, 2002), it is difficult to adequately model the dynamics of these substances within the ecosystem given just one pool. These properties, however, fall across a wide spectrum, making it difficult to separate the DOM into distinct pools. In much of the literature (Hedges, 2002), marine DOM is separated into two sets of two DOM classes. One set separates DOM according to size (Benner, 2002) into high molecular weight (HMW) and low molecular weight (LMW) fractions. The other separates DOM according to its reactivity (Carlson, 2002) into refractory and labile components. Unfortunately, these groups are not mutually exclusive, ie. HMW DOM can be both refractory and labile. Furthermore, in terms of ecosystem models, a separation by size is useful for light attenuation since HMW compounds are typically the colored component of marine DOM (Kirk, 1995), but a separation by reactivity is far more useful when calculating the relation of DOM to nutrient cycling.

For the purposes of this model, two reactively distinct pools of DOM are used to calculate the model's nutrient cycles. A mean value of 25% of the total DOM will be considered to be high molecular weight (Benner, 2002), and therefore CDOM affecting light attenuation (Kirk, 1995). Labile DOM (LDOC) is thus described in terms of carbon by:

$$\frac{\partial \mathrm{dLDOC}}{\partial \mathrm{t}} = \mathrm{Tr(dLDOC)} + \mathrm{d}\begin{bmatrix} \upsilon \mathrm{mB_{a1}} + \upsilon \mathrm{mB_{n1}} + \psi_1 \mathrm{P_1} + \psi_2 \mathrm{P_2} \\ + (1-\alpha_1)\gamma_1 \mathrm{P_1} + \mathrm{k_{fp}\, Z_1} + \mathrm{k_{fp}\, Z_2} \\ + \mathrm{k_D\, D_1} + \mathrm{k_D\, D_2} - \mathrm{g_4\, B_{a1}} - \mathrm{bLDOC} \end{bmatrix} \qquad (17a)$$

where m is equal to the mortality rate of all functional groups of bacteria and υ is the fraction of the dying bacterial biomass which becomes labile (Ogawa *et al.*, 2001). In contrast, the fecal pellet and detrital material are fully labile (Amon and Benner, 1996) and are calculated as a function of available substrate and the respective coefficients k_{fp} and k_d. The coefficient, b, is the fraction of dissolved organic matter undergoing photodegradation to inorganic products. The sediment pool of labile DOC is then:

$$\frac{\partial \mathrm{dLDOC}}{\partial \mathrm{t}} = \mathrm{Tr(hLDOC)} + \mathrm{d}\begin{bmatrix} \upsilon \mathrm{mB_{a2}} + \upsilon \mathrm{mB_{n2}} + \psi_3 \mathrm{P_3} \\ + (1-\alpha_3)\gamma_3 \mathrm{P_3} + \mathrm{k_{fp}\, Z_3} + \mathrm{k_D\, D_3} \\ - \mathrm{g_6\, B_{a2}} - \mathrm{bLDOC} \end{bmatrix} \qquad (17b)$$

Based on available data (Mopper *et al.*, 1991), b is usually zero in the sediments and much of the lower portion of the water-column.

The model's refractory pool of DOM (RDOC) is then described in the water-column by:

$$\frac{\partial \mathrm{dRDOC}}{\partial \mathrm{t}} = \mathrm{Tr(dRDOC)} + \mathrm{d}\begin{bmatrix}(1-\upsilon)\mathrm{mB_{a1}} + (1-\upsilon)\mathrm{mB_{n1}} \\ -\mathrm{bRDOC}\end{bmatrix} \tag{18a}$$

and in the sediments by:

$$\frac{\partial \mathrm{dRDOC}}{\partial \mathrm{t}} = \mathrm{Tr(hRDOC)} + \mathrm{h}\begin{bmatrix}(1-\upsilon)\mathrm{mB_{a2}} + (1-\upsilon)\mathrm{mB_{n2}} \\ -\mathrm{bRDOC}\end{bmatrix} \tag{18b}$$

Since refractory organic matter exists in the model only due to initial conditions and production by bacteria, refractory dissolved organic nitrogen (RDON) and dissolved organic phosphorus (RDOP) are assumed to be related to RDOC by the respective bacterial C/N and C/P ratios. The model's labile organic matter, however, has bacterial and microalgal origins such that labile dissolved organic nitrogen (LDON) is described in the model's water-column by:

$$\begin{aligned}\frac{\partial \mathrm{dLDON}}{\partial \mathrm{t}} = \mathrm{Tr(dLDON)} &+ \mathrm{d}\ (\mathrm{N/C})_{\mathrm{r}}\begin{bmatrix}\psi_1 \mathrm{P_1} + \psi_2 \mathrm{P_2} + (1-\alpha_1)\gamma_1 \mathrm{P_1} \\ +\mathrm{k_{fp}}(\mathrm{Z_1}+\mathrm{Z_2}) + \mathrm{k_D}(\mathrm{D_1}+\mathrm{D_2})\end{bmatrix} \\ &+ \mathrm{d}\ \left[(\mathrm{N/C})_{\mathrm{b}}(\upsilon \mathrm{mB_{a1}} + \upsilon \mathrm{mB_{n1}} - \mathrm{g_4 B_{a1}})\right] - \mathrm{bLDON}\end{aligned} \tag{19a}$$

and in the sediments by:

$$\frac{\partial \text{hLDON}}{\partial t} = \text{Tr(hLDON)} + \text{h}\ (\text{N}/\text{C})_r \begin{bmatrix} \psi_3 \text{P}_3 + (1-\alpha_3)\gamma_3 \text{P}_3 \\ + \text{k}_{fp} \text{Z}_3 + \text{k}_D \text{D}_3 \end{bmatrix} + \text{h}\ [(\text{N}/\text{C})_b (\upsilon \text{mB}_{a2} + \upsilon \text{mB}_{n2} - \text{g}_6 \text{B}_{a2})] - \text{bLDON} \quad (19b)$$

Labile dissolved organic phosphorus (LDOP) is described in the water-column by:

$$\frac{\partial \text{dLDOP}}{\partial t} = \text{Tr(dLDOP)} + \text{d}\ (\text{P}/\text{C})_r \begin{bmatrix} \psi_1 \text{P}_1 + \psi_2 \text{P}_2 + (1-\alpha_1)\gamma_1 \text{P}_1 \\ + \text{k}_{fp}(\text{Z}_1 + \text{Z}_2) + \text{k}_D(\text{D}_1 + \text{D}_2) \end{bmatrix} + \text{d}\ [(\text{P}/\text{C})_b (\upsilon \text{mB}_{a1} + \upsilon \text{mB}_{n1} - \text{g}_4 \text{B}_{a1})] - \text{bLDOP} \quad (20a)$$

while the pore-water LDOP is described by:

$$\frac{\partial \text{hLDOP}}{\partial t} = \text{Tr(hLDOP)} + \text{h}\ (\text{P}/\text{C})_r \begin{bmatrix} \psi_3 \text{P}_3 + (1-\alpha_3)\gamma_3 \text{P}_3 \\ + \text{k}_{fp} \text{Z}_3 + \text{k}_D \text{D}_3 \end{bmatrix} + \text{h}\ [(\text{P}/\text{C})_b (\upsilon \text{mB}_{a2} + \upsilon \text{mB}_{n2} - \text{g}_6 \text{B}_{a2})] - \text{bLDOP} \quad (20b)$$

3.3 Dissolved Inorganic matter

Remineralization, in terms of carbon, is described in the water-column by:

$$\frac{\partial \mathrm{dDIC}}{\partial \mathrm{t}} = \mathrm{Tr(dDIC)} + \mathrm{d}\begin{bmatrix} \varepsilon_1 \mathrm{P_1} + \varepsilon_2 \mathrm{P_2} + \beta_{\mathrm{a1}} \mathrm{B_{a1}} + \beta_{\mathrm{n1}} \mathrm{B_{n1}} + \\ \mathrm{bRDOC} + \mathrm{bLDOC} + \delta_1 \alpha_1 \gamma_1 \mathrm{P_1} \\ + \delta_2 \gamma_2 \mathrm{P_2} - \mathrm{g_1 P_1} - \mathrm{g_2 P_2} - \mathrm{g_5 B_{n1}} \end{bmatrix} \qquad (21a)$$

where carbon is respired by pelagic microalgae, bacteria and grazers, and is further produced by the photolysis of dissolved organic carbon. The DIC is then a carbon source for the phytoplankton and the nitrifying bacteria (del Giorgio and Cole, 2000), but not for the ammonifying bacteria, which make use of the labile organic carbon. Similarly, pore-water DIC is described by:

$$\frac{\partial \mathrm{hDIC}}{\partial \mathrm{t}} = \mathrm{Tr(hDIC)} + \mathrm{h}\begin{bmatrix} \varepsilon_3 \mathrm{P_3} + \beta_{\mathrm{a2}} \mathrm{B_{a2}} + \beta_{\mathrm{n2}} \mathrm{B_{n2}} + \\ \mathrm{bRDOC} + \mathrm{bLDOC} + \delta_3 \alpha_3 \gamma_3 \mathrm{P_3} \\ - \mathrm{g_3 P_3} - \mathrm{g_7 B_{n2}} \end{bmatrix} \qquad (21b)$$

The only form of new nitrogen in the water-column of the model is described by:

$$\begin{aligned} \frac{\partial \mathrm{dNO_3}}{\partial \mathrm{t}} &= \mathrm{Tr_t(dNO_3)} - \mathrm{d}\left[(\mathrm{N/C})_{\mathrm{r}}(\mathrm{g_{1NO3} P_1} + \mathrm{g_{2NO3} P_2})\right] \\ &\quad + \mathrm{d}\left[(\mathrm{N/C})_{(\mathrm{b})} \beta_{\mathrm{n1}} \mathrm{B_{n1}}\right] \end{aligned} \qquad (22a)$$

where $(N/C)_r$ is a Redfield nitrogen to carbon ratio for the model's phytoplankton and $(N/C)_b$ is the nitrogen to carbon ratio of the model's bacteria. The simulated nitrification in the model occurs through the nitrogen equivalent of respiration (β_{n1}) of the model's nitrifying bacteria (B_{n1}). "New" nitrogen in the sediments is similarly described by:

$$\frac{\partial hNO_3}{\partial t} = Tr_t(hNO_3) - h\left[(N/C)_r(g_{3NO3}P_3)\right] + h\left[(N/C)_{(b)}\beta_{n2}B_{n2}\right] \quad (22b)$$

Regenerated nitrogen is described in the water-column by:

$$\frac{\partial dNH_4}{\partial_t} = Tr_t(dNH_4) + d\left[(N/C)_r\begin{pmatrix}\varepsilon_1 P_1 - g_{1NH4}P_1 + \varepsilon_2 P_2 \\ - g_{2NH4}P_2 + \delta_1\alpha_1\gamma_1 P_1 + \delta_2\gamma_2 P_2\end{pmatrix}\right] + d\left[(N/C)_b(\beta_{a1}B_{a1} - g_{5NH4}B_{n1})\right] + bLDON \quad (23a)$$

where the pelagic nitrifying bacteria are in competition with the pelagic diatoms and microflagellates for ammonium. In addition to ammonification, which occurs through the respiration (β_{a1}) of the model's ammonifying bacteria (B_{a1}), ammonium is produced through the nitrogen equivalent of respiration of the model's pelagic grazers. The fraction of carbon respired is represented by δ.

Regenerated nitrogen in the sediments is described by:

$$\frac{\partial hNH_4}{\partial_t} = Tr_t(hNH_4) + h\left[(N/C)_r(\varepsilon_3 P_3 - g_{3NH4}P_3 + \delta_3\alpha_3\gamma_3 P_3)\right] + h\left[(N/C)_b(\beta_{a2}B_{a2} - g_{7NH4}B_{n2})\right] + bLDON \quad (23b)$$

The nitrifying bacteria are also in competition with the microalgae for phosphate, which is described in the model's water-column by:

$$\frac{\partial \mathrm{dPO_4}}{\partial_t} = \mathrm{Tr_t(dPO_4)} + \mathrm{d}\left[(\mathrm{P/C})_r \begin{pmatrix} \varepsilon_1 \mathrm{P_1} - \mathrm{g_{1PO4}} \mathrm{P_1} + \varepsilon_2 \mathrm{P_2} \\ - \mathrm{g_{2PO4}} \mathrm{P_2} + \delta_1 \alpha_1 \gamma_1 \mathrm{P_1} + \delta_2 \gamma_2 \mathrm{P_2} \end{pmatrix}\right] + \mathrm{d}\left[(\mathrm{P/C})_b (\beta_{a1} \mathrm{B_{a1}} + \beta_{n1} \mathrm{B_{n1}} - \mathrm{g_{5PO4}} \mathrm{B_{n1}})\right] + \mathrm{bLDOP} \quad (24a)$$

where $(P/C)_r$ and $(P/C)_b$ are the phosphorus to carbon ratios of the phytoplankton and bacteria, respectively. Note that phosphate is taken up by the nitrifying bacteria, but is regenerated through the respiration of both the nitrifying and ammonifying bacteria (del Giorgio & Cole, 2000). The functional group of ammonifying bacteria, instead, uses dissolved organic phosphorus (DOP) as a source of phosphorus during the break down of organic matter.

Sediment phosphate dynamics are described by:

$$\frac{\partial \mathrm{hPO_4}}{\partial_t} = \mathrm{Tr_t(hPO_4)} + \mathrm{h}\left[(\mathrm{P/C})_r (\varepsilon_3 \mathrm{P_3} - \mathrm{g_{3PO4}} \mathrm{P_3} + \delta_3 \alpha_3 \gamma_3 \mathrm{P_3})\right] + \mathrm{d}\left[(\mathrm{P/C})_b (\beta_{a2} \mathrm{B_{a2}} + \beta_{n2} \mathrm{B_{n2}} - \mathrm{g_{7PO4}} \mathrm{B_{n2}})\right] + \mathrm{bLDOP} \quad (24b)$$

Silicate dynamics are simply described in the model's water-column by:

$$\frac{\partial \mathrm{dSiO_4}}{\partial_t} = \mathrm{Tr_t(dSiO_4)} - \mathrm{d}\left[(\mathrm{Si/C})_r (\mathrm{g_{1SiO4}} \mathrm{P_1} - \psi_1 \mathrm{P_1})\right] + \mathrm{d}\eta \quad (25a)$$

where the sole silicate loss term is due to uptake by the pelagic diatoms. Silicate is then regenerated through the dissolution (η) of particulate silica upon the death of the diatoms. A small amount of silicate is also regenerated as dissolution of silica frustules from living diatoms to maintain a simple mass balance within the model upon excretion of organic material. Likewise, silicate dynamics in the sediments are described by:

$$\frac{\partial dSiO_4}{\partial_t} = Tr_t(hSiO_4) - h\left[(Si/C)_r\left(g_{3SiO4}P_3 - \psi_1 P_3\right)\right] + d\eta \qquad (25b)$$

4. Boundary conditions

The model employs a no-flux boundary condition along solid coastal boundaries, ignoring estuaries. Cross shelf open boundaries exist off Mobile Bay and Charlotte Harbor, and an along shelf open boundary exists at the 200 m isobath. At these boundaries, time-dependent nitrate, ammonium, and silicate values are prescribed at inflow points using the NEGOM and ECOHAB data sets (Table 2). Estuarine nutrients and DOM are added to the model as boundary conditions at various points according to observations made during the NEGOM and ECOHAB cruises in 1998. Nutrient concentrations are linearly interpolated spatially for grid points between stations and temporally between observations.

At the bottom of the sediment layer, a constant boundary condition is employed (Table 3), ignoring groundwater input of nutrients in this examination of water column nutrients. Atmospheric deposition of chemical species are ignored in this model such that fluxes for all chemical species across the air-sea interface are zero, with the exception of DIC for which the diffusive flux at the air-sea interface is described by:

$$\left(\frac{k_h}{d}\frac{\partial DIC}{\partial \sigma}\right)_0 = 1.11x10^{-5} W\phi\left[\left(pCO_2\right)_{air} - \left(pCO_2\right)_0\right] \quad (26)$$

where W is the wind speed, and ϕ is the solubility of CO_2 in seawater. In the upper layer of the water-column, the partial pressure of CO_2 $(pCO_2)_0$ is calculated (Peng *et al.*, 1987) as a function of POM's temperature and salinity, using alkalinity = 520 + 51.2 salinity (Millero *et al.*, 1998), while $(pCO_2)_{air}$ is assumed to be 365 μatm.

All simulations are forced by daily average flow fields from a 1998 case of a circulation model of the West Florida Shelf (Weisberg & He, 2003). Model runs simulate the spring and summer of 1998 in two cases: 1) The "standard case", considering only the available observations during the spring and summer 1998 from the NEGOM and ECOHAB:Florida programs (Fig. 8a), and 2) a case of different initial conditions, considering the fallout of an initialized spring diatom bloom off the coast of the "Big Bend" region of Florida, such as those that are produced in low salinity plumes of the Apalachicola and Mississippi rivers (Gilbes *et al.*, 1996) and similar to that analyzed in a previous 1-D simulation (Darrow *et*

al, 2003). Case 1 tests whether upwelled nutrients on their own are sufficient to grow benthic diatoms. Case 2 tests the ability of upwelled nutrients in conjunction with recycled nutrients from a dying phytoplankton bloom to grow benthic microalgae.

Model parameters are summarized in table 4.

Table 2. The depth dependent water-column conditions applied at the open boundaries over the entire model run, and applied over the entire model grid in the initial time step.

Depth (m)	Diatoms (μmol C l^{-1})	Flagellates (μmol C l^{-1})	NH_4 (μmol kg^{-1})	NO_3 (μmol kg^{-1})	PO_4 (μmol kg^{-1})	SiO_4 (μmol kg^{-1})
1	0.55	0.3125	0.2	0.05	0.025	1
10	0.55	0.3125	0.2	0.05	0.025	1
50	0.55	0.3125	0.2	0.75	0.1	1
100	0.55	0.3125	0.2	2.5	0.125	1
150	0.55	0.3125	0.2	5.64	0.225	1
200	0	0	0.2	10	0.34	6
250	0	0	0.2	10.5	0.425	7.5
300	0	0	0.2	10.6	0.51	9
350	0	0	0.2	11	0.595	10.5
400	0	0	0.2	12.08	0.68	12
450	0	0	0.2	13.59	0.765	13.5
500	0	0	0.2	15.1	0.85	15
600	0	0	0.2	18.12	1.02	18
700	0	0	0.2	21.14	1.19	21
800	0	0	0.2	24.16	1.36	24
900	0	0	0.2	27.18	1.53	27
1000	0	0	0.2	27.5	1.75	27.5
1500	0	0	0.2	27.5	1.75	27.5
2000	0	0	0.2	27.5	1.75	27.5
2500	0	0	0.2	27.5	1.75	27.5

Table 2 (cont)

Depth (m)	DON (μmol kg^{-1})	DOP (μmol kg^{-1})	DOC (μmol kg^{-1})	DIC (μmol kg^{-1})	Siliceous Fecal Pellets (μmol C kg^{-1})
1	11.3	0.7	75	2100	0
10	11.3	0.7	75	2100	0
50	11.3	0.7	75	2100	0
100	11.3	0.7	75	2100	0
150	11.3	0.7	75	2100	0
200	10.3	0.64	68	2120	0
250	10.05	0.625	66.25	2125	0
300	9.8	0.61	64.5	2130	0
350	9.55	0.595	62.75	2135	0
400	9.3	0.58	61	2140	0
450	9.05	0.565	59.25	2145	0
500	8.8	0.55	57.5	2150	0
600	8.3	0.52	54	2160	0
700	7.8	0.49	50.5	2170	0
800	7.3	0.46	47	2180	0
900	6.8	0.4	45	2190	0
1000	6.8	0.4	45	2200	0
1500	6.8	0.4	45	2200	0
2000	6.8	0.4	45	2200	0
2500	6.8	0.4	45	2200	0

Table 2 (cont)

Depth (m)	Non-Siliceous Fecal Pellets (μmol C kg^{-1})	Nitrifying Bacteria (μmol C kg^{-1})	Ammonifying Bacteria (μmol C kg^{-1})	Siliceous Detritus (μmol C kg^{-1})	Non-Siliceous Detritus (μmol C kg^{-1})
1	0	0.05	0.35	0.0075	0.005
10	0	0.05	0.35	0.0075	0.005
50	0	0.05	0.35	0.0075	0.005
100	0	0.05	0.35	0.0075	0.005
150	0	0.05	0.35	0.0075	0.005
200	0	0.05	0.35	0.0075	0.005
250	0	0.05	0.35	0.0075	0.005
300	0	0.05	0.35	0.0075	0.005
350	0	0.05	0.35	0.0075	0.005
400	0	0.05	0.35	0.0075	0.005
450	0	0.05	0.35	0.0075	0.005
500	0	0.05	0.35	0.0075	0.005
600	0	0.05	0.35	0.0075	0.005
700	0	0.05	0.35	0.0075	0.005
800	0	0.05	0.35	0.0075	0.005
900	0	0.05	0.35	0.0075	0.005
1000	0	0.05	0.35	0.0075	0.005
1500	0	0.05	0.35	0.0075	0.005
2000	0	0.05	0.35	0.0075	0.005
2500	0	0.05	0.35	0.0075	0.005

Table 3. The depth based initial conditions applied to the sediments over the entire model grid based on measurements in the South Atlantic Bight (Marinelli *et al.*, 1998).

Depth (mm)	Diatoms (mmol C m^3)	NH_4 (μmol kg^{-1})	NO_3 (μmol kg^{-1})	PO_4 (μmol kg^{-1})	SiO_4 (μmol kg^{-1})	DON (μmol kg^{-1})
2	4000	10	2	0.1	1.5	3.773585
4	0	10	2	0.1	1.5	22.64151
6	0	10	2	0.1	1.5	45.28302
8	0	10	2	0.1	1.5	75.4717
10	0	10	2	0.1	1.5	113.2075
12	0	10	2	0.2	1.5	135.8491
14	0	10	1	0.3	1.5	166.0377
16	0	10	1	0.4	1.5	181.1321
18	0	10	1	0.5	1.5	196.2264
20	0	10	1	0.6	1.5	211.3208
22	0	10	1	0.7	1.5	226.4151
24	0	10	1	0.8	1.5	241.5094
26	0	10	1	0.9	1.5	256.6038
28	0	10	1	1	1.5	271.6981
30	0	10	1	1.1	1.5	279.2453
32	0	10	1	1.2	1.5	283.0189
34	0	10	0	1.3	1.5	286.7925
36	0	10	0	1.4	1.5	292.8302
38	0	10	0	1.5	1.5	295.8491
40	0	10	0	1.6	1.5	301.8868

Table 3 (cont)

Depth (mm)	DOP (μmol kg^{-1})	DOC (μmol kg^{-1})	DIC (μmol kg^{-1})	Siliceous Fecal Pellets (μmol C kg^{-1})	Non-Sliceous Fecal Pellets (μmol C kg^{-1})
2	0.235849	25	2200	0	0
4	1.415094	150	2200	0	0
6	2.830189	300	2200	0	0
8	4.716981	500	2200	0	0
10	7.075472	750	2200	0	0
12	8.490566	900	2200	0	0
14	10.37736	1100	2200	0	0
16	11.32075	1200	2200	0	0
18	12.26415	1300	2200	0	0
20	13.20755	1400	2200	0	0
22	14.15094	1500	2200	0	0
24	15.09434	1600	2200	0	0
26	16.03774	1700	2200	0	0
28	16.98113	1800	2200	0	0
30	17.45283	1850	2200	0	0
32	17.68868	1875	2200	0	0
34	17.92453	1900	2200	0	0
36	18.30189	1940	2200	0	0
38	18.49057	1960	2200	0	0
40	18.86792	2000	2200	0	0

Table 3 (cont)

Depth (mm)	Siliceous Detritus (μmol C kg^{-1})	Non-Siliceous Detritus (μmol C kg^{-1})	Nitrifying Bacteria (μmol C kg^{-1})	Ammonifying Bacteria (μmol C kg^{-1})	Denitrifying Bacteria (μmol C kg^{-1})
2	0.0075	0.005	0.05	0.35	0
4	0.007125	0.00475	0.05	0.35	0
6	0.00675	0.0045	0.05	0.35	0
8	0.006375	0.00425	0.05	0.35	0
10	0.006	0.004	0.05	0.35	0
12	0.005625	0.00375	0.05	0.35	0
14	0.00525	0.0035	0.05	0.35	0.05
16	0.004875	0.00325	0.05	0.35	0.05
18	0.0045	0.003	0.05	0.35	0.075
20	0.004125	0.00275	0.05	0.35	0.1
22	0.00375	0.0025	0.05	0.35	0.125
24	0.003375	0.00225	0.05	0.35	0.15
26	0.003	0.002	0.05	0.35	0.175
28	0.002625	0.00175	0.05	0.35	0.2
30	0.00225	0.0015	0.05	0.35	0.225
32	0.001875	0.00125	0.05	0.35	0.25
34	0.0015	0.001	0.05	0.35	0.275
36	0.001125	0.00075	0.05	0.35	0.3
38	0.00075	0.0005	0.05	0.35	0.325
40	0.000375	0.00025	0.05	0.35	0.35

Table 4. Model parameters.

Symbol	Description	Units
B	Bacteria	mmol m^{-3}
B_{a1}	Pelagic ammonifying bacteria	mmol m^{-3}
B_{a2}	Benthic ammonifying bactera	mmol m^{-3}
B_{n1}	Pelagic nitrifying bacteria	mmol m^{-3}
B_{n2}	Benthic nitrifying bacteria	mmol m^{-3}
b 1.9 x 10^{-9}	Coefficient of phototransformation of DOM	s^{-1}
CDOM	Colored dissolved organic matter	mmol m^{-3}
D	Detritus	mmol m^{-3}
d	Depth of level	m
g_1	Realized growth rate of pelagic diatoms	s^{-1}
g_2	Realized growth rate of pelagic microflagellates	s^{-1}
g_3	Realized growth rate of benthic diatoms	s^{-1}
g_4	Realized growth rate of pelagic ammonifyign bacteria	s^{-1}
g_5	Realized growth rate of pelagic nitrifying bacteria	s^{-1}
g_6	Realized growth rate of benthic ammonifying bacteria	s^{-1}
g_7	Realized growth rate of benthic nitrifying bacteria	s^{-1}
h 0.002	depth of each sediment level	m
$I_{0(\lambda)}$	Solar irradiance at wavelength, λ, just below the surface	μE m^{-2} s^{-1}
I_{sat}	Saturation intensity effecting photoinhibition for a given microalgal functional group	μE m^{-2} s^{-1}
$I_{z(\lambda)}$	Incident irradiance at depth, z and wavelength, λ	μE m^{-2} s^{-1}
$l_{1\ 0.03}$	Pelagic diatom lysis rate	s^{-1}
$l_{2\ 0.03}$	Pelagic microflagellate lysis rate	s^{-1}
$l_{3\ 0.03}$	Benthic diatom lysis rate	s^{-1}
$k_{B(\lambda)}$	Specific attenuation coefficient of bacteria at wavelength, λ	m^{-1}
$k_{C(\lambda)}$	Specific attenuation coefficient of CDOM at wavelength, λ	m^{-1}
$k_{D(\lambda)}$	Specific attenuation coefficient of detritus at wavelength, λ	m^{-1}
k_d 5.7 x 10^{-7}	Degredation rate of detritus	s^{-1}
k_{fp} 5.7 x 10^{-7}	Degredation rate of fecal pellets	s^{-1}
k_h	Coefficient of vertical eddy diffusivity	cm s^{-1}
$k_{M(\lambda)}$	Specific attenuation coefficient of benthic diatoms at wavelength, λ	m^{-1}
k_{NH4}	Michaelis-Menten half-saturation constant for Ammonium uptake for a given functional group	mmol m^{-3}
k_{NO3}	Michaelis-Menten half-saturation constant for Nitrate uptake for a given functional group	mmol m^{-3}
k_{PO4}	Michaelis-Menten half-saturation constant for Phosphate uptake for a given functional group	mmol m^{-3}
$k_{P1(\lambda)}$	Specific attenuation coefficient of pelagic diatoms at wavelength, λ	m^{-1}
$k_{P2(\lambda)}$	Specific attenuation coefficient of pelagic microflagellates at wavelength, λ	m^{-1}
$k_{s(\lambda)}$	Specific attenuation coefficient of wet, sandy sediment at wavelength, λ	m^{-1}
k_{SiO4}	Michaelis-Menten half-saturation constant for Silicate uptake for a given functional group	mmol m^{-3}
$k_{w(\lambda)}$	Specific attenuation coefficient of water at wavelength, λ	m^{-1}
k_λ	Total attenuation coefficient at wavelength, λ	m^{-1}

Table 4 (cont)

Symbol	Description	Units
LDOC	Concentration of labile DOC	mmol m^{-3}
LDON	Concentration of labile DON	mmol m^{-3}
LDOP	Concentration of labile DOP	mmol m^{-3}
M	Benthic diatoms	mmol m^{-3}
$(N/C)_b$ 0.15	Carbon to Nitrogen ratio for bacteria	
$(N/C)_r$ 0.15	Redfieldian Carbon to Nitrogen ratio for microalgae	
NH_4	Ammonium concentration	mmol m^{-3}
NO_3	Nitrate concentration	mmol m^{-3}
$(P/C)_b$ 0.0188	Carbon to phosphorus ratio for bacteria	
$(P/C)_r$ 0.009	Redfieldian carbon to phosphorus ratio for microalgae	
P_1	Pelagic diatoms	mmol m^{-3}
P_2	Pelagic microflagellates	mmol m^{-3}
PO_4	Phosphate concentration	mmol m^{-3}
RDOC	Concentration of refractory DOC	mmol m^{-3}
RDON	Concentration of refractory DON	mmol m^{-3}
RDOP	Concentration of refractory DOP	mmol m^{-3}
Si	Particulate silica	mmol m^{-3}
$(Si/C)_r$ 0.15	Silica to carbon ratio for benthic and pelagic diatoms	
SiO_4	Silicate concentration	mmol m^{-3}
T	Temperature	C
Tr_a	Transport due to advection	cm s^{-1}
Tr_b	Transport across the sediment/water interface	cm s^{-1}
Tr_d	Transport due to diffusion	cm s^{-1}
Tr_s	Trasport within the sediments	cm s^{-1}
Tr_t	Total transport	cm s^{-1}
t	Time step	s^{-1}
u	Velocity component in the ξ direction	cm s^{-1}
v	Velocity component in the ζ direction	cm s^{-1}
W	Wind speed	m s^{-1}
w_1 5.7 x 10^{-6}	Sinking rate of pelagic diatoms	m s^{-1}
w_{D1} 5.7 x 10^{-6}	Sinking rate of detritus of diatom origin	m s^{-1}
w_{D2} 0	Sinking rate of detritus of flagellate origin	m s^{-1}
w_{Z1} 1.16 x 10^{-3}	Sinking rate of siliceous fecal pellets	m s^{-1}
w_{Z2} 1.16 x 10^{-3}	Sinking rate of non-siliceous fecal pellets	m s^{-1}
z	Depth interval within the water-column	
α_h	Rate of non-local exchange at depth, h, in the sediments	s^{-1}
α_1 .8	Fraction of material grazed by copepods which is ingested	
α_2 .8	Fraction of material grazed by protozoans which is ingested	
α_3 .8	Fraction of material grazed by benthic grazers which is ingested	

Table 4 (cont)

Symbol	Description	Units
β_{a1} 0.45	Respiration rate of pelagic ammonifying bacteria	
β_{n1} 0.45	Respiration rate of pelagic nitrifying bacteria	
δ_1 0.20	Respiration rate of pelgaic copepods grazing pelagic diatoms	
δ_2 0.20	Respiration rate of protozoans grazing pelagic microflagellates	
ξ	Cross-shelf curvilinear coordinate	
ε_1 0.10	Respiration rate of pelagic diatoms	
ε_2 0.10	Respiration rate of pelagic microflagellates	
ε_3 0.10	Respiration rate of benthic diatoms	
γ_1	Grazing rate of copepods on pelagic diatoms	
γ_2	Grazing rate of protozoans microflagellates	
γ_3	Grazing rate of benthic grazers on benthic diatoms	
λ	Wavelength of radiation	nm
μ_1 1.45 x 10^{-5}	Maximal growth rate for pelagic diatoms	s^{-1}
μ_2 1.16 x 10^{-5}	Maximal growth rate for pelagic microflagellates	s^{-1}
μ_3 1.45 x 10^{-5}	Maximal growth rate for benthic diatoms	s^{-1}
μ_τ	Functional group specific maximum growth rate normalized to a 24 h period at 27 ˚C	s^{-1}
ζ	Alongshore curvilinear coordinate	
η 6.9 x 10^{-6}	Dissolution of silica	mmol m^{-3} s^{-1}
σ	Sigma coordinate	
υ 0.9	Fraction of dying bacterial biomass which is labile	
ψ_1 0.04	Pelagic diatom excretion rate	
ψ_2 0.04	Pelagic microflagellate excretion rate	
ψ_3 0.04	Benthic diatom excretion rate	
ω	Velocity component in the σ direction	

Results

1. Case 1

1.1 Spring 1998

Compared to the previous 20 year climatological mean, the wind field over the eastern Gulf of Mexico during March-May 1998 was anomalous, featuring persistent eastward, upwelling favorable winds along the Panhandle of Florida (Walsh et al, 2003). Although the 1 μmol kg^{-1} isopleth of nitrate was initially located at the shelf break in the eastern Gulf of Mexico due to the model's initial conditions (Table 2), the circulation model's flow fields transported nitrate to the continental shelf during the first week of the simulation. In the absence of loop current forcing in this simulated scenario, the 1 μmol kg^{-1} isopleth of nitrate penetrated to the 35 m isobath along the northern gulf coast and the southern West Florida Shelf by May 9 (Fig. 17A). In the real world, the combined effect of strong coastal upwelling, loop current impingement at the shelf break, and light limitation of microalgae (Walsh et al., 2003) drove the 1 μmol kg^{-1} isopleth of nitrate all the way to the 20 m isobath (Fig. 4B).

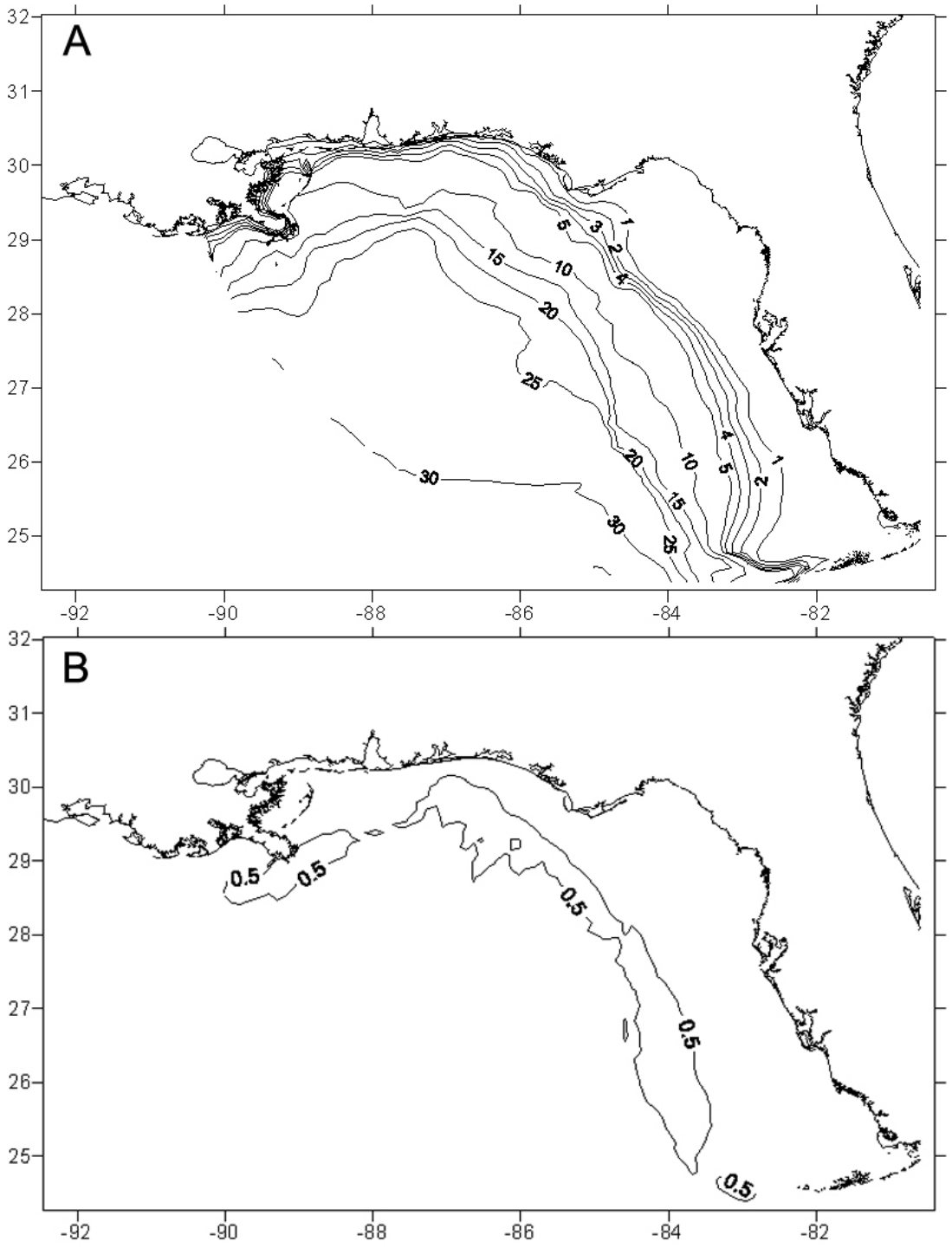

Figure 17. The simulated near-bottom A) NO_3 (μmol kg^{-1}), B) NH_4 (μmol kg^{-1}), during 9 May 1998 in case 1 of the model.

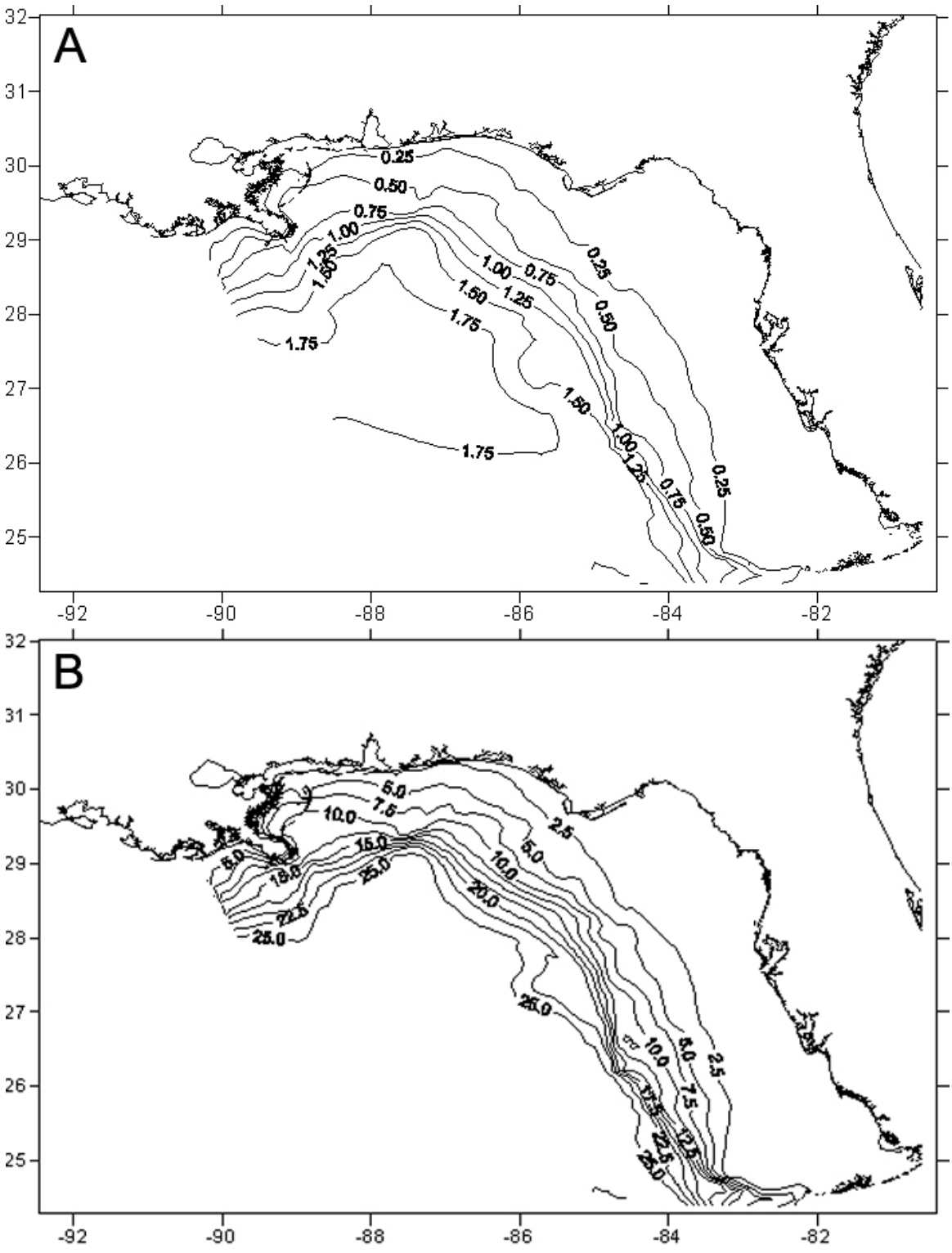

Figure 18. The simulated near-bottom A) PO_4(μmol kg^{-1}) and B) SiO_4 (μmol kg^{-1}), during 9 May 1998 in case 1 of the model.

The recycled NH_4, was elevated along the shelf-break, reaching concentrations as high as 0.8 μmol kg^{-1} at 1 m off the bottom (Fig. 17B). These are similar to near-bottom concentrations measured during the NEGOM program (Walsh *et al*, 2003), with the exception of the Big Bend region where the model did not match elevated concentrations.

Phosphate concentrations in the present simulation (Fig. 18A) were similar to the real world (Fig. 7A), where the 0.25 μmol kg^{-1} isopleth of phosphate penetrated the 20 m isobath across the entire Eastern Gulf of Mexico. Like the nitrate, silica did not penetrate as far onto the continental shelf in the simulation as it did in the real world. Here, the simulated 2.5 μmol kg^{-1} isopleth of silica did not penetrate to the 20 m isobath over most of the shelf (Fig. 18B), while it made it all the way to the shore in most regions in the real world (Fig. 5B).

Unlike, previous one-dimensional simulations of the West Florida shelf (Darrow et al, 2003) in which advective porewater exchange was not considered, the present simulation parameterized stronger flushing of the interstitial waters of the top 4 cm of sediments. Porewater ammonium concentrations (Fig. 19B) were now less than those of the previous analysis. They were also less than those observed by Marinelli *et al*. (1998) in the South Atlantic Bight. Phosphate (Fig. 20A) and nitrate (Fig. 19A) concentrations of the surficial sediments on the continental shelf were, however, similar to those observed at the same depths in the South Atlantic Bight. Porewater silicate concentrations (Fig. 20D) in the

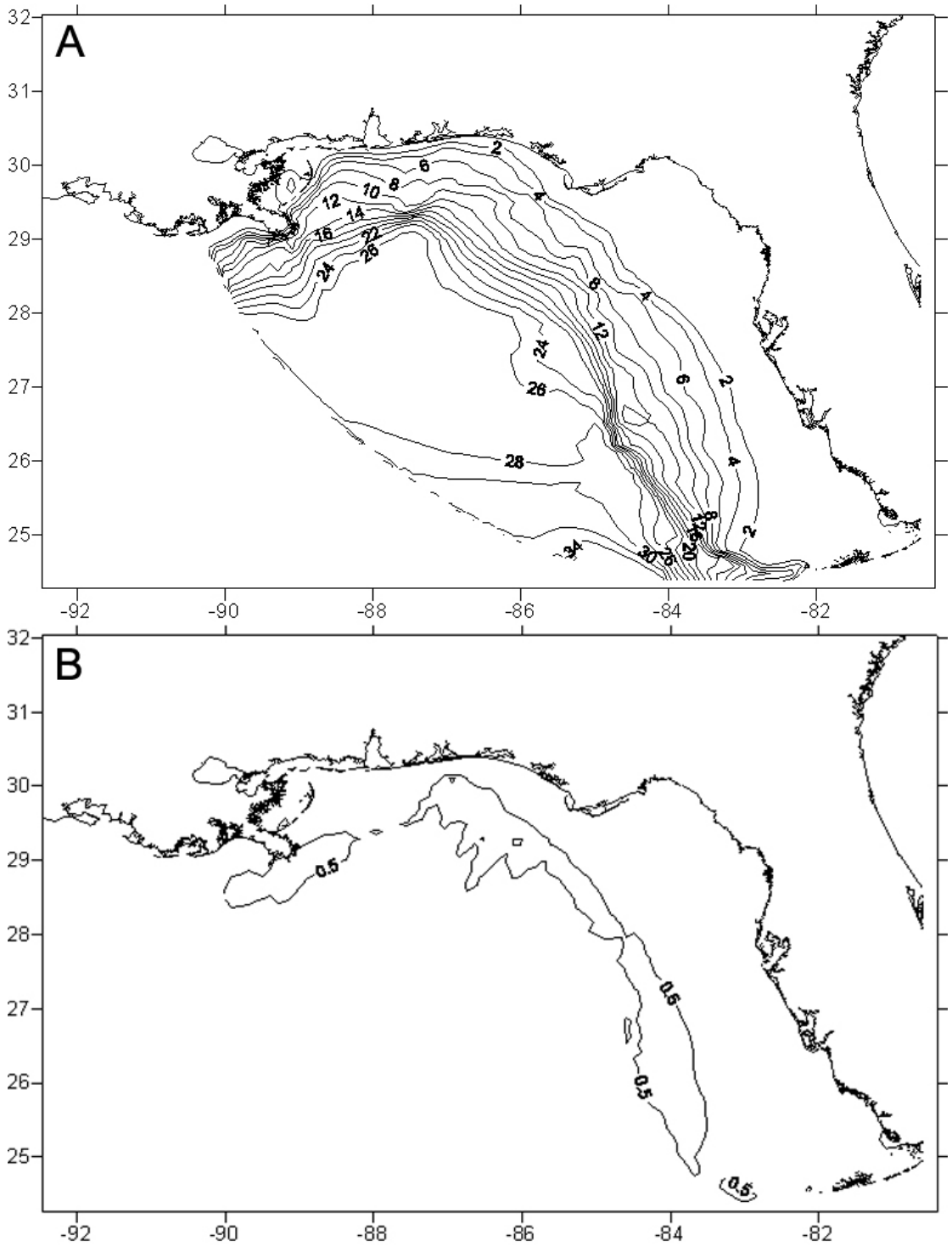

Figure 19. The simulated concentrations of A) NO_3 (μmol kg^{-1}) and B) NH_4 (μmol kg^{-1}) in the surface sediment layer during 9 May 1998 in case 1 of the model.

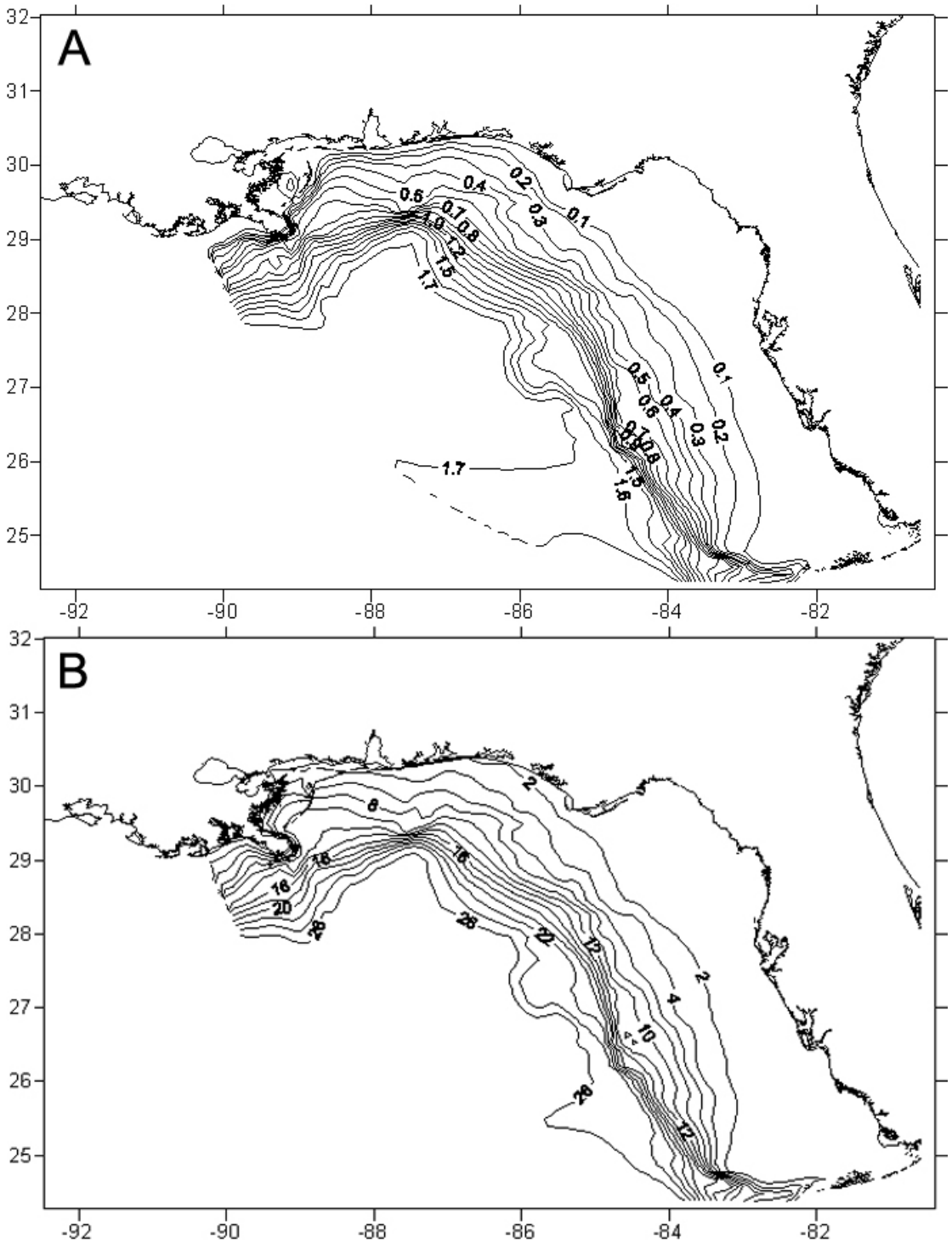

Figure 20. The simulated concentrations of A) PO_4 (μmol kg^{-1}) and B) SiO_4 (μmol kg^{-1}) in the surface sediment layer during 9 May 1998 in case 1 of the model.

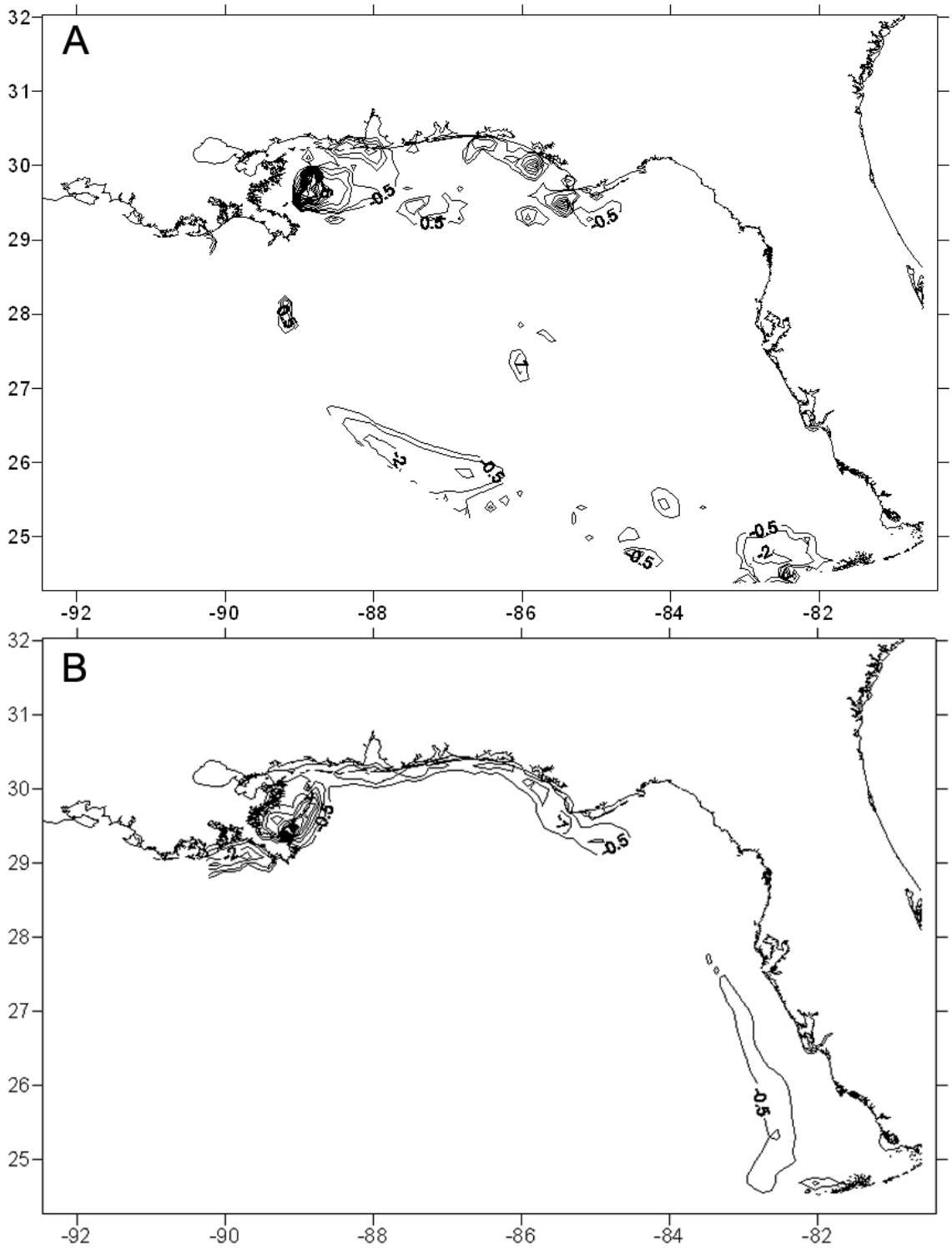

Figure 21. The simulated flux (mmol m^{-2} day^{-1}) of A) total inorganic nitrogen and B) inorganic phosphorus across the sediment water interface during 9 May 1998 in case 1 of the model.

present simulation were significantly less than those of the previous analysis, but were consistent with observations at the 27 m isobath in the South Atlantic Bight where similar sediment permeabilities are found. Overall, simulated nutrient concentrations in the surface sediment pore waters (Figs. 19,20) were nearly equal to those of the near-bottom water (Figs. 17,18) due to the rapid flushing of these highly permeable sediments. Although flushing of the sediments was rapid, net fluxes of nutrients across the sediment/water interface were small and predominantly into the sediment (Fig. 21), rather than out of the sediments as calculated in the one-dimensional analysis and observed in the South Atlantic Bight. Large influxes of nitrogen and phosphorus were simulated near the mouth of the Mississippi river. In the real world, particles are transported deeper than 4 cm into the sediments where they are eventually broken down to dissolved organic and inorganic nutrients through digenetic processes. This cycle, absent from the present model, typically leads to high concentrations of dissolved nutrients in the deep sediments relative to the water column and therefore an efflux of nutrients from the sediments to the bottom waters.

Simulated surface chlorophyll concentrations in the water column were approximately 0.5 $\mu g\ l^{-1}$ over most of the West Florida Shelf (Fig. 22A). This is higher than concentrations observed during the NEGOM program on the West Florida Shelf (Fig. 22B). Simulated and observed surface chlorophyll concentrations were both elevated along the northern Gulf coast.

Near-bottom chlorophyll concentrations in the model were similar to most of the real world observations, but the simulation missed some of the enhanced

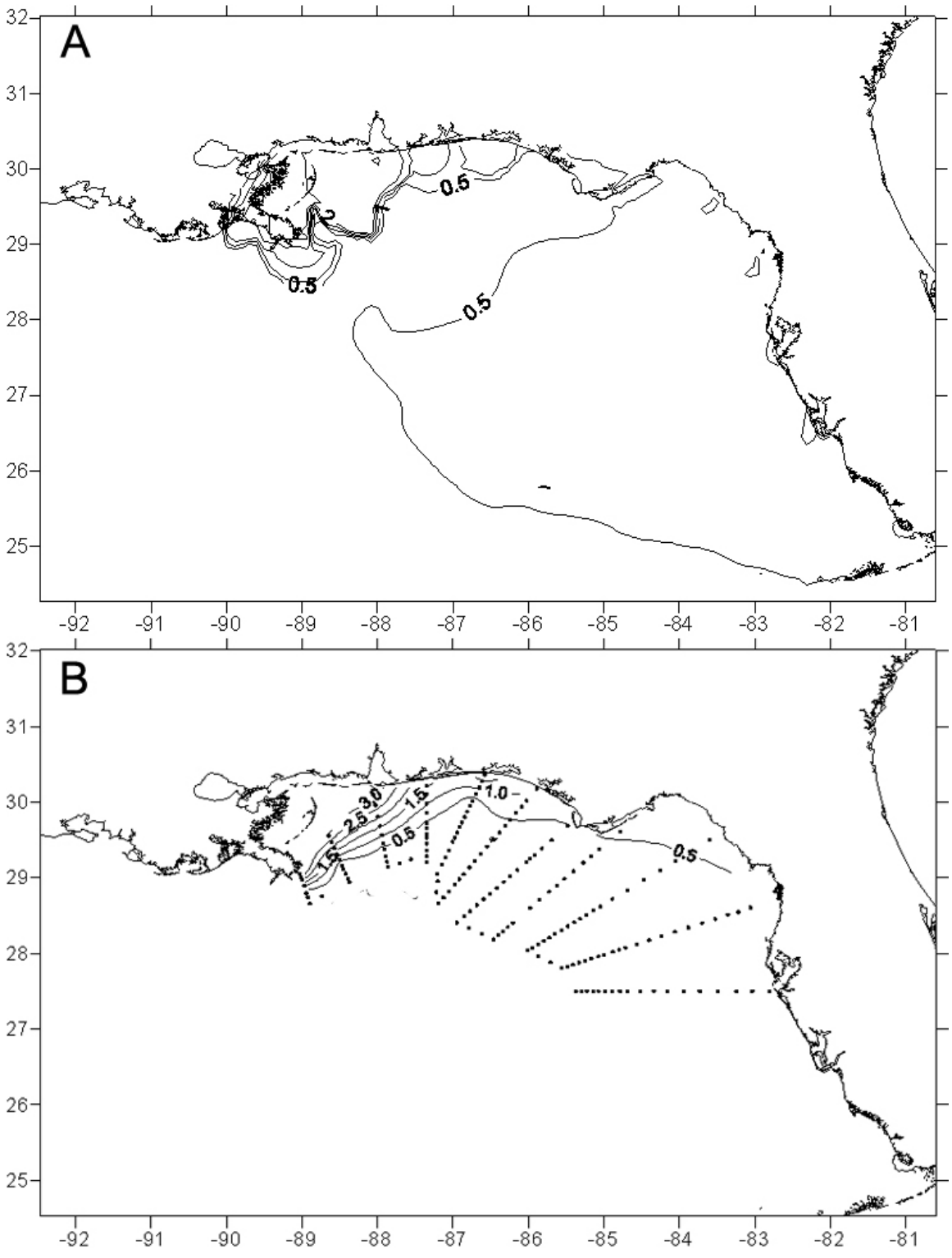

Figure 22. The A) simulated and B) observed surface chlorophyll concentrations ($\mu g\ l^{-1}$) in the eastern Gulf of Mexico during 9 May, 1998.

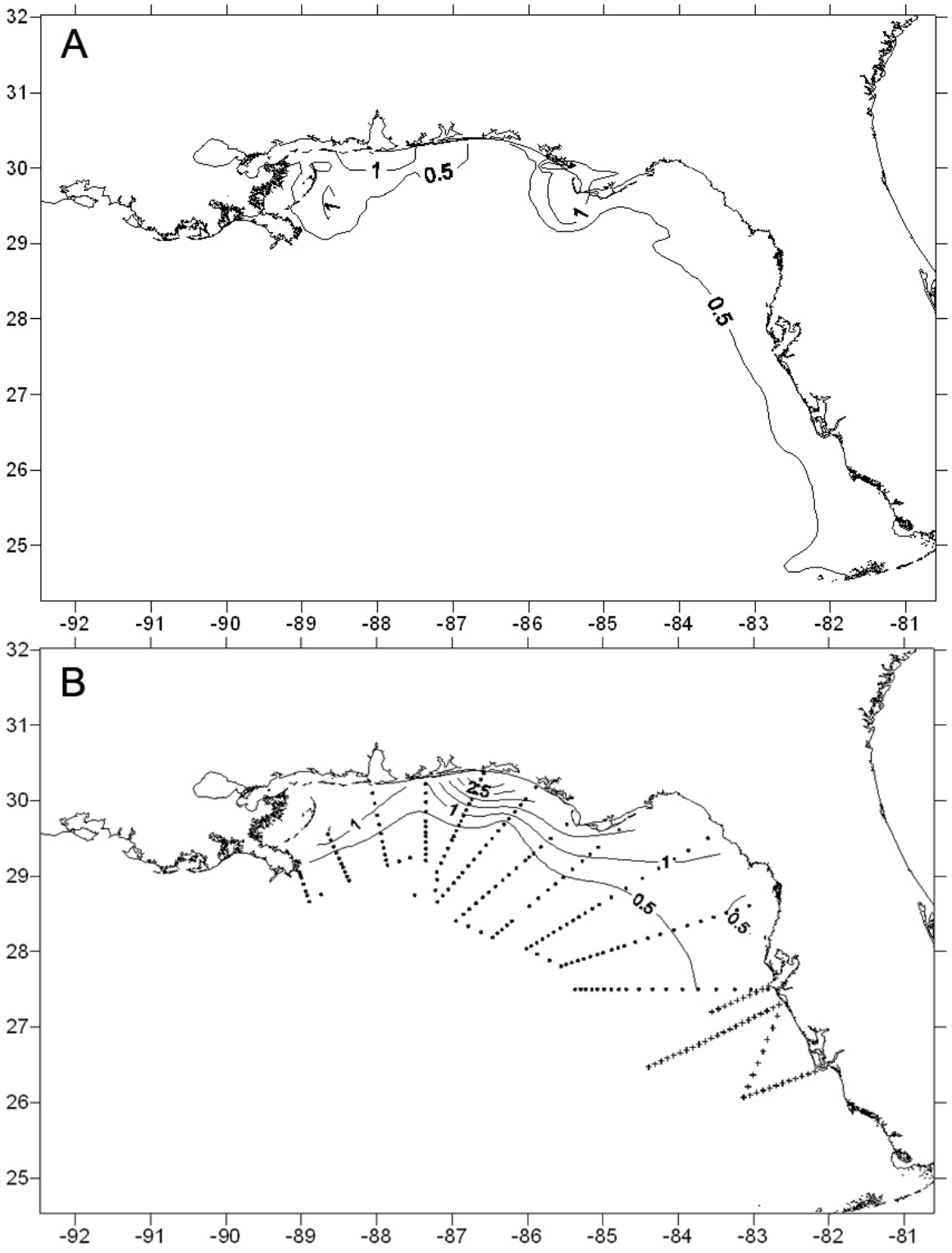

Figure 23. The A) simulated and B) observed near-bottom chlorophyll concentrations ($\mu g\ l^{-1}$) in the eastern Gulf of Mexico during 9 May, 1998.

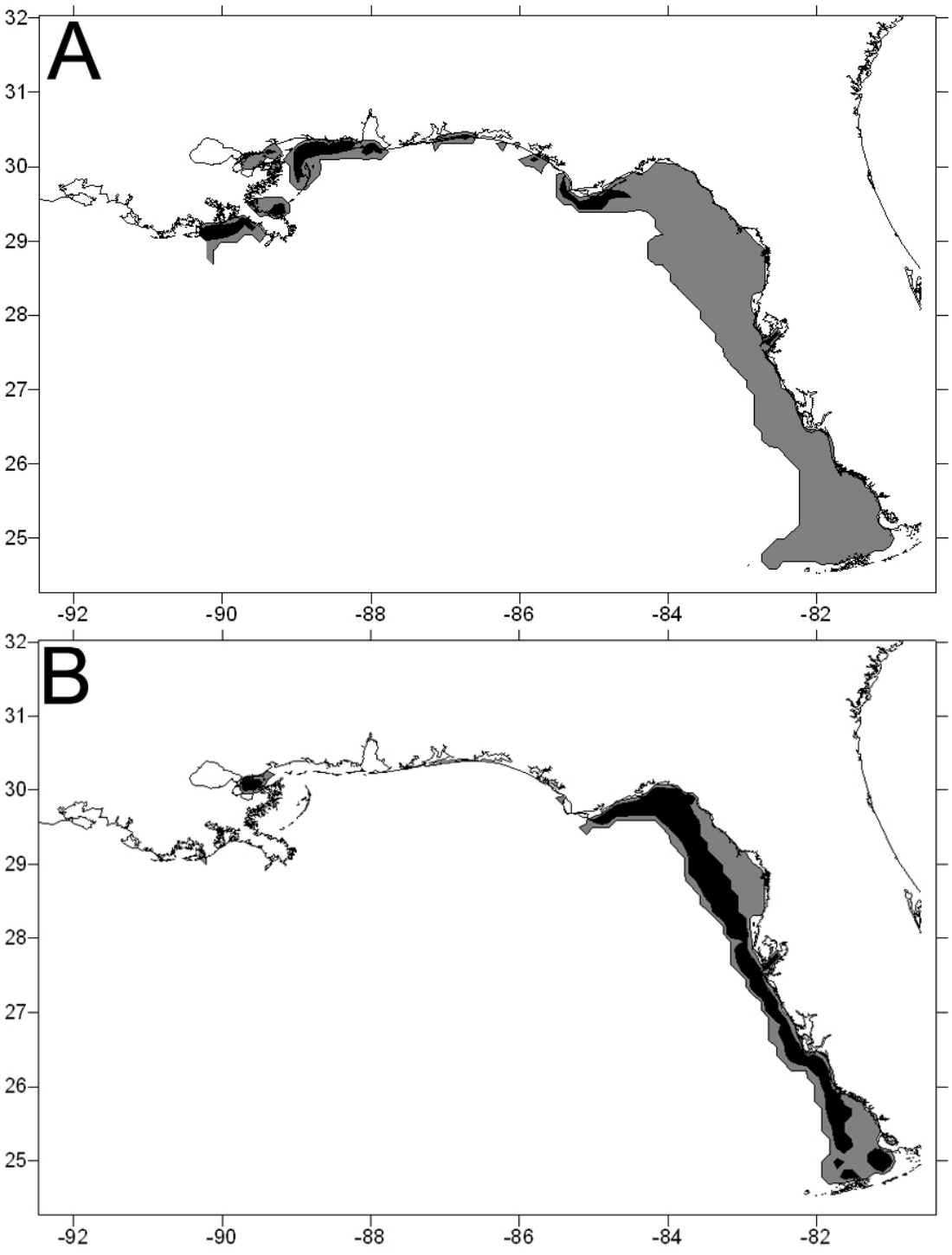

Figure 24. Simulated limiting factors in the growth of near-bottom A) diatoms and B) flagellates during 9 May, 1998. White represents light, grey represents nitrogen and black represents phosphorus.

near-bottom concentrations along the northern Gulf coast. Although the simulated near-bottom chlorophyll concentrations were highest near the northern coast, reaching 1.4 $\mu g\ l^{-1}$ (Fig. 23A), the observed concentrations there were as high as 2 $\mu g\ l^{-1}$ (Fig. 23B). While light was a limiting factor for much of the day, the diatoms were limited mostly by nitrogen availability when light levels were at their highest (Fig. 24A). The diatoms were limited by phosphorus in some areas along the northern Gulf coast. Flagellates were limited by phosphorus where they reached their highest concentrations on the West Florida Shelf (Fig. 24B). In lower concentrations, the flagellates were limited by nitrogen.

Simulated benthic chlorophyll only reached maximum stocks of approximately 5 mg m^{-2} over the top 2 mm of sediment on the West Florida Shelf and Gulf Coast by May 9 (Fig. 25A), compared to similar stocks observed by G. Vargo in April 1993 (Fig. 11A). Benthic chlorophyll stocks reached as high as 10 mg m^{-2} near the mouth of the Mississippi River.

In the narrow band on the West Florida shelf, where benthic chlorophyll stocks were greater than 5 $\mu g\ l^{-1}$, the benthic diatoms were limited by light for the first 3 hours after sunrise. As light levels continued to increase, the benthic diatom growth became nitrogen limited and remained so for the next 6.5 hours (Fig 26). As light levels decreased, the diatoms were again limited by light beginning about 3 hours before sunset. Similar patterns were observed elsewhere across the model domain, although phosphorus was the mid-day limiting factor along the northern Gulf coast.

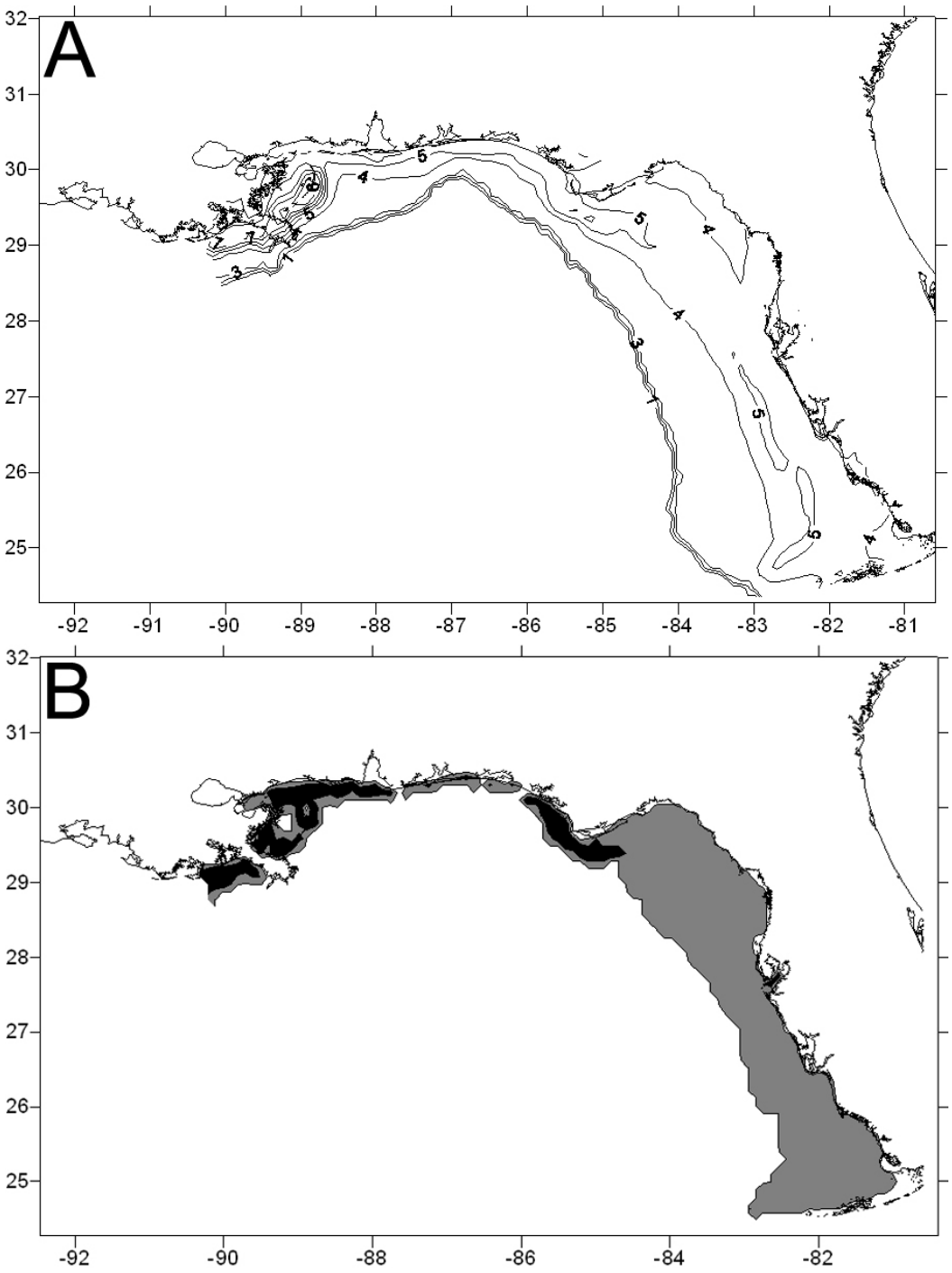

Figure 25. Simulated A) benthic chlorophyll stocks (mg m^{-2}) integrated over the top 2 mm of sediment on 9 May, 1998 and B) their limiting factors. White represents light, grey represents nitrogen and black represents phosphorus.

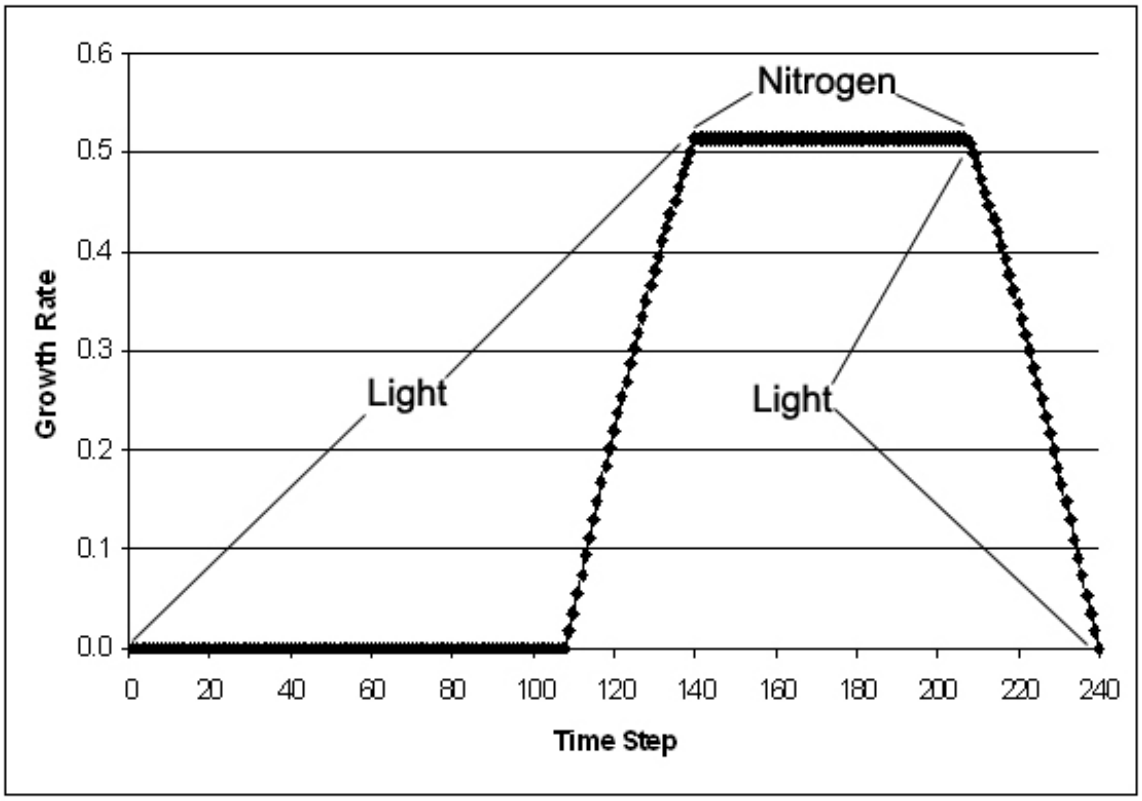

Figure 26. Simulated growth rate (day^{-1}) and limiting factors affecting the growth rate of benthic diatoms in the Florida Middle Grounds during 9 May, 1998.

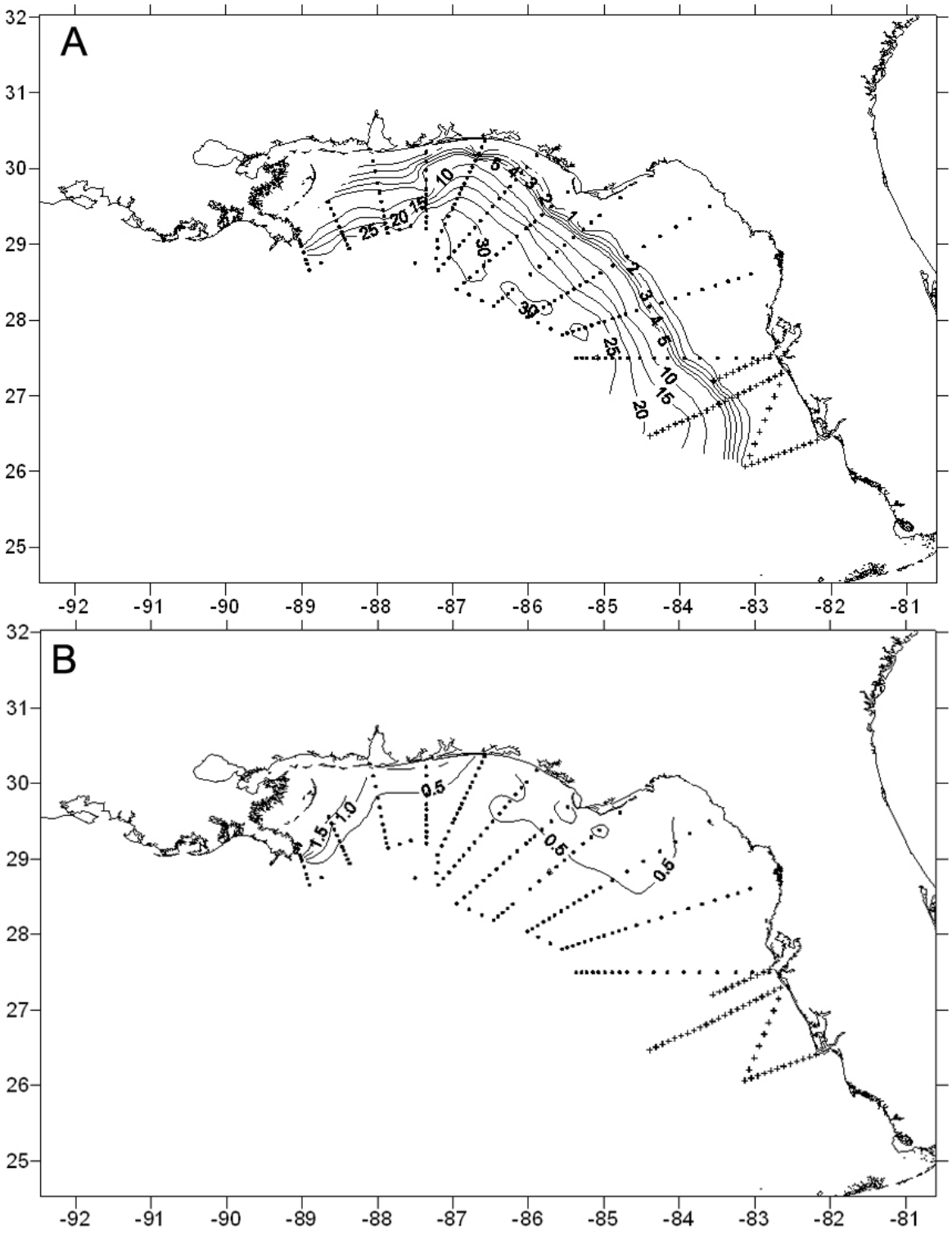

Figure 27. Observations of A) NO_3 (μmol kg^{-1}) and B) NH_4 (μmol kg^{-1}) in the near bottom waters of the eastern Gulf of Mexico during August 1998 from the NEGOM (◆) and ECOHAB Florida (+) programs.

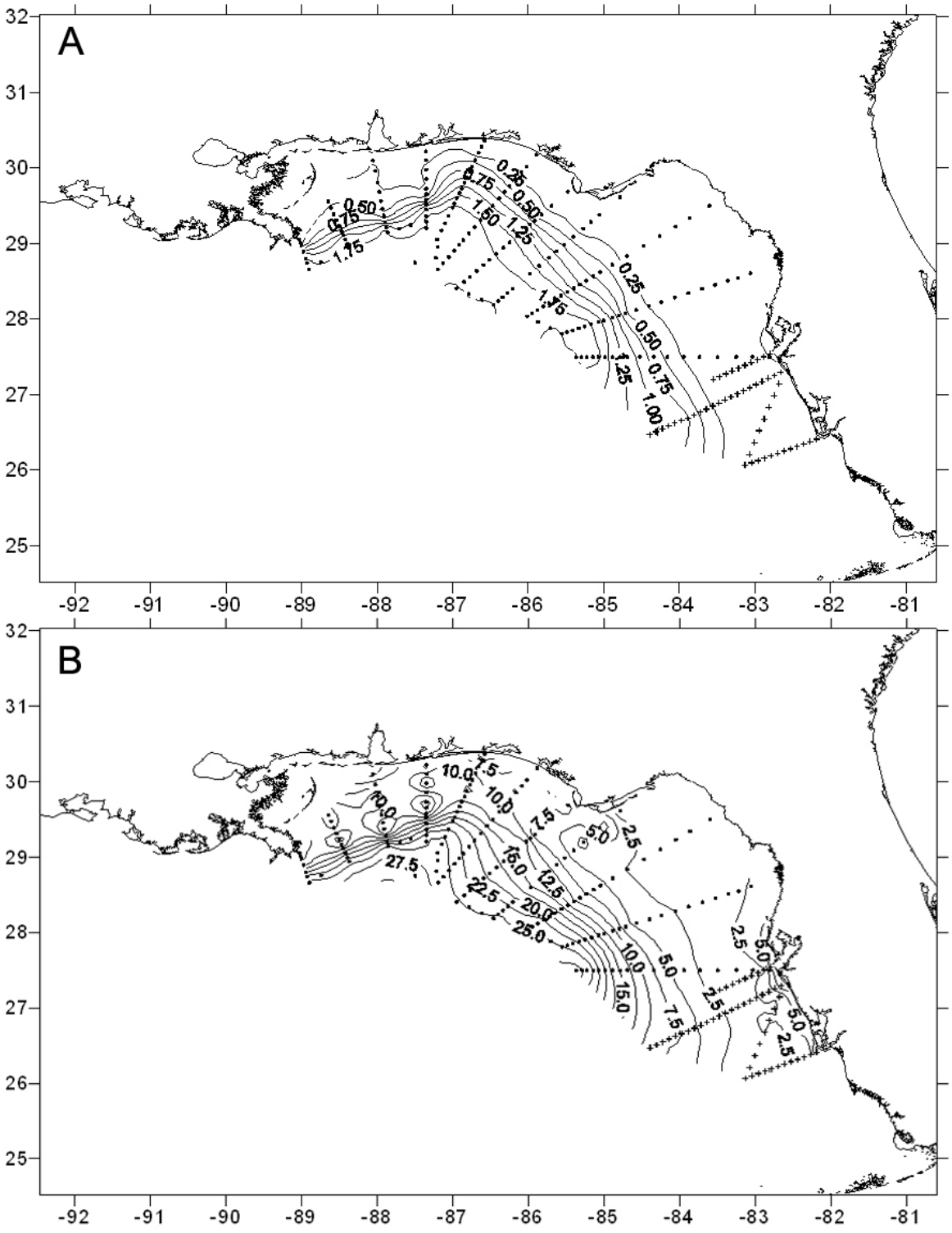

Figure 28. Observations of A) PO_4 (μmol kg^{-1}) and B) SiO_4 (μmol kg^{-1}) in the near bottom waters of the eastern Gulf of Mexico during August 1998 from the NEGOM (◆) and ECOHAB Florida (+) programs.

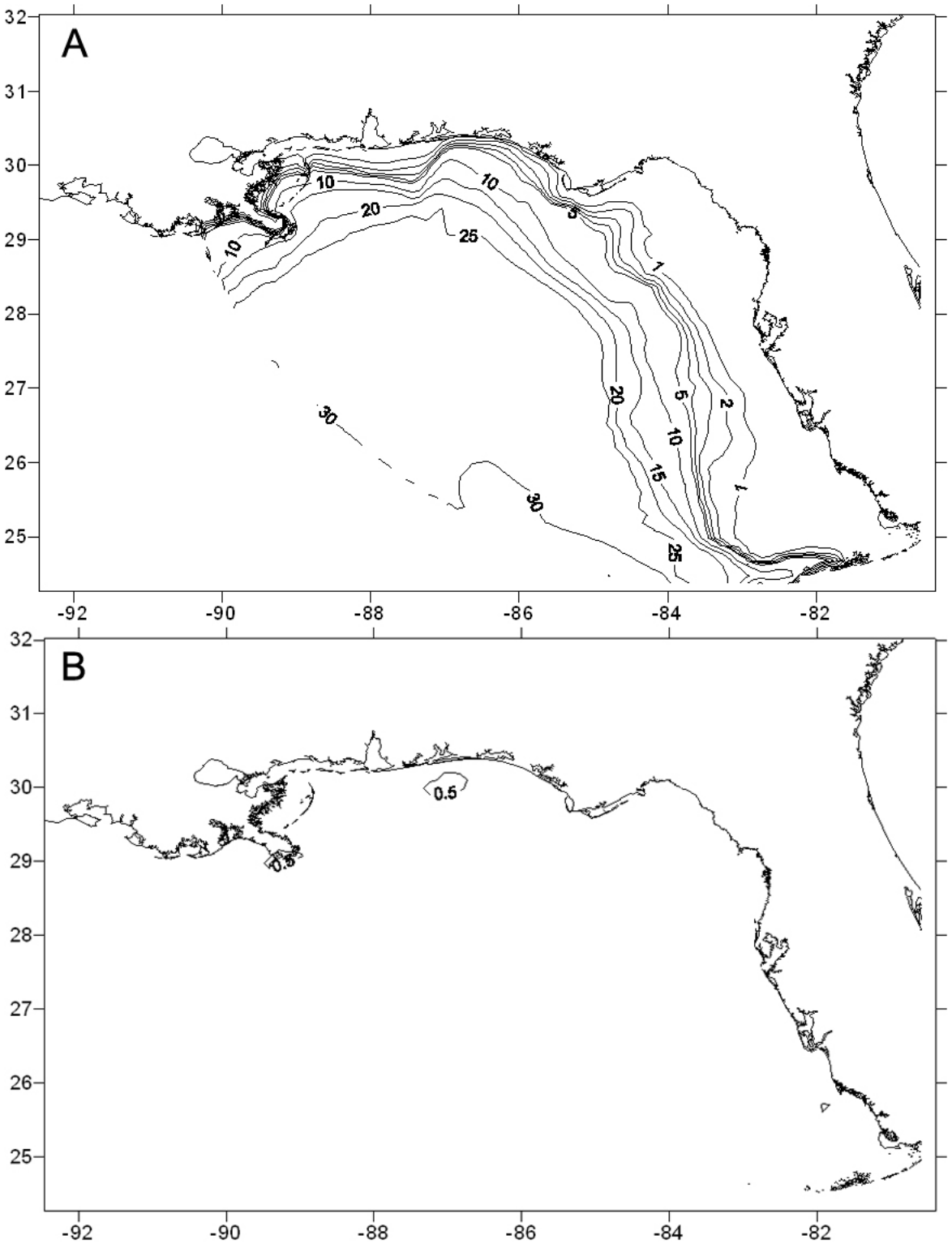

Figure 29. Simulated near-bottom concentrations of A) NO_3 (μmol kg^{-1}) and B) NH_4 (μmol kg^{-1}) during 6 August, 1998.

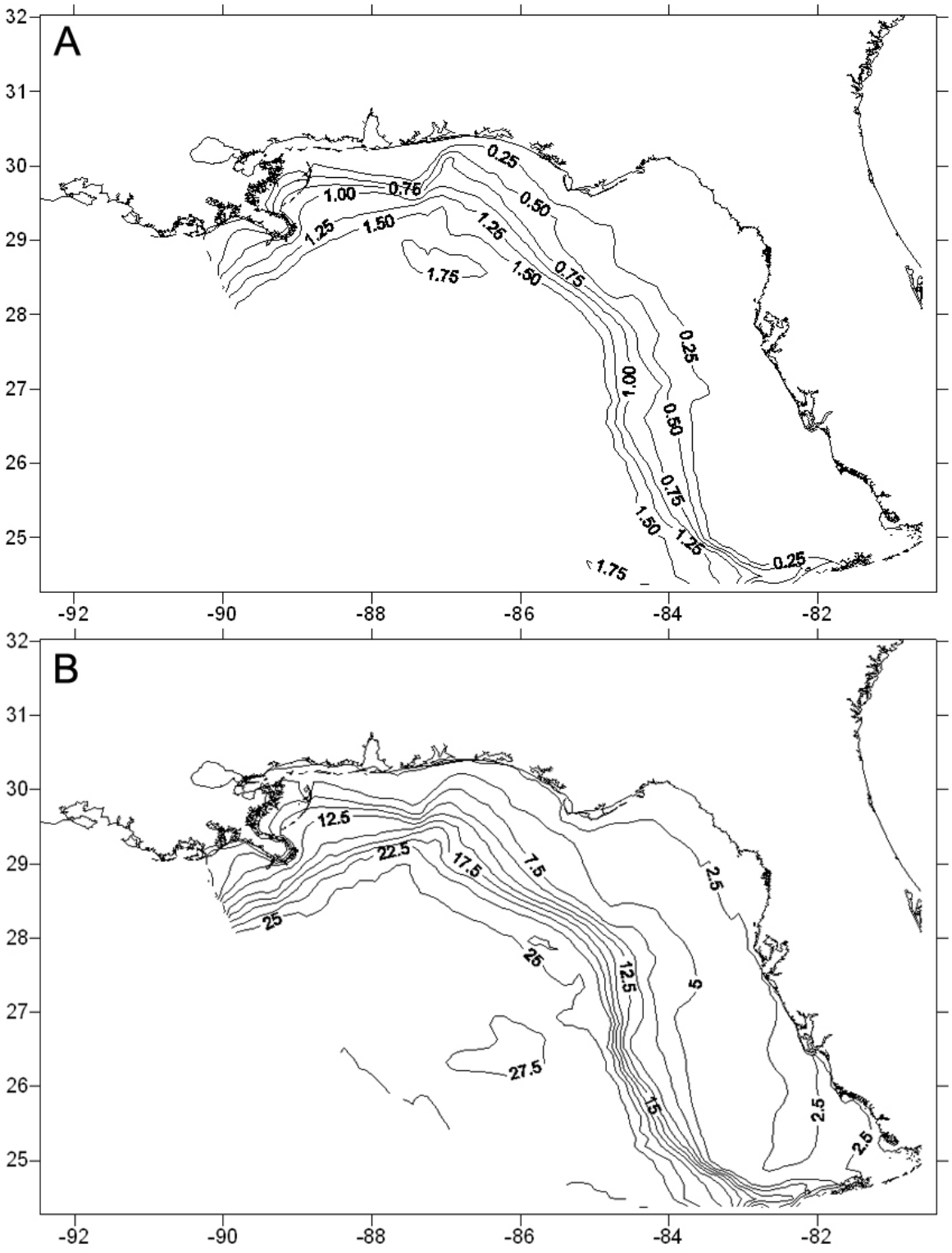

Figure 30. Simulated near-bottom concentrations of A) PO_4 (μmol kg^{-1}) and B) SiO_4 (μmol kg^{-1}) during 6 August, 1998.

1.2 Summer 1998

As observed during the NEGOM and ECOHAB:Florida cruises (Fig. 27A), the simulated near-bottom algae (Fig. 35) had depleted near-bottom nitrate stocks over the continental shelf by early August 1998, with the 1 μmol kg^{-1} isopleth now penetrating only to the 50 m isobath (Fig. 29A). On the southern West Florida Shelf, where the near-bottom algae was limited primarily by phosphorus (Fig. 36), the 1 μmol kg^{-1} isopleth of nitrate still penetrated as far as the 20 m isobath (Fig. 29).

Near-bottom NH_4 concentrations were elevated only in isolated areas near the mouth of the Mississippi river and Mobile Bay (Fig. 29B). The locations of elevated NH_4 coincide with field measurements of increased near-bottom ammonium during the July 1998 NEGOM cruise (Fig. 27B), but the observed NH_4 occupied a much wider area.

Simulated near-bottom PO_4 concentrations (Fig. 30A) were very similar to those observed (Fig. 28A), with the 0.25 μmol kg^{-1} isopleth penetrating nearly all the way to coast near the Alabama/Florida border. Elsewhere, the 0.25 μmol kg^{-1} isopleth of PO_4 penetrated only to the 50 m isobath.

In August 1998, elevated near-bottom silicate concentrations of 7.5 μmol SiO_4 kg^{-1} (Fig. 28B) were measured nearshore on the West Florida Shelf, especially near the mouth of Tampa Bay. Along the northern Gulf of Mexico coast, silicate concentrations as high as 10 μmol kg^{-1} reached the shore. The simulation reflected elevated silica concentrations from the deep water source

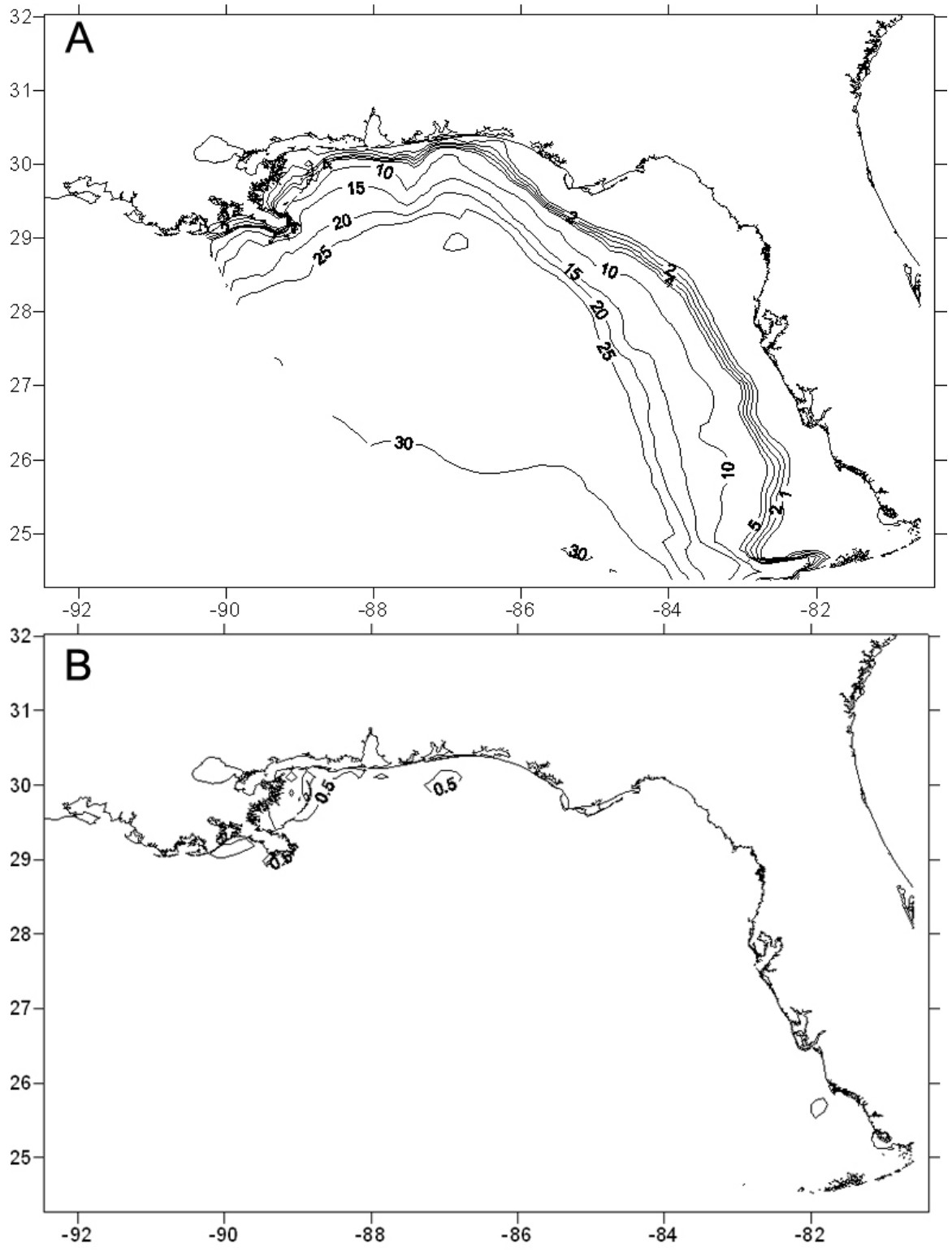

Figure 31. Simulated porewater concentrations (μmol kg^{-1}) of A) NO_3 and B) NH_4 during 7 August, 1998.

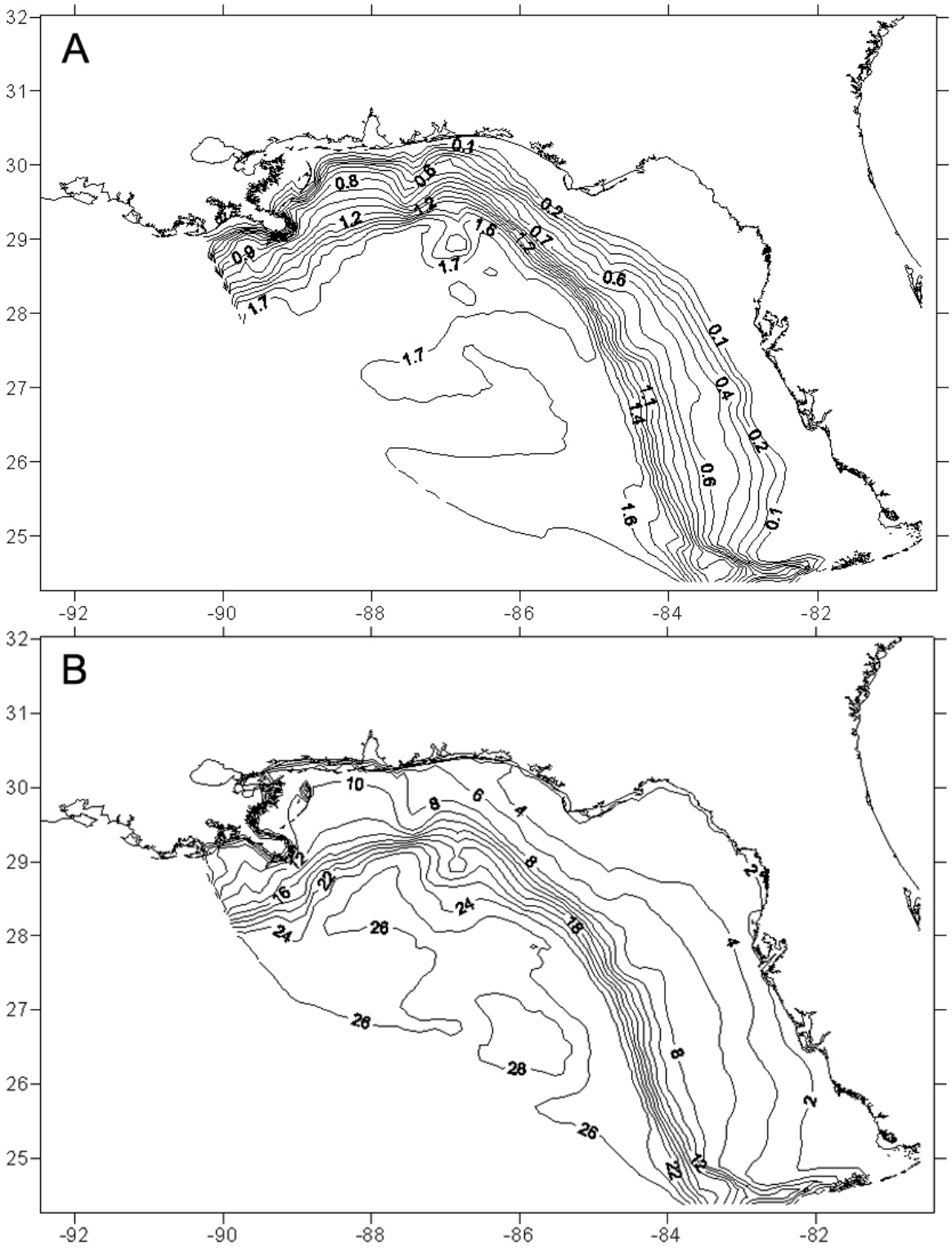

Figure 32. Simulated porewater concentrations (μmol kg^{-1}) of A) PO_4 and B) SiO_4 during 7 August, 1998.

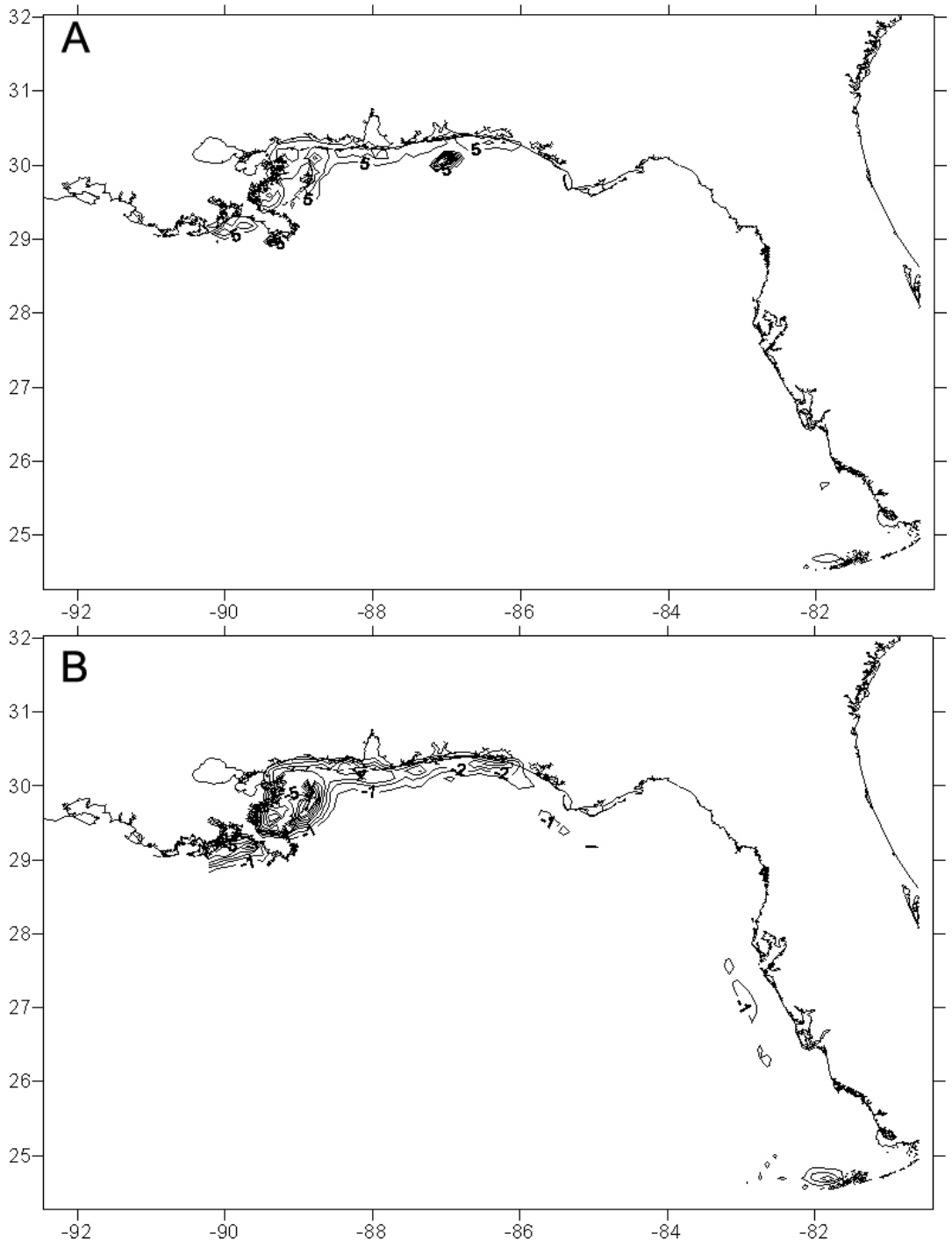

Figure 33. The simulated flux (mmol m^{-2} day^{-1}) of A) dissolved inorganic nitrogen and B) dissolved inorganic phosphorus across the sediment water interface during 7 August, 1998. Negative numbers indicate a flux into the sediments.

penetrating all the way to the shore near Tampa Bay and along the southern west coast of Florida (Fig. 30B), but did not replicate the estuarine source of silicate suggested by the real world observations. Simulated summer local stocks of silicate in the Big Bend region of Florida were larger than those observed. In contrast, the May silicate observations were greater than those simulated there.

Simulated sediment NH_4 concentrations in August (Fig. 31B) were the same as simulated near-bottom NH_4 concentrations. Elevated stocks of ammonium near the mouth of the Mississippi River and southeast of Mobile Bay amounted to 6 μmol NH_4 kg^{-1}. Large fluxes of Nitrogen out of the sediments (Fig. 33A) occurred at these locations. Simulated porewater nitrate concentrations (Fig. 31A) also mirrored simulated near-bottom nitrate concentrations (Fig 29A) over most of the eastern Gulf of Mexico.

Simulated porewater phosphate concentrations (Fig. 32A) were also similar to their near-bottom counterparts (Fig 30A). On the whole, however, porewater phosphate concentrations were elevated nearer to the shore on the West Florida Shelf than the near-bottom phosphate concentrations. Flux of phosphate was predominantly into the sediments over the entire Eastern Gulf of Mexico (Fig. 33B), with the greatest influx of PO_4 near the mouth of the Mississippi River, like nitrogen. Again, the influx of phosphate at the sediment surface is likely an artifact of this model's lack of deep sediments.

The total simulated surface chlorophyll (Fig. 34A) was consistent with surface observations of chlorophyll (Fig. 34B) offshore, where concentrations

reached 1.5 μg l^{-1}. The modeled pythoplankton stocks were not as high as those measured near the mouth of the Mississippi River and Tampa Bay. Simulated near-bottom chlorophyll (Fig. 35A) was elevated in the Southern West Florida Shelf, the Northeastern Gulf Coast and the Northwestern Gulf Coast. Both simulated functional groups of near-bottom phytoplankton were limited primarily by phosphorus in their greatest concentrations (Fig. 36). Light was the primary limiting factor for flagellates along the northern Gulf coast, while the near-bottom diatoms there managed to outcompete the flagellates under phosphorus limitation. There was no silica limitation at any point in the simulation.

Benthic chlorophyll was greatest along the 50 m isobath, where light limitation and nutrient remineralization yielded chlorophyll stocks of 8.6 mg m^{-2}. Maximum stocks of 12 mmol m^{-2} over the top 2 mm sediment were simulated near the Mississippi River (Fig. 37A). In their greatest concentrations, these benthic diatoms were limited mostly by phosphorus (Fig. 37B), like those simulated in the previous 1-D analysis (Darrow et al 2003). Like the spring, CO_2 evaded the water column almost the entire eastern Gulf of Mexico during the summer of 1998.

2. Case 2

After initiating an artificial bloom on 1 April 1998 to simulate the effects of recycled nutrients from a surface phytoplankton bloom on the benthos, the simulated surface chlorophyll in case 2 reached maximum levels of 1.7 μg l^{-1} on

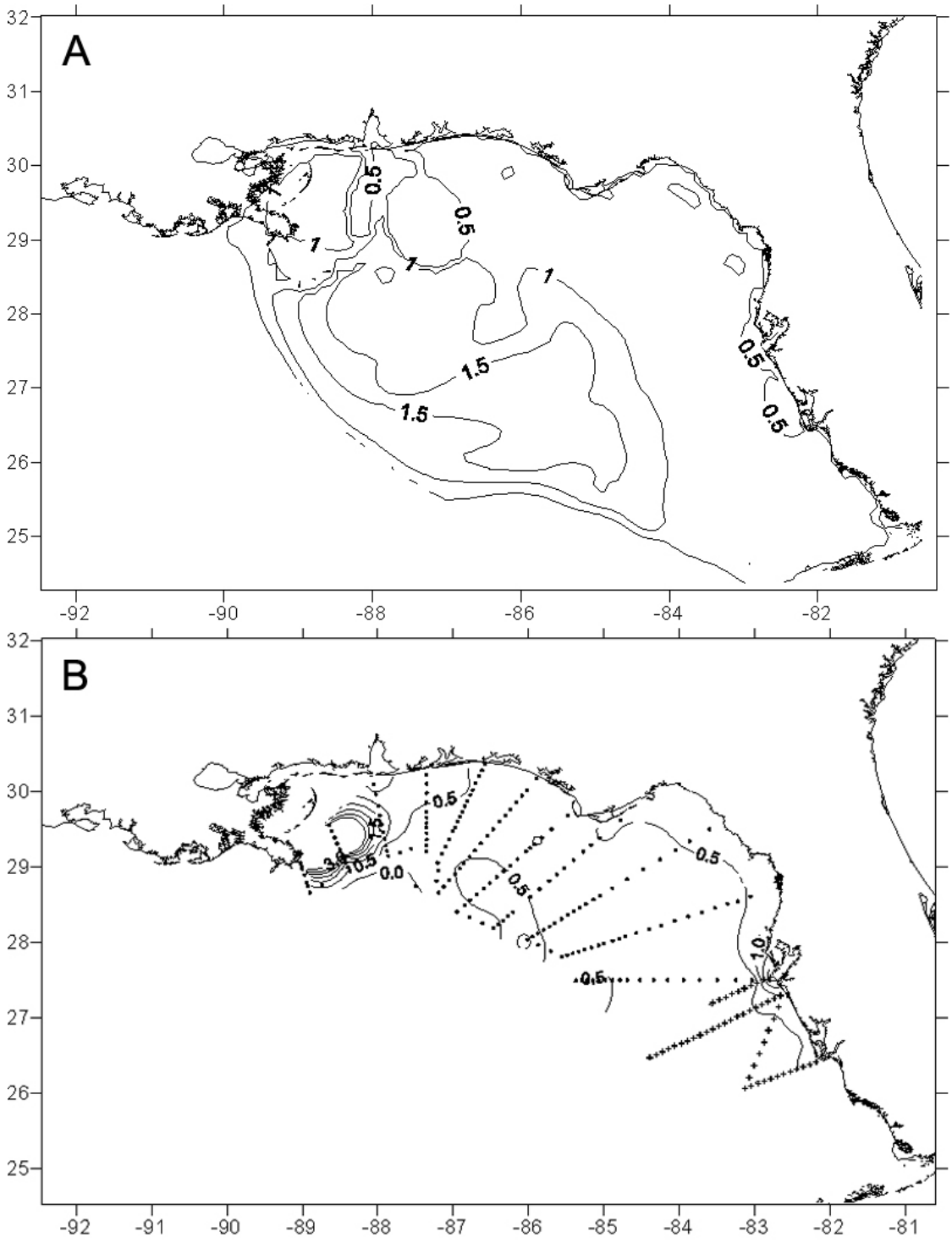

Figure 34. Cumulative surface chlorophyll concentrations ($\mu g\ l^{-1}$) A) from diatoms and flagellates simulated in case 1 of the model and B) observed during the NEGOM (◆) and ECOHAB (+) cruises of August 1998.

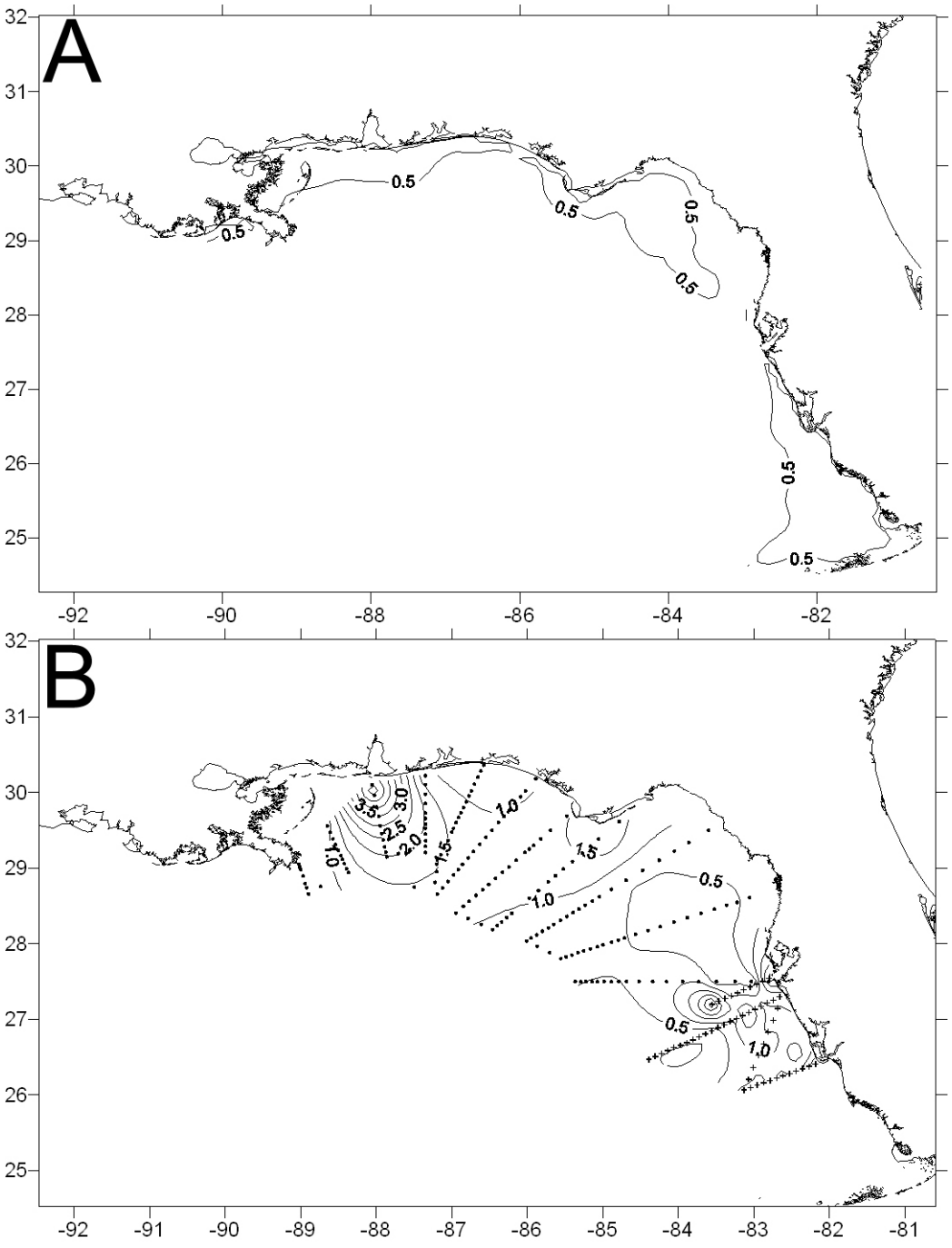

Figure 35. Cumulative near-bottom chlorophyll concentrations ($\mu g\ l^{-1}$) A) from diatoms and flagellates simulated in case 1 of the model and B) observed during the NEGOM (◆) and ECOHAB: Florida (+) cruises of August 1998.

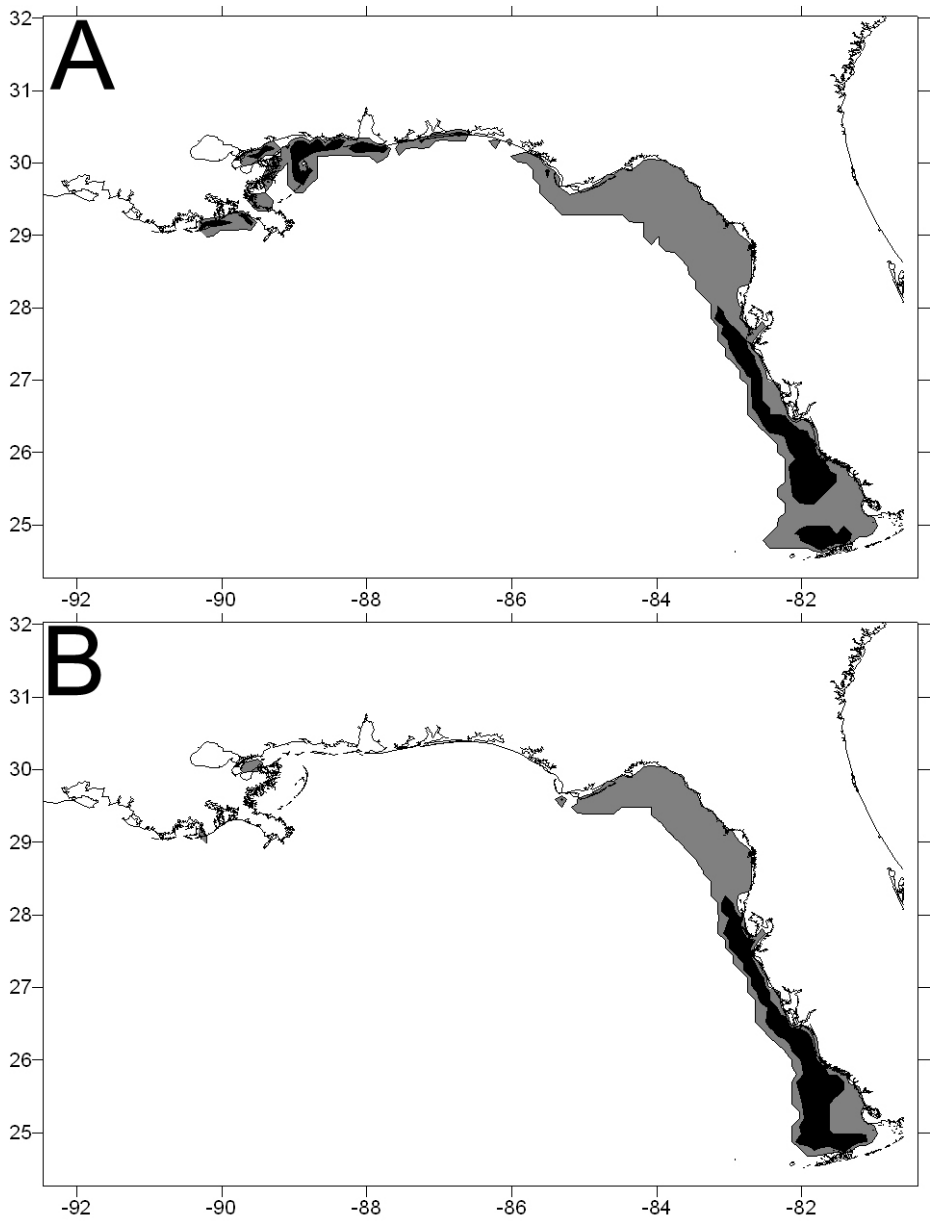

Figure 36. The simulated factors limiting the growth of A) diatoms and B) flagellates in the near-bottom waters of case 1 of the model during 7 August, 1998. White represents light, grey represents nitrogen and black represents phosphorus.

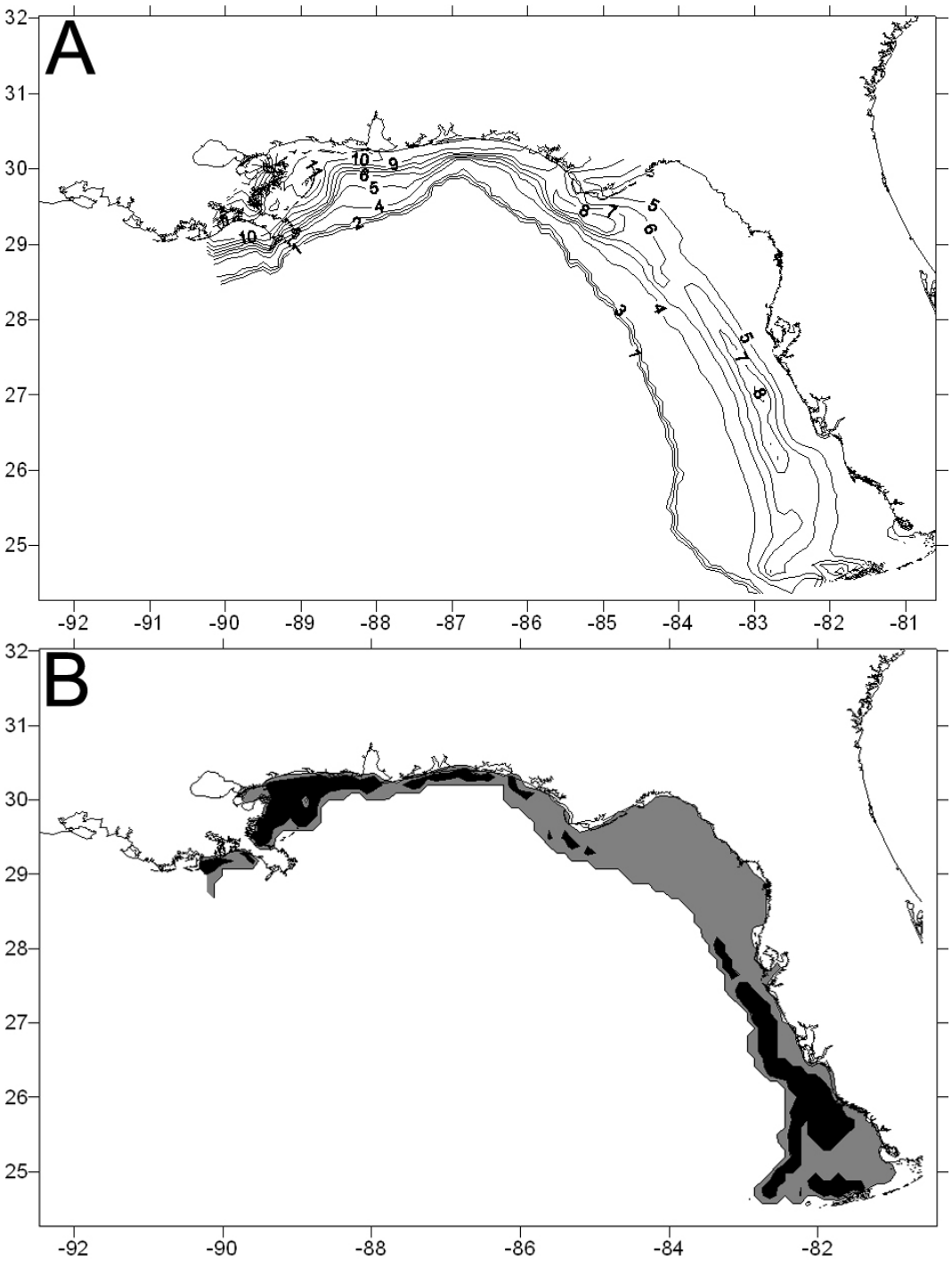

Figure 37. Simulated A) Benthic chlorophyll stocks (mg m^{-2}) integrated over the top 2 mm of sediment during 7 August , 1998 and B) the factors limiting their growth. White represents light, grey represents nitrogen and black represents phosphorus.

15 April 1998 (Fig. 38A). By contrast, maximum simulated surface chlorophyll stocks on 15 April 1998 in case 1 of the model were only 0.765 $\mu g\ l^{-1}$ (Table 5). From the site of the artificial bloom, surface phytoplankton drifted east-northeastward during the 14 day period, resulting in enhanced chlorophyll concentrations near the shore relative to case 1 of the model (Fig 39). Some chlorophyll was present in the near-bottom waters through the sinking of live diatoms such that phytoplankton grew there off the recycled nutrients from sinking detritus and fecal pellets. Although the maximum chlorophyll stocks in the near-bottom waters of the West Florida Shelf were not different from case 1 (Table 5), simulated near-bottom chlorophyll stocks, greater than 0.5 $\mu g\ l^{-1}$ covered a larger area than in case 1 of the model (Fig. 40) by 15 April, 1998. Near-bottom phytoplankton in case 2 continued to thrive a week later and a small near-bottom chlorophyll plume extended northwestward, reaching the 20-m isobath by 23 April, 1998 (Fig. 41) in case 2.

The simulated near-bottom phytoplankton assemblage on the West Florida Shelf during 23 April, 1998 in both cases of the model was evenly mixed between diatoms and flagellates, with flagellates more prevalent near shore and diatoms more prevalent offshore. The near shore extent of diatom domination was greater, however, during case 2 of the model. Diatoms constituted more than 50% of the total phytoplankton assemblage nearly all the way to the coast in this case of the model, in contrast to case 1 where the diatom domination extended only to the 10-m isobath (Fig 42). In both cases of the model, the near-bottom diatoms were limited by nitrogen availability and the near-bottom

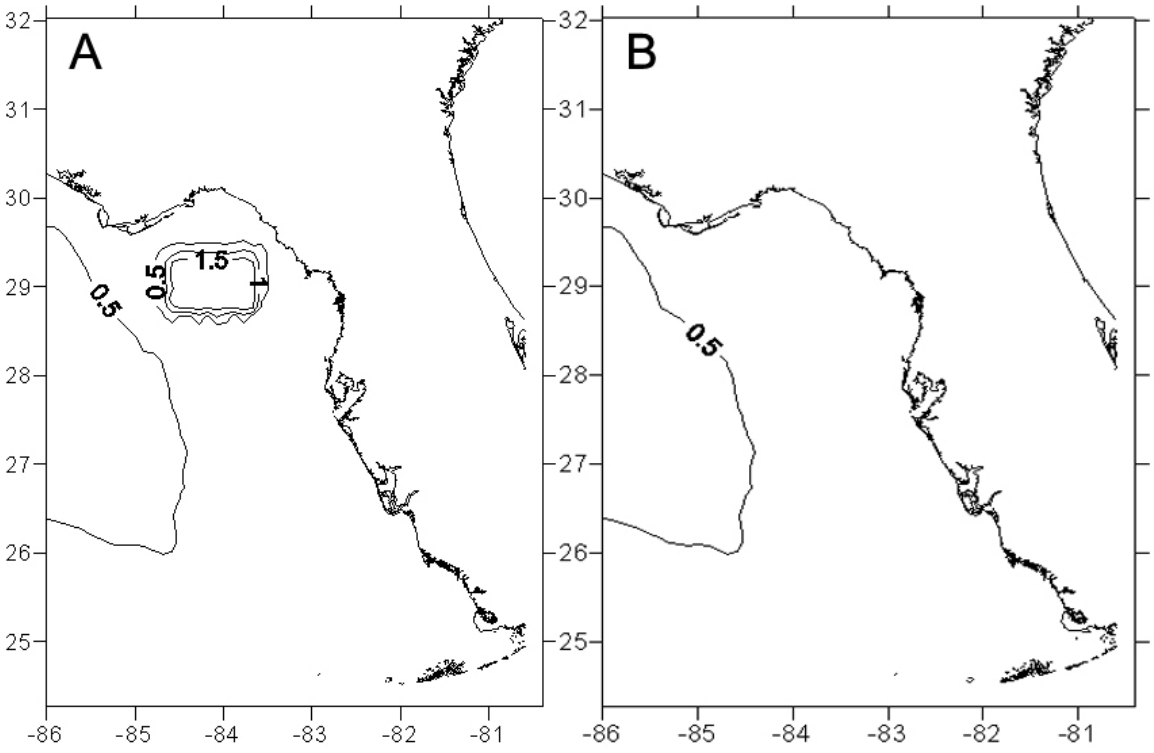

Figure 38. Simulated total surface chlorophyll (μg/l) from diatoms and flagellates during 1 April, 1998 in the A)case 2 and B) case 1 of the model.

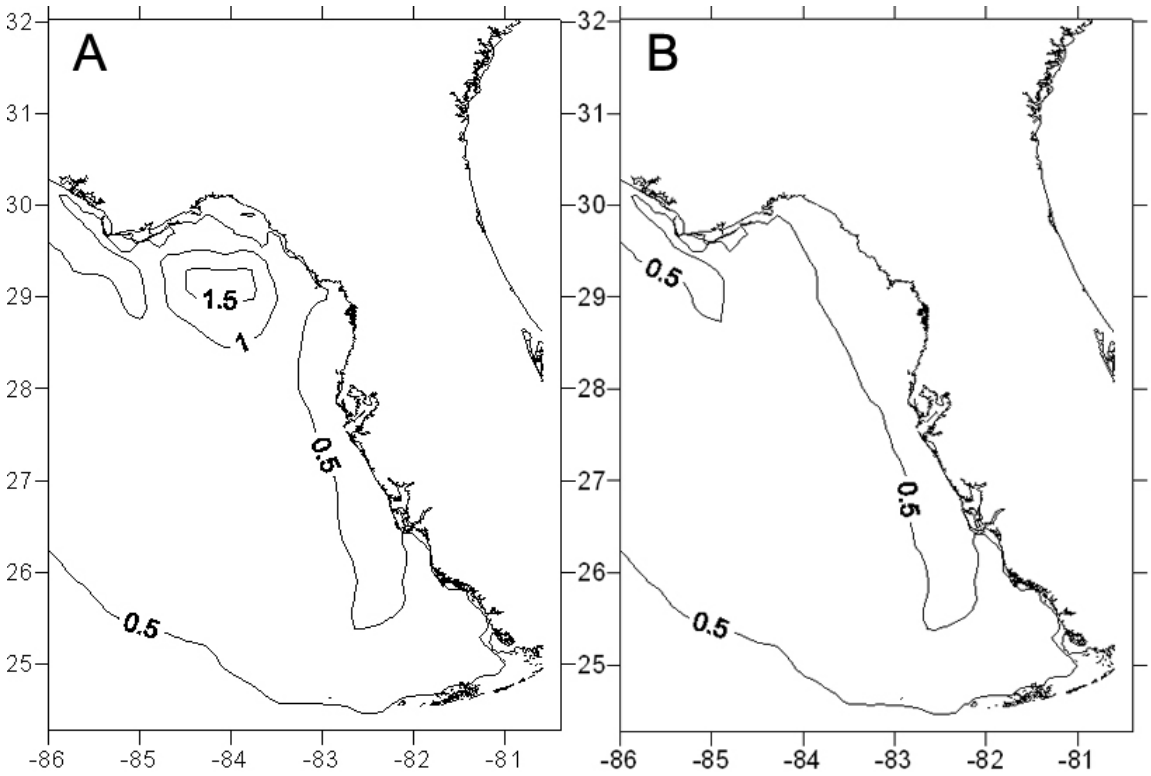

Figure 39. Simulated total surface chlorophyll (μg/l) from diatoms and flagellates during 15 April, 1998 in the A) case 2 and B) case 1 of the model.

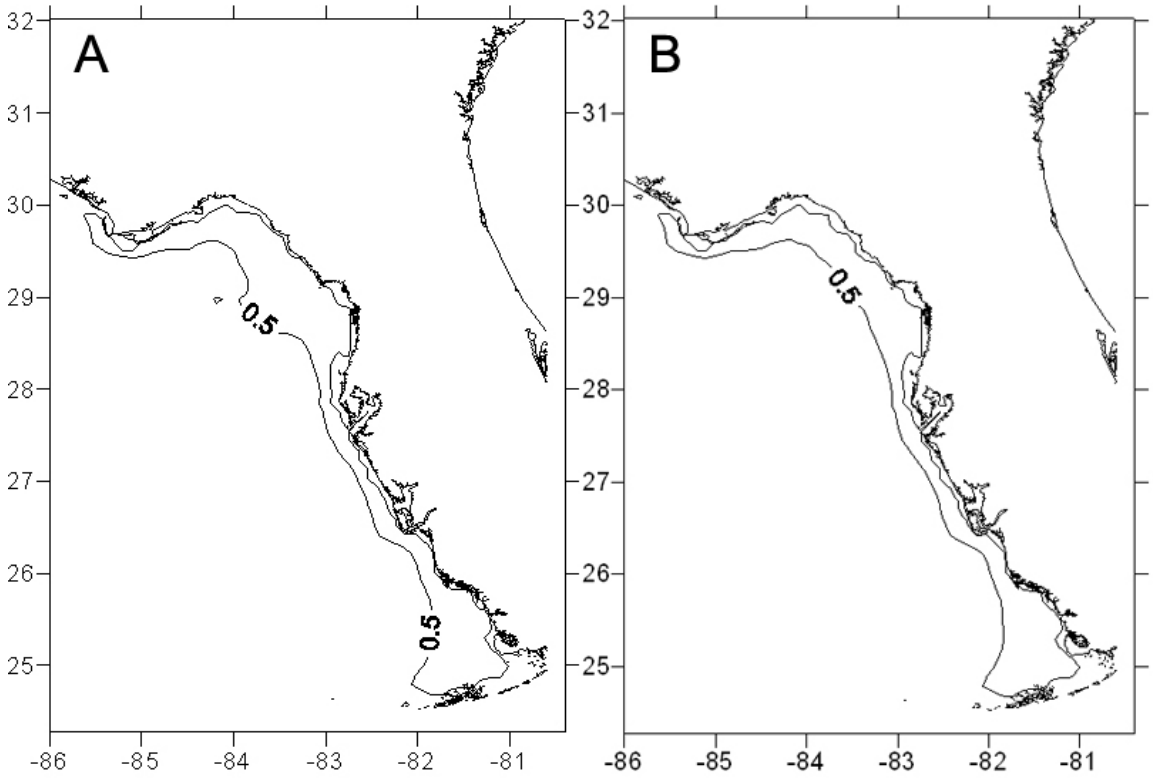

Figure 40. Simulated total near-bottom chlorophyll (μg/l) from diatoms and flagellates during 15 April 1998 in A) case 2 of the model and B) case 1 of the model.

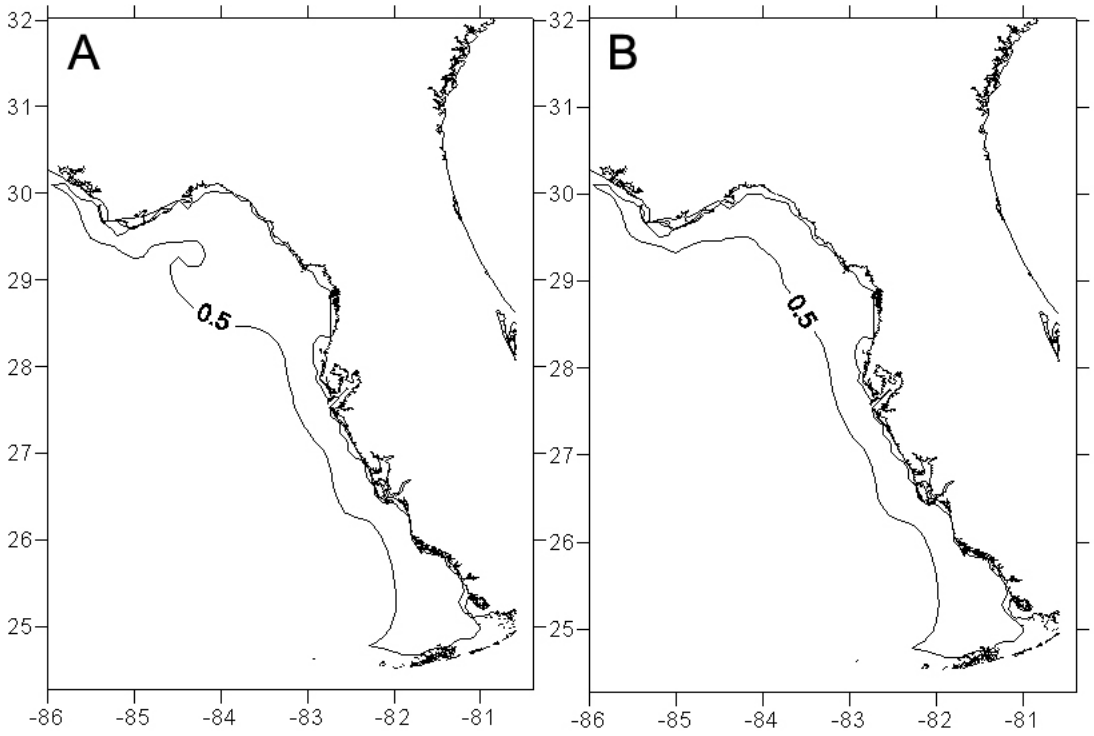

Figure 41. Simulated total near-bottom chlorophyll (μg/l) from diatoms and flagellates during 23 April 1998 in A) case 2 of the model and B) case 1 of the model.

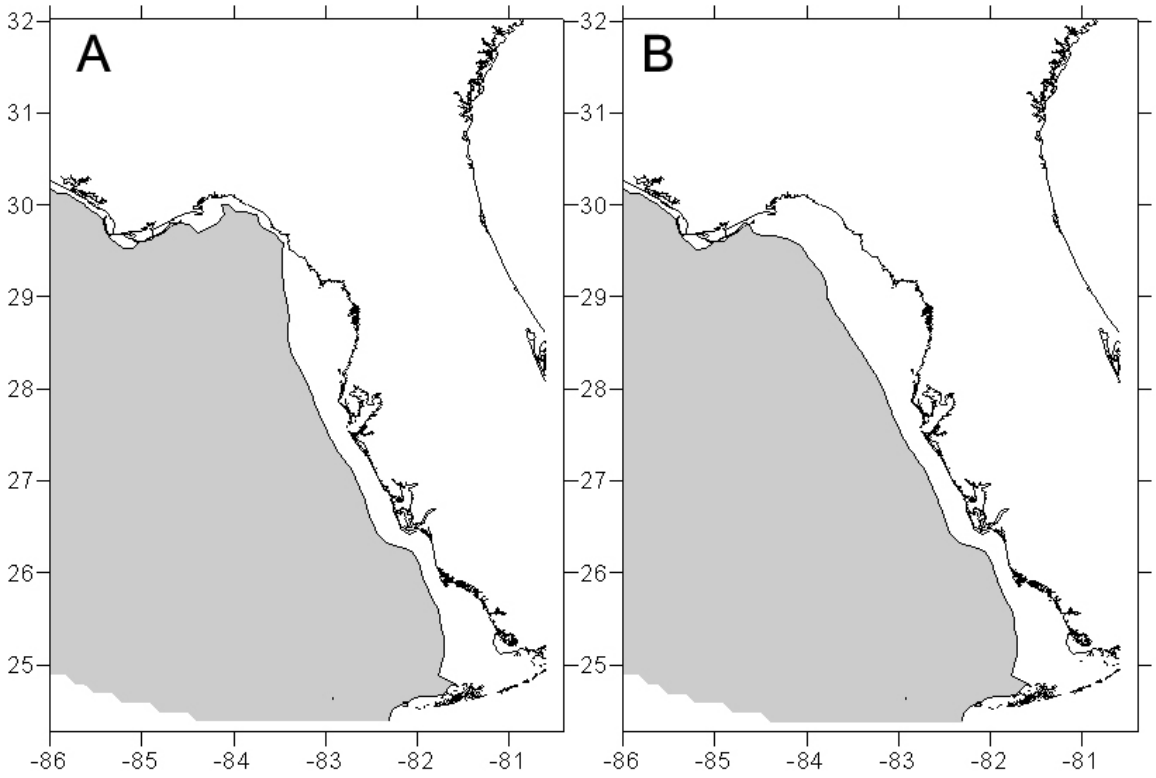

Figure 42. Simulated phytoplankton dominance in the near-bottom waters of the eastern Gulf of Mexico during 23 April 1998 in A) case 2 of the model and B) case 1 of the model. Grey indicates that diatoms were the dominant functional group, while white indicates that flagellates were the dominant functional group.

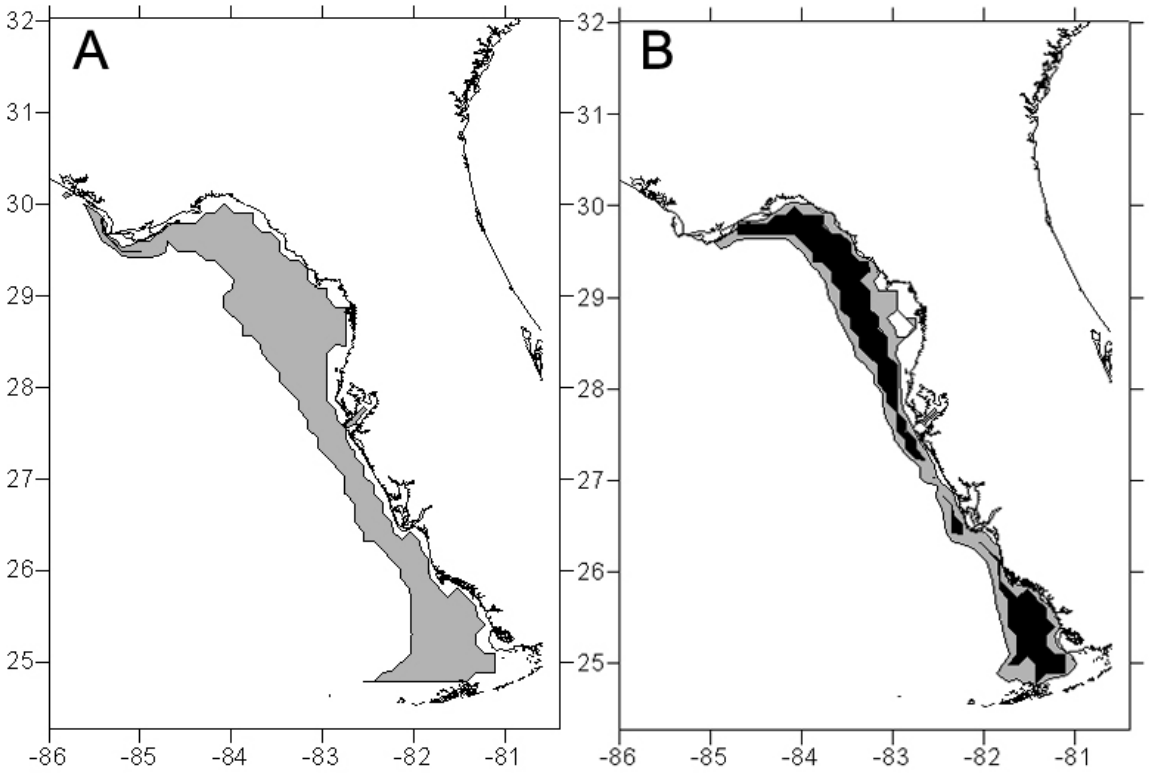

Figure 43. The simulated factors limiting the growth of A) diatoms and B) flagellates in the near-bottom waters of the eastern Gulf of Mexico during 23 April, 1998 in the case 2 of the model. White represents light, grey represents nitrogen and black represents phosphorus.

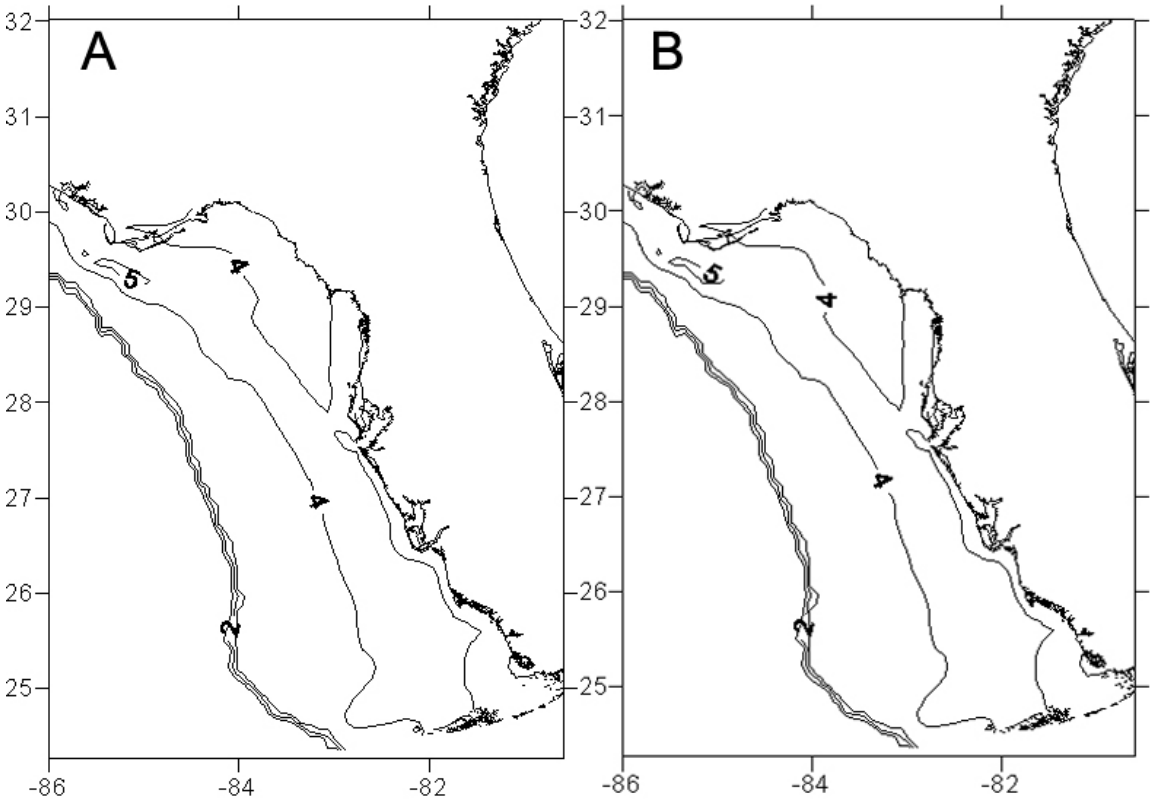

Figure 44. Simulated benthic chlorophyll stocks (mg m^{-2}) integrated over the top 5 mm of sediment during 23 April, 1998 in the A) case 2 and B) case 1 of the model.

Table 5. Comparison of the model's simulated chlorophyll stocks during the 2 model cases.

	Case 1	Case 2
WFS Max Surface Chl ($\mu g\ l^{-1}$) on April 1	0.651	1.63
WFS Max Surface Chl ($\mu g\ l^{-1}$)on April 15	0.765	1.53
WFS Max Surface Chl ($\mu g\ l^{-1}$) on April 23	0.765	0.798
WFS Max Near-Bottom Chl ($\mu g\ l^{-1}$) on April 15	0.649	0.767
WFS Max Near-Bottom Chl ($\mu g\ l^{-1}$) on April 23	0.735	0.757
WFS Max Benthic Chl ($mg\ m^{-2}$) on April 15	6.99	6.99
WFS Max Benthic Chl ($mg\ m^{-2}$) on April 23	8.42	8.42

flagellates, which are more efficient nitrogen users were limited by phosphorous availability (Fig 43).

Unlike previous studies (Darrow *et al*, 2003), where a “dump” of diatoms led to increased benthic chlorophyll concentrations following a two week phytoplankton bloom, benthic chlorophyll concentrations did not differ from case 1 following the simulated surface bloom in case 2 (Fig 44). Near-bottom nutrient concentrations and porewater nutrient concentrations in case 2 of the model were also the same as case 1.

Discussion

The consistency of the simulated nutrient profiles produced by the calculated non-local exchange rates (Figs 14-16) with nutrient profiles observed on the SAB (Jahnke et al 2005) suggests that the present methodology for determining the non-local exchange rate is viable for future simulations. Indeed, calculated non-local exchange rates ranged from 0-3 day^{-1} at the sediment surface compared to the exchange rate of 1.5 day^{-1} required to match observed sediment $Si(OH)_4$ profiles on the SAB (Jahnke et al, 2005).

By using a non-local exchange parameterization to represent the exchange of particles and solutes across the sediment/water interface, one is essentially turning a local 3 dimensional process into a 1 dimensional process. This is not a problem for the water-column because particles and solutes are rapidly mixed (relative to the 6 minute time interval of the model) on the horizontal length scales of the porewater advective processes.

Concentrations of any given chemical species can be assumed to be fairly homogeneous across any given sigma layer below the multi-kilometer scale grid squares of the model. Such an assumption is not valid in the sediments, where horizontal variability occurs on the scale of millimeters. By contrast, the

underlying sediment environment is likely quite heterogeneous across the same grid squares as evidenced by variability in replicate samples of chlorophyll and nutrients (Fig 7., Table 1).

Thus, the present parameterization of porewater advection as a non-local exchange process should not be used to make conclusions about the sediment environment itself. While it is likely a good estimation of the exchange of dissolved chemical species across the sediment/water interface, it is not an accurate depiction of the process of porewater advection itself, particularly with the respect to the transport of particles to the deep sediments. A true coupling of the sediments to the water column would likely require a much more detailed and deeper, millimeter scale model of the sediment environment.

Such inadequacies in the resolution of the sediment model may be responsible for this model's failure to replicate high concentrations of benthic chlorophyll as previously simulated on the West Florida Shelf (Darrow et al 2003) and observed on the South Atlantic Bight (Nelson et al 1999). On the continental shelf off the coast of North Carolina, benthic diatom stocks have been observed as high as 41 mg m^{-2} on the crests of sand ripples (Cahoon *et al.*, 1990). The diatoms are typically not present, or present in much lower concentrations in the troughs of the sand ripples. The lack of particulate transport to the deep sediments in the present model likely led to a significant underestimation of the overall nutrient flux from the water column to the sediments, thus leading to nutrient limitation of the simulated benthic diatoms.

The flume experiments of Huettel *et al* (1996) show that water tends to enter the sediments at the base of a sand ripple due to the pressure gradient generated by flow over the sand ripple. Pressure is lowest at the crest of the ripple, resulting in an upwelling of deep nutrient rich pore waters out of the sediments at the crest of the ripple. This mechanism of pore water nutrient upwelling is consistent with the patterns of diatoms observed by Cahoon *et al.* (1990) off the coast of North Carolina. Because the current simulation is unable to resolve the horizontal scale of such ripples, the simulated benthic diatom populations are more representative of average concentrations over the a given grid space, rather than populations that might actually be observed at any given point in that particular grid space.

In fact, average simulated concentrations of benthic chlorophyll in both cases of the model were similar to those observed on the West Florida shelf by G. Vargo in April and August 1993 (Fig. 11) and during July 2000 (Table 1). However, far higher average concentrations have been measured by G. Vargo in July and October 1992 (Fig 10) and August 2000 (Table 1) and also by J. Nelson in November 2001 (Table 1). Some sort of seasonal variability in the overlying water column must lead to increased chlorophyll in the benthos, but this model was unable to replicate any such conditions.

1998 and 1993 were, however, similar years in terms of freshwater nutrient input. Drought conditions existed over the southeastern United States (Lott, 1994)) and freshwater from the Mississippi River did not reach the West Florida Shelf for another 3 months following the coastal production cruises during

which chlorophyll concentrations in the benthos were sampled (Weisberg, 1994). Thus, the model did at least match benthic algal growth observations on the West Florida Shelf in similar conditions lacking freshwater nutrient input.

The highest simulated benthic chlorophyll stocks occurred near the mouth of the Mississippi River (Fig. 18) where the nutrient limited benthic diatoms benefited from fluxes of inorganic nitrogen and phosphorus into the sediments (Fig 21). In contrast to the chlorophyll stocks of > 30 mg m^{-2} simulated in the previous 1-D analysis (Darrow *et al.*, 2001), the maximum chlorophyll stocks integrated over the top 5 mm of sediments in any case of this simulation were ~ 12 mg m^{-2}. The benthic diatoms at the chlorophyll maxima in both models were limited primarily by phosphorus availability (Fig. 25) and the near-bottom phytoplankton overlying the benthic chlorophyll maxima were light limited (Fig. 24). The benthic diatoms were also light limited to some extent in this area, perhaps explaining why they did not reach the levels simulated in the 1-D analysis, despite high porewater nutrient oncentrations.

In the second case of the model, an artificial surface phytoplankton bloom was mimicked to represent the chlorophyll plumes that grow in the riverine discharge of the Mississippi and Apalachicola Rivers and are transported to the West Florida Shelf during the springtime when the prevailing winds favor eastward surface circulation (Gilbes *et al.*, 1996). The present 3-D simulation was unable to match previous 1-D results (Darrow et al, 2003) for benthic algal growth following the decline of such a surface phytoplankton bloom. There are a few possible reasons:

The 1-D simulation provided no mechanism for particles to enter the sediments. Any particle sinking through the water column was trapped in the deepest vertical layer of the model where it remained until it was consumed or dissolved. This artificial “trapping” mechanism in the model led to an equally artificial buildup of nutrients in the deepest vertical layer of the water column and a very large concentration gradient across the sediment/water interface. Furthermore, only one sediment layer was represented in the 1-D simulation. So, rapid diffusion of nutrients into that layer early in that simulation led to a very nutrient rich environment for the benthic algae.

In the present simulation, particles were actively transported to multiple layers of sediment through pore water advection processes. There was neither a trapping effect in the near-bottom water column, nor in the surficial sediments. Also, in the present, 3-D simulation particles were mixed horizontally as they sank, diluting their concentrations as they were transported toward the seafloor.

The biggest reason that the benthic diatoms in case 2 of the present model did not experience the rapid growth simulated during the 1-D analysis is that the near-bottom phytoplankton grew instead. Although there was an unrealistic buildup of nutrients in the near-bottom waters of the 1-D simulation (Darrow et al., 2003), the simulated near-bottom diatoms were unable to use those nutrients because they were light limited. The fallout of the surface bloom instead made it to the sediments where the shade adapted benthic diatoms grew on the recycled nutrients. In the present simulation, the near-bottom

phytoplankton were not light limited, so they grew on the fallout of the surface bloom, using up the nutrients before they could be transported to the sediments.

The lack of near-bottom light limitation in the present simulation can chiefly be explained by the treatment of dissolved organic matter. In the 1-D analysis, 50% of all CDOM was considered to be colored and thus light absorbing (Darrow et al., 2003). Based on research that was not available at the time of the 1-D model construction, the present simulation assumes 25% of all CDOM to be colored and thus light absorbing (Benner, 2002). Therefore, under similar surface irradiance conditions, more light made it to the near-bottom water in the present simulation than in the previous 1-D analysis.

In the real world, diagenetic processes in the deep sediments result in enhanced nutrient concentrations there. Once these nutrients are upwelled as water flows over sediment ripples, they likely enhance benthic microalgal growth at the crests of the ripples. The present simulation, testing the role of nutrients from the water column in enhancing benthic microalgal populations, assumes sediments are only 4 cm deep over the entire model grid. Such an assumption is unrealistic. In fact, some of the deepest sediments on the West Florida Shelf are located just northwest of Tampa Bay (Hafen, 2001) where the November 2000 observations were made and also in the Florida Middle Grounds where the August 2000 observations were made. In any case, deep sediments and their interactions with surficial sediments were not adequately modeled in the present simulation, so in that regard, a potentially important nutrient source for the benthic diatoms was ignored.

Conclusions

Although several observations show that benthic microalgae grow on the West Florida Shelf, it is still difficult to determine what causes variability in benthic microalgal populations over time. Clearly, nutrient concentrations in the shallow sediments of this model were not adequate to produce the high benthic chlorophyll concentrations observed in the field.

Given the rapid flushing of most continental shelf sediments in the simulated Eastern Gulf of Mexico, pore water nutrient concentrations are often the same as nutrient concentrations in the near-bottom waters. In nature, these gradients are typically steeper and nutrients coming from the deeper sediments are more likely available to algae living in the surface sediments. In deeper waters, where sediments are not as rapidly flushed, insufficient light exists to grow benthic microalgae.

Nutrients are, however, efficiently transferred to the benthos on the continental shelf upon the decline of a surface phytoplankton bloom. Whether those nutrients are used up by near-bottom phytoplankton or make it all the way to the sediments is dependent on the amount of light reaching the bottom. There exists an irradiance window where near-bottom phytoplankton are light limited

and the more shade adapted benthic algae are not. It is within this window that benthic algae have the opportunity to use nutrients from the overlying water column to grow – whether they are new, upwelled nutrients or recycled nutrients from a dying surface bloom.

References

Admiraal, W. 1977. Experiments with mixed populations of benthic estuarine diatoms in laboratory microecosystems. *Botanica Marina* 20, 479-485.

Amon, R.M.W. and R. Benner. 1996. Bacterial utilization of different size classes of dissolved organic matter. *Limnology and Oceanography* 41, 41-51.

Azam, F., T.Fenchel, J.G. Field, J.S. Gray, L.A. Meyer-Reil and F. Thingstad. 1983. The ecological role of water-column microbes in the sea. *Marine Ecology* 10, 257-263.

Banse, K. 1992. Grazing, temporal changes of phytoplankton, and the microbial loop in the open sea. *Primary Productivity and Biogeochemical Cycles in the Sea* ed: P.G. Falkowski and A.D. Woodhead. Plenum Press.

Bates, J. D. 1963. Heavy mineral roconnaissance Florida west coast. *Economic Geology* 58, 1237-1245.

Benner, R. 2002. Chemical composition and reactivity. In: *Biogeochemistry of Marine Dissolved Organic Matter*, eds: D. Hansell and C. Carlson. Academic Press.

Bidigare, R.R., M.E. Ondrusek, J.H. Morrow, and D.A. Kiefer. 1990. *In vivo* absorption properties of algal pigments. *SPIE* 1302, 290-302.

Birdsall, B. C. 1977. Eastern Gulf of Mexico, Continental Shelf Phosphorite Deposits. Masters thesis. University of South Florida. Tampa, FL. 87 pages.

Blumberg, A.F. and G.L. Mellor. A description of a three dimensional coastal ocean circulation model. In “Three-dimensional Coastal Ocean Models”, ed N. Heaps, AGU, Washington D.C., pp 208-233, 1987.

Bolden, S. 1990. Abundance, diet and foraging migrations of the tomtate (Haemulon aurolineatum) on an artificial and a natural reef in Onslow Bay, North Carolina. Masters thesis. University of North Carolina, Wilmington. pages.

Boudreau, B.P. 1997. *Diagenetic Models and their Implementation*. 417p. Springer-Verlag.

Brooks, H. K. 1973. Geological oceanography. In: A Summary of Knowledge of the Eastern Gulf of Mexico, ed. Jones, J. I., R. E. Ring, M. O. Rinkel and R. E. Smith, State Univeristy System of Florida Institute of Oceanography, St. Petersburg. IIE1 - IIE49.

Cahoon, L. B. and J. E. Cooke. 1992. Benthic microalgal production in Onslow Bay, North Carolina, USA. *Marine Ecology Progress Series* 84, 185-196.

Cahoon, L. B. and C. R. Tronzo. 1992. Quantitative estimates of demersal zooplankton abundance in Onslow Bay, North Carolina, USA. *Marine Ecology Progress Series* 87, 197-200.

Cahoon, L. B., R. S. Redman and C. R. Tronzo. 1990. Benthic microalgal biomass in sediments of Onslow Bay, North Carolina. *Estuarine and Coastal Marine Science* 31, 805-816.

Carder, K.L., R.G. Steward, G.R. Harvey, and P.B. Ortner. 1989. Marine humic and fulvic acids: Their effects on remote sensing of ocean chlorophyll. *Limnology and Oceanography* 34, 68-81.

Carlson C.A. 2002. Production and Consumption Processes. In: *Biogeochemistry of Dissolved Organic Matter in the Ocean* eds. D.A. Hansell and C.A. Carlson. Academic Press, San Diego. Pp. 91-151

Conmy, R. N. and P. G. Coble. 2002. Changes in the optical properties of colored dissolved organic matter in coastal regions of the Gulf of Mexico between the Mississippi River and Florida Bay. *AGU/ASLO conference abstract*

Darrow, B. P. 2002. Adventures in modeling: The West Florida benthic diatom massacre. *XHAB 2002 Conferance Abstract*

Darrow, B. P., J. J. Walsh, G. A. Vargo, R. T. M. Jr., K. A. Fanning and J.-Z. Zhang. 2002. A simulation study of the growth of benthic microalgae following the decline of a surface phytoplankton bloom. *Continental Shelf Research* 23, 1265-1283.

Davis, C.C. 1948. Gymnodinium brevis pp. nov., A cause of discolored water and animal mortality in the Gulf of Mexico. *Botanical Gazette*. 109, 358-360.

De Jonge, V. N. and J. v. d. Bergs. 1987. Experiments on the resuspension of estuarine sediments containing benthic diatoms. *Estuarine, Coastal and Shelf Science* 24, 725-740.

De Jonge, V. N. and J. E. E. V. Beusekom. 1995. Wind and tide induced resuspension of sediment and microphytobenthos from tidal flats in the Ems estuary. *Limnology and Oceanography* 40, 766-778.

Del Castillo, C. E., F. Gilbes, P. G. Coble and F. E. Muller-Karger. 2000. On the dispersal of riverine colored dissolved organic matter over the West Florida shelf. *Limnology and Oceanography* 45, 1425-1432.

Delgado, M., V. N. D. Jonge and H. Peletier. 1991. Effect of sand movement on the growth of benthci diatoms. *Journal of Experimental Marine Biology and Ecology* 145, 221-231.

Del Giorgio, P.A. and J.J. Cole. 2000. Bacterial energetics and growth efficiency. In: *Microbial Ecology of the Ocean*. Ed: D.L. Kirchman. Wiley-Liss 289-324.

Dortch, Q. and T. E. Whitledge. 1991. Does nitrogen or silicon limit phytoplankton production in the Mississippi River plume and nearby regions? *Continental Shelf Research* 12, 1296-1309.

Ducklow, H. 2000. Bacterial production and biomass in the oceans. In: *Microbial Ecology of the Oceans* ed. D. Kirkman. Wiley Liss.

El-Sayed, S. Z., W. M. Sackett, L. M. Jeffrey, A. D. Fredricks, R. P. Saunders, P. S. Conger, G. A. Fryxell, K. A. Steidinger and S. A. Earle. 1972. Chemistry, primary productivity, and benthic algae of the Gulf of Mexico. Serial Atlas of the Marine Environment, Folio 22. American Geographic Society.

Eppley, R.W. 1972. Temperature and phytoplankton growth in the sea. *Fishery Bulletin* 70, 1063-1085.

Eriksson, P.G. and S.E.B. Weisner. 1999. An experimental study on effects of submersed macrophytes on nitrification and denitrification in ammonium-rich aquatic systems. *Limnology and Oceanography* 44, 1993-1999.

Fanning, K. A., K. L. Carder and P. R. Betzer. 1982. Sediment resuspension by coastal waters: a potential mechanism for nutrient re-cycling on the ocean's margins. *Deep-Sea Research* 29, 953-965.

Fanning, K.A., R.H. Byrne, J.A. Breland, and P.R. Betzer. 1981. Geothermal springs of the West Florida continental shelf: evidence of dolomitization and radionuclide enrichment. *Earth and Planetary Science Letters* 52, 345-354.

Gilbes, F., C. Tomas, J. J. Walsh and F. E. Muller-Karger. 1996. An episodic chlorophyll plume on the West Florida shelf. *Continental Shelf Research* 16, 1201-1224.

Gordon, H.R., O.B. Brown, R.H. Evans, J.W. Brown, R.C. Smith, K.S. Baker, and D.K. Clark. 1988. A semianalytic radiance model of ocean color. *Journal of Geophysical Research* 93, 10909-10924.

Gregg, W.W. and K.L. Carder. 1990. A simple spectral solar irradiance model for cloudless maritime atmospheres. *Limnology and Oceanography.* 35: 1657-1675.

Hafen, M. 2001. *West Florida Shelf Sand Waves*. Doctoral dissertation. University of South Florida.

Hedges, J. 2002. Why dissolved organics matter. In: *Biogeochemistry of Marine Dissolved Organic Matter*, eds: D. Hansell and C. Carlson. Academic Press.

He, R. and R. H. Weisberg. 2003. A Loop Current intrusion case study on the West Florida shelf. *Journal of Physical Oceanography* 33, 465-477.

Hu, C., F.E. Muller-Karger and P.W. Sawrzenski. 2006. Hurricanes, submarine groundwater discharge and Florida's red tides. *Geophysical Research Letters* 33, L11601.

Huettel, M. and G. Gust. 1992. Impact of bioroughness on interfacial solute exchange in permeable sediments. *Marine Ecology Progress Series* 89, 253-267.

Huettel, M., W. Ziebis and S. Forster. 1996. Flow-induced uptake of particulate matter in permeable sediments. *Limnology and Oceanography* 41, 309-322.

Humm, H. J. 1957. Rediscovery of Anadyomene menziesii, a deep-water green alga from the Gulf of Mexico. *Bulletin of Marine Science Gulf Caribbean* 6, 346-348.

Hutchinson, G.E. 1961. The Paradox of the Plankton. *American Naturalist.* 95, 137-145.

Iverson, R. L. and H. F. Bittaker. 1986. Seagrass distribution and abundance in Eastern Gulf of Mexico coastal waters. *Estuarine, Coastal and Shelf Science* 22, 577-602.

Jahnke, R. A., J. R. Nelson, R. L. Marinelli and J. E. Eckman. 2000. Benthic flux of biogenic elements on the southeastern US continental shelf: influence of pore water advective transport and benthic microalgae. *Continental Shelf Research* 20, 109-127.

Jahnke, R, M Richards, J Nelson, C Robertson, A Rao and D Jahnke. 2005. Organic matter remineralization and porewater exchange rates in permeable South Atlantic Bight continental shelf sediments. *Continental Shelf Research* 25:1433-1452.

Joyce, E. A. J. and J. Williams. 1969. Rationale and pertinent data. In: Memoirs of the Hourglass Cruises, ed. Florida Department of Natural resources, St. Petersburg, FL. 1-50.

Jumars, P.A., D.L. Penry, J.A. Baross, M.J. Perry, and B.W. Frost. 1989. Closing the microbial loop: dissolved carbon pathway to heterotrophic bacteria from incomplete ingestion, digestion, and absorption in animals. *Deep-Sea Research* 20, 109-127.

Kirk, J.T.O. 1995. *Light and Photosynthesis in Aquatic Ecosystems.* 511p. Cambridge University Press.

Khromov, N. S. 1969. Distribution of plankton in the Gulf of Mexico and some aspects of its seasonal dynamics. In: Soviet-Cuban Fishery Research, ed. Bogdanov, A. S., Washington, DC, USA. 36-56.

Kuhl, M. and B.B. Jorgensen. 1994. The light field and microbenthic communities: radiance distributions and microscale optics of sandy coastal sediments. *Limnology and Oceanography* 39, 1368-1398.

Lenes, J. M., B. P. Darrow, C. Cattrall, C. A. Heil, M. Callahan, G. A. Vargo, R. H. Byrne, J. M. Prospero, D. E. Bate, K. A. Fanning and J. J. Walsh. 2001. Iron fertilization and the Trichodesmium response on the West Florida shelf. *Limnology and Oceanography* 46, 1261-1277.

Li, M.Z. and C.L. Amos. 1995. SEDTRANS92: a sediment transport model for continental shelves. *Computers and Geosciences.* 21, 533-554.

Lott, J.N. 1994. The U.S. summer of 1993. *Weather*. 49, 370-383.

Mallin, M. A., J. M. Burkholder and M. J. Sullivan. 1992. Contributions of benthic microalgae to coastal fishery yield. *Transactions of the American Fisheries Society* 121, 691-695.

Manooch, C. S. I. 1977. Foods of the Red Porgy, Pagrus Pagrus Linnaeus (Pisces: Sparidae), from North Carolina and South Carolina. *Bulletin of Marine Science* 27, 776-787.

Marinelli, R. L. 1992. Effects of polychaetes on silicate dynamics and fluxes in sediments: Importance of species, animal activity and polychaete effects on benthic diatoms. *Journal of Marine Research* 50, 745-779.

Marinelli, R. L., R.A. Jahnke, D.B. Craven, J.R. Nelson, and J.E. Eckman. 1998. Sediment nutrient dynamics on the South Atlantic Bight continental shelf. *Limnology and Oceanography*. 43, 1305-1320.

Masserini, R. T. J. and K. A. Fanning. 2000. A sensor package for the simultaneous determination of nanomolar concentrations of nitrite, nitrate, and ammonia in seawater by flourescence detection. *Marine Chemistry* 68, 323-333.

Miller, D. C., R. J. Geider and H. L. MacIntyre. 1996. Microphytobenthos: The ecological role of the "secret garden" of unvegetated, shallow-water marine habitats. II. Role in sediment stability and shallow-water food webs. *Estuaries* 19, 202-212.

Millero, F. J., A. G. Dickson, G. Eischeid, C. Goyet, P. Guenther, K. M. Johnson, R. M. Key, K. Lee, D. Purkerson, C. L. Sabine, R. G. Schottle, D. R. W. Wallace, E. Lewis, and C. D. Winn. 1998. Assessment of the quality of the shipboard measurements of total alkalinity on the WOCE Hydrographic Program Indian Ocean CO2 survey cruises 1994–1996. *Marine Chemistry* 63, 9–20.

Millie, D. F., G. J. Kirkpatrick and B. T. Vinyard. 1995. Relating photosynthetic pigments and in vivo optical density spectra to irradiance for the Florida red tide dinoflagellate, Gymnodinium breve. *Marine Ecology Progress Series* 120, 65-75.

Moe, M. A. J. 1969. *Biology of the Red Grouper Epinephelus Morio (Valenciennes) from the eastern Gulf of Mexico*. Florida Department of Natural Resources, St. Petersburg, FL.

Mopper, K., X. Zhou, R.J. Kieber, D.J. Kieber, R.J. Sikorski, and R. D. Jones. 1991. Photochemical degradation of dissolved organic carbon and its impact on the oceanic carbon cycle. *Nature* 353 60-61.

Morel, A. and Y-H. Ahn. 1990. Optical efficiency factors of free-living marine bacteria: Influence of bacterioplankton upon the optical properties and particulate organic carbon in oceanic waters. *Journal of Marine Research* 48, 145-175.

Morgan, M.G. and V. Dale. 2007. *Hypoxia in the Northern Gulf of Mexico. An update by the EPA Science Advisory Board*. Environmental Protection Agency, United States of America.

Muller-Karger, F. E., J. J. Walsh, R. H. Evans and M. B. Meyers. 1991. On the seasonal phytoplankton concentration and sea surface temperature cycles of the Gulf of Mexico as determined by satellites. *Journal of Geophysical Research* 96, 12645-12665.

Mullin, M.M., E.F. Stewart, and F.J. Fuglister. 1975. Ingestion by planktonic grazers as a function of concentration of food. *Limnology and Oceanography* 20, 259-262.

Nelson, D. M. and Q. Dortch. 1996. Silicic acid depletion and solicon limitation in the plume of the Mississippi River: evidence from kinetic studies in the spring and summer. *Marine Ecology Progress Series* 136, 163-178.

Nelson, J. R., J. E. Eckman, C. Y. Robertson, R. L. Marinelli and R. A. Jahnke. 1999. Benthic microalgal biomass and irradiance at the sea floor on the continental shelf on the South Atlantic Bight: Spatial and temporal variability and storm effects. *Continental Shelf Research* 19, 477-505.

Nelson, J.R. and C.Y. Roberston, 1993. Detrital spectral absorption: Laboratory studies of visible light effects on phytodetritus absorption, bacterial spectral signal, and comparison to field measurements. *Journal of Marine Researc ,*51, 181-207.

Nordlie, F. G. 1990. Rivers and springs. In: Ecosystems of Florida, ed. Myers, R. L. and J. J. Ewel, Unviersity of Central Florida Press, Orlando. 393-425.

Ogawa, H., Y. Amagai, I. Koike, K. Kaiser, and R. Benner. 2001. Production of refractory dissolved organic matter by bacteria. *Science* 292, 917-920.

Pakulski, J.D., R. Benner, T. Whitledge, R. Amon, B. Eadie, L. Cifuentes, J. Ammerman and D. Stockwell. 2000. Microbial metabolism and nutrient cycling in the Mississippi and Atchafalaya river plumes. *Estuarine, Coastal and Shelf Science* 50, 173-184.

Paluszkiewicz, T., L. P. Atkinson, E. S. Posmentier and C. R. McClain. 1983. Observations of a loop current frontal eddy intrusion onto the West Florida Shelf. *Journal of Geophysical Research* 88, 9639-9651.

Peng, T., T. Takahashi, W.S. Broeker and J. Olasfsson. 1987. Seasonal variability of carbon dioxide, nutrients and oxygen in the northern North Atlantic surface water: observations and a model. *Tellus* 39B, 439-458.

Pope, R.M. and E.S. Fry. 1997. Absorption spectrum (380-700 nm) of pure water. II. Integrating cavity measurements. *Applied Optics* 36, 8710-8723.

Reid, J. A.; Jenkins, C. J.; Field, M. E.; Gardner, J. V.; Zimmermann, M.; Box, C. E.; Kneeshaw, T. A. 2001. usSEABED: Database Efforts in Marine Surficial Sediments of the US EEZ. *American Geophysical Union, Fall Meeting 2001*, *abstract #OS11B-0367*.

Riedl, R.J., Machan, R., 1972. Hydrodynamic patterns in lotic intertidal sands and their bioclimatological implications. *Marine Biology* 13, 179-209.

Riedl, R.J., Huang, N., Machan, R., 1972. The subtidal pump: a mechanism of interstitial water exchange by wave action. *Marine Biology* 13, 210-221.

Roesler, C.S., M.J. Perry, and K.L. Carder. 1989. Modeling in situ phytoplankton absorption from total absorption spectra in productive inland marine waters. *Limnology and Oceanography* 34, 1510-1534.

Ryder, P. D. 1985. Hydrology of the Floridan Aquifer System in West-Central Florida. United States Geological Survey Professional Paper 1403-F. Washington, DC.

Schirripa, M. J., C. M. Legault and M. Ortiz. 1999. The Red Grouper fishery of the Gulf of Mexico: Assessment 3.0. Southeast Fisheries Science Center, Sustainable Fisheries Division. Miami, FL.

Sinclair, W. C., J. W. Stewart, R. L. Knutilla, A. E. Gilboy and R. L. Miller. 1985. Types, features, and occurence of sinkholes. United States Geological Survey water-resources report 85-4126. Tallahassee, FL.

Smith, R.C. and K.S. Baker. 1981. Optical properties of the clearest natural waters (200-800 nm). *Applied Optics* 20, 177-184.

Smith, S. M. and G. L. Hitchcock. 1994. Nutrient enrichments and phytoplankton growth in the surface waters of the Louisiana Bight. *Estuaries* 17, 740-753.

Sundback, K. and W. Graneli. 1988. Influence of microphytobenthos on the nutrient flux between sediment and water: a laboratory study. *Marine Ecology Progress Series* 43, 63-69.

Thomas, C. J. and L. B. Cahoon. 1993. Stable isotope analyses differentiate between different trophic pathways supporting rocky-reef fishes. *Marine Ecology Progress Series* 95, 19-24.

Vargo, G. A., K. L. Carder, W. Gregg, E. Shanley, C. Heil, K. A. Steidinger and K. D. Haddad. 1987. The potential contribution of primary production by red tides to the West Florida shelf ecosystem. *Limnology and Oceanography* 32, 762-767.

Walker, S.T. 1884. Fish mortality in the Gulf of Mexico. *Proc U.S. Natl Mus* 6, 105-109.

Walsh, J.J. and D.A. Dieterle. 1994. CO2 cycling in the coastal ocean. I – A numerical analysis of the southeastern Bering Sea with applications to the Chukchi Sea and the northern Gulf of Mexico. *Progress in Oceanography* 34, 335-392.

Walsh, J. J. and K. A. Steidinger. 2001. Saharan dust and Florida red tides: the cyanophyte connection. *Journal of Geophysical Research* 106, 11597-11612.

Walsh, J. J., R. H. Weisberg, D. A. Dieterle, R. He, B. P. Darrow, J. K. Jolliff, K. M. Lester, G. A. Vargo, G. J. Kirkpatrick, K. A. Fanning, T. T. Sutton, A. E. Jochens, D. C. Biggs, B. Nababan, C. Hu and F. E. Muller-Karger. 2003. The phytoplankton response to intrusions of slope water on the West Florida shelf: models and observations. *Journal of Geophysical Research.* 108, 3190-3213.

Walsh, J.J., J.K. Jolliff, B.P. Darrow, J.M. Lenes, S.P. Milroy, D.A. Dieterle, K.L. Carder, F.R. Chen, G.A. Vargo, R.H. Weisberg, K.A. Fanning, F.E. Muller-Karger, K.A. Stedinger, C.A. Heil, C.R. Tomas, J.S. Prospero, T.N. Lee, G.J. Kirkpatrick, T.E. Whitledge, D.A. Stockwell, T.A. Villareal, A.E. Jochens, and P.S. Bontempi. 2006. Red Tides in the Gulf of Mexico: Where, when, and why? *Journal of Geophysical Research*. 111, 1003-1065.

Weisberg, R.H. 1994. Transport of Mississippi River water to the west Florida shelf. In: *Special NOAA Report-Coastal Oceanographic Effects of Summer 1993 Mississippi River Floodin.* EdL M.J. Dowgiallo. USDOC/NOAA Coastal Ocean Office/National Weather Service.

Brian Darrow has been interested in computers since an early age. He wrote his first working computer program at age 9, beginning a lifelong journey as a self taught software engineer. Prior to his doctoral work in computer modeling marine ecosystems, Brian received a Bachelor of Science degree in biology from St. Louis University and a Master of Science degree in Marine Science from the University of South Florida. Dubbed an honorary “parrothead” for his work studying the scum on the bottom of the ocean, Brian has thus far participated in 17 coastal research cruises and logged over 75 days at sea. He is the recipient of several awards and fellowships, including the Gulf Oceanographic Charitable Trust Fellowship in Coastal Science.